

Ninevah University

College of Electronics Engineering



Investigation of Radar Cross-Section Reduction of Planar Surfaces

Mustafa Basim Jasim Al-Obadi

M.Sc. Dissertation

in

Communication Engineering

Supervised by

Prof. Dr. Khalil Hassan Sayidmarie

2022 A.D.

1444 A.H.

Investigation of Radar Cross-Section Reduction of Planar Surfaces

Dissertation Submitted by

Mustafa Basim Jasim Al-Obadi

To

The Council of College of Electronic Engineering

Ninevah University

In Partial Fulfillment of the Requirements

For the Degree of Master of Sciences

In

Communication Engineering

Supervised by

Prof. Dr. Khalil Hassan Sayidmarie

2022 A.D.

1444 A.H

بِسْمِ اللَّهِ الرَّحْمَنِ الرَّحِيمِ

فَتَعَالَى اللَّهُ الْمَلِكُ الْحَقُّ وَلَا تَعْجَلْ بِالْقُرْآنِ مِنْ

قَبْلِ أَنْ يُقْضَىٰ إِلَيْكَ وَحْيُهُ وَقُلْ رَبِّ زِدْنِي

عِلْمًا ﴿١١٤﴾

سورة طه : ١١٤

Supervisor's Certification

I certify that the dissertation entitled (**Investigation of Radar Cross-Section Reduction of Planar Surfaces**) was prepared by **Mustafa Basim Jasim** under my supervision at the Department of Communication Engineering, Ninevah University, as a partial requirement for the Master of Science Degree in Communication Engineering.

Signature:

Name: Prof. Dr. Khalil H. Sayidmarie

Department of Communication Engineering

Date: / /2022

Report of Linguistic Reviewer

I certify that the linguistic reviewer of this dissertation was carried out by me and it is accepted linguistically and in expression.

Signature:

Name:

Date: / /2022

Report of the Head of Department

I certify that this dissertation was carried out in the Department of Communication Engineering. I nominate it to be forwarded to discussion.

Signature:

Name: Dr: Mahmud A. Mahmud

Date: / /2022

Report of the Head of Postgraduate Studies Committee

According to the recommendations presented by the supervisor of this dissertation and the linguistic reviewer, I nominate this dissertation to be forwarded to discussion.

Signature:

Name:

Date: / /2022

Committee Certification

We the examining committee, certify that we have read this dissertation entitled (**Investigation of Radar Cross-Section Reduction of Planar Surfaces**) and have examined the postgraduate student (**Mustafa Basim Jasim**) in its contents and that in our opinion; it meets the standards of a dissertation for the degree of Master of Science in Communication Engineering.

Signature:

Name: Assist Prof. Dr. Yessar E.
Mohammed Ali

Head of committee

Date: / /2022

Signature:

Name: Assist Prof. Dr. Mohamad A.
Ahmed

Member

Date: / /2022

Signature:

Name: Assist Prof. Dr. Ahmed M.
Salama

Member

Date: / /2022

Signature:

Name: Prof. Dr. Khalil H. Sayidmarie

Member and Supervisor

Date: / /2022

The college council, in its meeting on / /2022, has decided to award the degree of Master of Science in Communication Engineering to the candidate.

Signature:

Name: Prof. Dr. Khalid K. Mohammed
Dean of the College

Date: / /2022

Signature:

Name: Assist Prof. Dr. Sedki B. Thanoon
Council registrar

Date: / /2022

Acknowledgements

First and foremost, praises and thanks to God, the Almighty, for His showers of blessings throughout my research work to complete the dissertation successfully.

I would like to express my sincere gratitude and special thanks to my dear supervisor Dr. Khalil H. Sayidmarie for his ongoing support, scientific supervision, training, and encouragement during the composition of my dissertation. His candid comments have really sharpened my viewpoint and enhanced my comprehension.

Additionally, I would like to express my appreciation to the staff of the department of Communication Engineering, in particular the head of the department. I also must mention my respected professors who gave me lectures throughout my academic career, as well as those who have provided me with a lot of support.

I want to express my sincere gratitude to my great parents for their support and inspiration during the entirety of my academic career, without their help and prayers, there is no way I could have accomplished this achievement. I attribute my accomplishment to them. I ask God to grant them a blessed life and good health.

Last but not the least, my sincere thanks also go to my older brothers Abdulla, and Yahya, as well may kindness sisters, Marwa, and Ansam whose encouraged me and prayed for me throughout the time of my research and gave me as much support and assistance as they could. May the Almighty God richly bless all of you.

Abstract

There is a growing interest in reducing the radar cross-section (RCS) of objects for a wide range of applications. Composite materials, such as wood and other synthetic materials were utilized in the construction of objects to lower RCS.

This dissertation examines the reduction of radar cross-section of the targets utilizing single layer frequency selective surfaces (FSS) unit cells. Creating FSS unit cells with a low reflection coefficient is the aim of this work in order to use them to minimize the radar cross-section. The research includes theoretical analysis as well as simulations with the CST Microwave Studio.

An FSS using double square rings printed on single side of the substrate was studied to enhance the performance of reducing of radar cross section. The effect of changing the rings size, and width on the resonance frequency was investigated. Also, to get a wide bandwidth from the intersection of two bands of frequency response of the double rings, a meander inner ring was used to bring its circumference close to the circumference of the outer ring, in addition to using an open inner ring because circumference of open ring approximately equal $0.5\lambda_e$ at resonance. Moreover, the effect of changing some parameters of the unit cell like size of ring, width of ring, and space between two ends of inner ring on the resonance frequency and the reflection coefficient were investigated.

In addition to the conducting parts, this dissertation also discusses whether it is possible to increase the FSS cell's absorber performance to reduce the radar cross-section. In order to minimize the reflected power from the FSS unit cells employing the double closed rings and double rings with an open inner ring were supplemented with a layer of carbon paste to increase the absorbance. The suggested FSS cells were examined using different combinations of shapes of copper ring and fillings by carbon paste, modifying ring dimensions, conductivity, and paste thickness for proposed forms of unit cells.

Published Research

Some of the results obtained in this work were published in the following:

Mustafa B. Jasim, and Khalil H. Sayidmarie, "Planar Absorbing FSS Unit Cells for Radar Cross-Section Reduction", 2022 International Conference on Innovation and Intelligence for Informatics, Computing, and Technologies (3ICT), 20-21 Nov. 2022, University of Bahrain.

TABLE OF CONTENTS

Subject		Page
Acknowledgments		V
Abstract		VI
Published Research		VII
Table of Contents		VIII
List of Tables		XII
List of Figures		XIII
List of Abbreviations		XVIII
List of Symbols		XIX
CHAPTER ONE – INTRODUCTION		1
1.1	Overview	1
1.2	Literature Survey	2
1.3	Aims of the Dissertation	9
1.4	Dissertation Layout	9
CHAPTER TWO – BASICS OF RADAR CROSS-SECTION REDUCTION		10
2.1	Introduction	10
2.2	Radar Cross Section Reduction Concepts	11
2.2.1	Absorption	12
2.2.2	Scattering	12
2.3	Classification of RCS Reduction Methods	12
2.3.1	Active Radar Cross-Section Reduction	13
2.3.2	Passive Radar Cross Section Reduction	14
2.4	Techniques of RCS reduction	15
2.4.1	Shaping	15
2.4.2	Absorbing Materials	16

2.4.3	Frequency-Selective Surface (FSS)	19
2.4.3.1	FSS used as Reflectors	20
2.4.3.2	FSS used as Antenna Radomes	22
2.4.4	Artificial Magnetic Conductors (AMC)	22
2.4.5	Electromagnetic Band Gap (EBG)	24
2.4.6	Polarization Rotation Reflecting Surface (PRRS)	25
2.4.7	Metasurface	26
2.4.8	Opposite Phase Cancellation (OPC)	27
CHAPTER THREE – RADAR CROSS-SECTION REDUCTION USING FSS WITH CONDUCTIVE UNIT CELLS		30
3.1	Introduction	30
3.2	Design of the FSS Unit Cell	30
3.3	Copper Unit Cell	31
3.3.1	Single Square Ring	31
3.3.2	Double Square Closed Ring	35
3.3.3	Double Ring Unit Cell with Meander Inner Ring	39
3.3.4	Double Ring Unit Cell with Open Inner Ring	41
3.3.5	Comparing the Performance of the Proposed Designs	45
3.4	The Ohmic Sheet or Resistive Sheet Unit Cell	46
3.4.1	Double ring Unit Cell	47
3.4.2	Double Ring with Open Inner Ring Unit Cell	49

CHAPTER FOUR – RADAR CROSS-SECTION REDUCTION USING RESISTIVE FSS UNIT CELLS		54
4.1	Introduction	54
4.2	Double Closed Copper Rings with Carbon Paste	55
4.2.1	Double Closed Copper Rings with a Carbon Ring	56
4.2.2	Double Closed Copper Rings with a Carbon Ring and Patch	58
4.3	Double Rings with Opened Inner Ring	60
4.3.1	Double Rings with Opened Inner Ring and Carbon Patch	62
4.3.2	Double Rings with Opened Inner and Carbon Paste at the Inner Ring Opening	63
4.3.3	Double Rings with Opened Inner and Carbon Ring	64
4.3.4	Double Rings with Opened Inner Ring Filled with Carbon Paste	66
4.3.5	Double Rings with Opened Inner Ring, Carbon Ring and Carbon Patch	67
4.3.6	Double Rings with Opened Inner and Carbon at the Inner Ring Opening and Carbon Ring	68
4.3.7	Double Rings with Opened Inner and Carbon Paste in Between Them	70
4.4	FSS Cells Using Rings of Carbon Paste	71
4.4.1	Double Closed Rings Carbon Paste Unit Cell	71
4.4.1.1	Carbon Ground Plane with Substrate Unit Cell	73
4.4.1.2	Ground Plane and Outer Ring of Carbon Paste	73
4.4.1.3	Carbon Ground Plane with Inner Ring	74

4.4.2	Double Ring (Open Inner Ring) Carbon Paste Unit Cell	76
4.4.2.1	Carbon Ground Plane with Substrate Unit Cell	77
4.4.2.2	Carbon Ground Plane with Outer Ring	78
4.4.2.3	Carbon Ground Plane with Opened Inner Ring	79
4.5	Effect of Changing Parameters on Single Ring Carbon Paste Unit Cell	81
4.5.1	Changing the Side Length of the Ring	81
4.5.2	Changing the Thickness of Ground Plane	84
4.5.3	Changing the Conductivity of the Carbon Paste	84
CHAPTER FIVE – CONCLUSIONS AND FUTER WORK		87
5.1	Conclusions	87
5.2	Futers Work	89
REFERENCES		90
References		90

LIST OF TABLES

CHAPTER THREE - RADAR CROSS-SECTION REDUCTION USING FSS WITH CONDUCTIVE UNIT CELLS		
Table	Title	Page
3.1	The Simulations of the Single Ring FSS with Various Ring Length	34
3.2	The Simulations Result of the Double Ring FSS with Various Dimensions	38
3.3	Simulations Results of the Double Ring (Open Inner Ring) with Various Length of L3	44
3.4	Comparing Between Previous Cases Results	46
3.5	1st and 2nd Minima Frequency for Each Resistive Value	50
3.6	The Simulations Result of the Unit Cell with Various Values of Resistivity, Ring Width=2mm, and $\epsilon\epsilon = 3.157$.	52
CHAPTER FOUR- RADAR CROSS-SECTION REDUCTION USING RESISTIVE FSS UNIT CELLS		
Table	Title	Page
4.1	Comparison of Best Results for Cases of Carbon Region Distribution	71
4.2	Simulation Results of Changing Side Ring Length, and Ring Width	83
4.3	Simulation Results of Changing Length, Width, and Conductivity	85

LIST OF FIGURES

Chapter One – INTRODUCTION		
Figure	Title	Page
1.1	Radar Cross Section (RCS) Concept	1
Chapter Two – BASICS OF RADAR CROSS-SECTION REDUCTION		
Figure	Title	Page
2.1	Radar Cross-Section Notion	11
2.2	Classification of the RCS Reduction Techniques	13
2.3	(a) Diagram of the Salisbury Screen (b) Transmission Line Equivalent Circuit	17
2.4	Variation of the Reflection Coefficient as a Function of Incidence Angle	18
2.5	Dallenbach Layer	19
2.6	Performance of the Dallenbach Layers	19
2.7	Some Typical FSS Element Shapes	21
2.8	(a) Dipole Antenna with the FSS Reflectors (b) Top view. (c) Ribcage Dipole Antenna (d) the FSS Unit Cell	21
2.9	FSS-Antenna-Radome System	22
2.10	(a) An AMC Formed of an Array of Unit Cells. Each via is Connected to the Ground Plane, (b) the Equivalent LC Circuit, and (c) the Corresponding Model	23
2.11	Reflection Phase of RCS-Reducing AMC	23
2.12	EBG Structure with Square Satch	24
2.13	The PRRS Unit Cell Design (a) Top view (b) Side view	25
2.14	Schematics of an Absorptive Array Metasurface	26
2.15	Chessboard Structure. The Black Squares Represent the PEC Elements and the White Squares the AMC Elements. The Inset Shows the Unit Cell	28
2.16	The Fabricated Hexagonal Checkerboard Ground Plane Combining EBG1 and EBG2 Structures	29
Chapter Three – RADAR CROSS-SECTION REDUCTION USING FSS WITH CONDUCTIVE UNIT CELLS		
Figure	Title	Page

3.1	The FSS Unit Cell Geometry of Single Ring (a)'' Front view'' (b)'' Side view''	31
3.2	The unit cell with waveguide port for simulation using the CST Microwave studio	32
3.3	The Reflection Coefficient (S_{11}) of the Single Ring FSS	33
3.4	The Surface Current Distribution on a Single Square Ring at 3.2 GHz Frequency	35
3.5	Double Ring Unit Cell Geometry (a)'' Front view'' (b)''Side view''	36
3.6	The Reflection Coefficient (S_{11}) of Double Ring Unit Cell	36
3.7	S_{11} of Different Values of the Inner Ring	37
3.8	The Surface Current on the Double Square Ring (a) at 3.2 GHz (b) at 5 GHz	39
3.9	Double Rings Unit Cell with Meandered Rings (a) Meandering the Horizontal Sides, (b) Meandering the Vertical Sides	40
3.10	The Reflection Coefficient S_{11} of Double Rings Unit Cell (Inner Ring is Meandered)	41
3.11	Geometry of Double Rings Unit Cell (Open Inner Ring)	42
3.12	Reflection Coefficient S_{11} of Double Rings Unit Cell (Open Inner Ring)	43
3.13	Geometry of Double Rings Unit Cell (Open Inner Ring)	45
3.14	Reflection Coefficient S_{11} of Double Rngs (Open Inner Ring) with Changed the Polarization	45
3.15	Geometry for Defining Resistivity (Left) and Sheet Resistance (Right)	47
3.16	Geometry of the Unit Cell (a) Ohmic Sheet case (b) Copper Case	48
3.17	Reflection Coefficient Response of the Double Ring Ohmic Sheet Compared to that for Using Copper	48
3.18	Geometry of the Double Ring with Open Inner Ring Unit Cell (a) Ohmic Sheet Case (b) Copper Case	49
3.19	Reflection Coefficient Response of the Double Ring (open Inner Ring) Ohmic Sheet Comparing with Copper Case	50
3.20	Reflection Coefficient Response for Variable Sheet Resistivity	53

3.21	Reflection Coefficient Response of GP and Substrate without the Rings	53
Chapter Four - RADAR CROSS-SECTION REDUCTION USING RESISTIVE FSS UNIT CELLS		
Figure	Title	Page
4.1	Double Ring Unit Cell Geometry (a) "Front view" (b) "Side view"	55
4.2	Double Ring Unit Cell Geometry with Carbon Paste Layer Placed in Between the Two Rings	56
4.3	Variation of the Reflection Coefficient with Frequency for the Double Ring Unit Cell with and without Carbon Paste	57
4.4	Variation of the Reflection Coefficient with Frequency for the Double Ring Unit Cell with Carbon Paste after decreasing the Size of the Inner Ring	57
4.5	Double Ring Unit Cell Geometry with Carbon Paste Ring and Patch	58
4.6	Reflection Coefficient Responses (S_{11}) of the Double Ring with Carbon Layers Between the Rings and at the Center of the Inner Ring	59
4.7	Reflection Coefficient of Double Ring Unit Cell with Carbon Ring and Patch after decreasing the Outer Ring Size	59
4.8	Geometry of Unit Cell (a) Copper Rings (b) Adding Carbon Ring (c) Adding Carbon Ring and Patch at the Center	60
4.9	Reflection Coefficient Results of the (Copper Rings, adding a Carbon Ring, and adding a Carbon Ring and Path at the Center)	60
4.10	Geometry of Double Rings Unit Cell (Open Inner Ring)	61
4.11	Reflection Coefficient of the Double Ring with Open Inner Ring Unit Cell	61
4.12	Double Ring (Open Inner Ring) with Carbon Square Patch	62
4.13	S_{11} of the Double Ring Unit Cell (with Open Inner Ring) when adding a Carbon Square Patch at the Center	62
4.14	Double Ring (Open Inner Ring) Unit Cell with Carbon in the Internal Ring Opening	63
4.15	S_{11} of the Double Ring Unit Cell (with Open Inner Ring) with Carbon in the Internal Ring Opening	63

4.16	Double Ring Unit Cell (Open Inner Ring) with Carbon Ring	64
4.17	S_{11} of the Double Ring Unit Cell (Open Inner Ring) with Carbon Ring	64
4.18	Geometry of the Double Ring Unit Cells (Open Inner Ring) Cases with Carbon in One Region of Unit Cell	65
4.19	Reflection Coefficient Comparison of Cases of Unit Cells with Carbon in One Region	65
4.20	Double Ring Unit Cell (Open Inner Ring) with Carbon in the Square Patch and at the Inner Ring Opening	66
4.21	S_{11} of the Double Ring Unit Cell (Open Inner Ring) with Carbon in the Square Patch and at the Space Between Two ends of the Inner Ring	66
4.22	Double Ring Unit Cell (Open Inner Ring) with Carbon Ring and Patch	67
4.23	Reflection Coefficient of the Double Ring Unit Cell (Open Inner Ring) with Carbon in the Square Patch and at the Space Between Two Rings	67
4.24	Double Ring Unit Cell (with Open Inner Ring) with Carbon Ring and Carbon in the Inner Ring Opening	68
4.25	S_{11} of the Double Ring Unit Cell (Open Inner Ring) with Carbon Ring and Carbon in the Inner Ring Opening Together	68
4.26	Geometries of the Unit Cells with Carbon in Two Regions Together Comparing with Copper Ring Case	69
4.27	Reflection Coefficient Comparison of Cases with Carbon in Two Regions	69
4.28	Unit Cell Geometry (a) Copper Rings (b) Carbon at Three Regions Together	70
4.29	Variation of the Reflection Coefficient Double Ring Unit Cell (Open Inner Ring) with Carbon in Three Rings Compared with the Copper Case	70
4.30	Geometry of the Carbon Rings Unit Cells (a) Carbon Ground Plane, (b) Copper Ground Plane	72
4.31	Reflection Coefficient of the Double Ring Unit Cell for Carbon Ground Plane and Copper Ground Plane	72
4.32	Unit Cell Geometry Contains Carbon GP and Substrate	73

4.33	Variation of the Reflection Coefficient of Unit Cell Contains Carbon GP and Substrate	73
4.34	Unit Cell Geometry Contains Carbon GP and Outer Ring	74
4.35	Variation of the Reflection Coefficient of Unit Cell which Contains Carbon GP and Outer Ring	74
4.36	Unit Cell Geometry Contains Carbon GP and Inner Ring	75
4.37	Reflection Coefficient of the Unit Cell that Contains Carbon GP and Inner Ring	75
4.38	Reflection Coefficient Comparison for Each Case of Closed Ring Carbon Unit Cell	76
4.39	Geometry of Double Ring (Open Inner Ring) Unit Cells (a) Carbon GP, (b) Copper GP	77
4.40	Reflection Coefficient of the Double Ring (Open Inner Ring) Unit Cell for Carbon GP and Copper GP	77
4.41	Variation of Reflection Coefficient of Unit Cell Contains Carbon GP and Substrate	78
4.42	Reflection Coefficient of the Unit Cell that Contains Carbon GP and Outer Ring	79
4.43	Unit Cell Geometry Contains Carbon GP and an Open Inner Ring	79
4.44	Reflection Coefficient for the Unit Cell that Contains Carbon GP and Inner Ring	80
4.45	Reflection Coefficient Comparison for Each Case of Carbon Unit Cell	80
4.46	Reflection Coefficient Comparison for Changing the Side Length of the Ring	82
4.47	Reflection Coefficient Comparison for Changing the Width of the Ring	83
4.48	Reflection Coefficient Comparison for Changing Carbon Ground Plane Thickness	84

LIST OF ABBREVIATIONS

Abbreviation	Name
AMC	Artificial Magnetic Conductors
BW	Bandwidth
CST Microwave Studio	Computer Simulation Technology
DGS	Defected Ground Structure
EBG	Electromagnetic Band Gap
EC	Equivalent Circuit
EM	Electromagnetic
FBW	Fragmentary Bandwidth
FSS	Frequency Selective Surface
GP	Ground Plane
HFSS	High frequency Structure Simulator
HMM	Hybrid Mechanism Metasurface
OPC	Opposite Phase Cancellation
PCA	Polarization Conversion Absorption
PEC	Perfect Electric Conductor
PMC	Perfect Magnetic Conductor
PRRS	Polarization Rotation Reflection Surface
RAM	Radar Absorbing Material
RCS	Radar Cross Section
RCSR	Radar Cross Section Reduction
RF	Radio Frequency
TE	Transvers Electric
TM	Transvers Magnetic

LIST OF SYMBOLS

Symbols	Name
A	Cross Sectional Area
C	Speed of Light
CR_{av}	Average Circumference of Ring
E_i	Incident Electric Field
E_s	Scattered Electric Field at Receiver
f	Resonance Frequency
GHz	Giga Hertz
h, h_1	Substrate Thickness
L	Side Length of Unit Cell
L_1	Side Length of Outer Ring
L_2	Side Length of Inner Ring
mt	Ground Plane and Ring Thickness
R	Radar Rang
Rho	Density of Carbon Paste
R_s	Sheet Resistance
S_{11}, Γ	Reflection Coefficient
S_r	Scattered Power Density
S_t	Power Density Intercepted by Target
W	Width of Ring
Z_o	Characteristic Impedance of Transmission Line
Z_i	Input Impedance
δ	Conductivity
δv	Volume Conductivity
ϵ_{eff}	Effective Relative Dielectric Constant
ϵ_o	Permittivity of free space
ϵ_r	Relative Dielectric Constant
θ	Off-Normal Angle
λ	Wavelength
λ_e	Effective wavelength
λ_1	Wavelength of Lowest Frequency
λ_o	Wavelength in the Air
σ	Radar Cross Section
Ω	Ohm
ρ	Resistivity of Sheet Material
ρv	Volume Resistivity
γ	Complex Propagation Constant

CHAPTER ONE
INTRODUCTION

CHAPTER ONE

INTRODUCTION

1.1 Overview:

Radar cross-section (RCS) is a measure of the capability of a target material to reflect the incident radar wave toward the radar receiver [1]. It is defined as the ratio of backscattered power per steradian (unit solid angle) in the direction of the radar to the power density that is intercepted by the target. Thus, one can define a target's RCS as a comparison between two radar signal intensities. One is the strength of the signal reflected strength from the target, while the other is the signal strength that is reflected from a perfectly smooth sphere of a cross-sectional area in (m^2) as shown in Fig. 1.1.

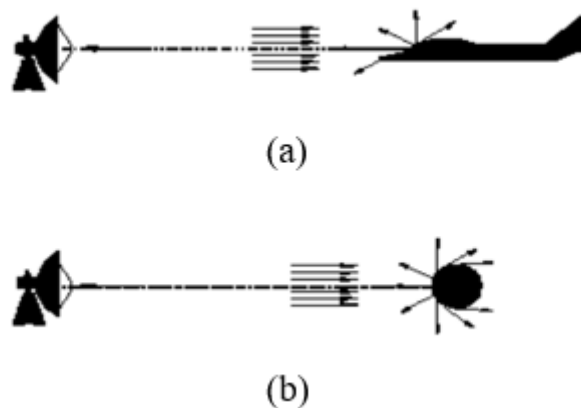


Figure 1.1 Radar Cross Section (RCS) concept, (a) reflection from a target, (b) reflection from a perfectly smooth sphere [2].

The need to reduce or control the radar cross-section has been a topic of interest since World War II. Initial attempts were made to reduce aircraft detectability by using wood and other composites as aircraft materials, as they exhibit lower reflection of radar waves compared to metals. It was then realized that molding and coating with radar absorbing materials (RAM), is the main techniques for RCS reduction. RCS reduction refers how radar may

make a target less visible. The target's invisibility is referred to as the ideal RCS reduction regardless of the frequency of the incident wave, incidence angle, or polarization. However, such goal for reduction is not easily attainable in a practical way. Recent times have seen a lot of attention paid to improving the RCS reduction bandwidth, for practical applications, and RCS reduction of 10 dB is typically deemed sufficient [3]. Obtaining a 10 dB RCS reduction for a target means a 90% reduction in the radar cross-section, and such reduction is obtained at a certain frequency or band of frequencies.

There are two main mechanisms that were used to achieve RCS reduction. These are scattering and absorption. Scattering means deflecting the incident wave away from the radar, whereas the absorption mechanism absorbs all or part of the incident wave in an absorbing layer. Shaping is one of the techniques that utilize the scattering principle, while radar-absorbing material (RAM) uses the absorption principle to operate. Both methods have been in use for many years, however, recently due to their superior characteristics, metasurfaces have attracted interest in this field. A metasurface is a periodic or aperiodic array of subwavelength resonant scatters that impact the surface's electromagnetic response [4].

1.2 Literature Survey:

In 1989, H.J. Li, N.H. Farhat, and Y. Shen experimentally studied the Radar cross-section (RCS) reduction using microwave diversity imaging. Experimental results showed that broadband absorber covering is useless in lowering the co-polarized (both the transmitting and receiving antennas have the same sense of circular polarization) RCS of a plate when the incident wave approximates the edge-on direction but is effective at lowering the cross-polarized (the transmitting and receiving antennas have an opposite sense of circular polarization) RCS for all incident directions. The surface current

absorber covering is effective at reducing the no specular energy and several bounces regardless of how polarized the measurement is [5].

In 1995, E. Ongareau, et al proposed a system formed by a cascade connection of meander-line strip grating surfaces that rotates the polarization plane of a linearly polarized wave. Reflectivity measurements of the system shaped on a reflector-backed metallic ground plane have shown reflectivity levels smaller than -20 dB over the 10.5 -17 GHz band [6].

In 1996, C. B. Wilsen, and D. B. Davidson studied the radar cross section (RCS) reduction of microstrip patch antennas for low-observable platforms, with emphasis on the application of lossy superstrates. The observed effect of these antenna parameters is related to expected RCS reduction. The RCS computed by a finite element method/method of moments code is also presented. Other RCS reduction techniques discussed included shorting posts and ferrite substrates [7]. While S. C. Zhao, B. Z. Wang, and Q. Q. in 2008 proposed a rectangular patch antenna having two circular apertures, a defected ground structure (DGS), and a shorting post. The radar cross section (RCS) of the antenna at operational frequency can be reduced by the novel structure. Simultaneously, the suggested antenna's return loss is maintained, moreover, the patch antenna's RCSs at the frequencies outside the operational range are minimized. High frequency electromagnetic modeling software was used to simulate the proposed antenna. The peak of RCSs was reduced by about 7 dB and the broadband RCSs are below -30 dB from 2 to 8 GHz [8].

In their turn S. S. Parit, and V. G. Kasabegoudar in 2016 presented an octagonal ultra-wideband antenna with reduced RCS. The proposed antenna operates in the frequency range of 3.6 GHz to 16 GHz with an impedance bandwidth of more than 115%. The antenna was optimized with an improved RCS of nearly 50% (without affecting the overall performance) than the works reported earlier [9]. On the same year, W. Chen in 2016 used an

electromagnetic band-gap checkerboard surface to reduce the RCS. The reflections from various parts of the checkboard are out of phase at the resonant frequency thus resulting in reducing the reflected wave. Checkerboard surfaces come in five distinct designs were analyzed, simulated with High frequency Structure Simulator (HFSS) and measured for verification [10].

Likewise, J. Su, et al, in 2018, presented a checkerboard metasurface based on a unique physical mechanism, optimized multielement phase cancellation, to significantly increase the bandwidth of radar cross section (RCS) reduction. The proposed primary interface achieved a 10 dB RCS reduction in an extremely wide frequency range from 5.5 to 32.3 GHz with a ratio bandwidth (f_H/f_L) of 5.87:1 when both polarizations are incident normally. Moreover, the RCS reduction was greater than 8 dB from 5.4 to 40 GHz with a bandwidth of 7.4:1. The super surface also performs well under a wide range of oblique incidence angles [11]. Parallel to this, G. Shen, et al in 2018 presented a broadband terahertz metamaterial absorber having four sub-cells, a metal ground plane, and several metal rings, all of which are separated by a layer of dielectric. The experimental results showed better broadband performance than both the previous single layer absorbers based on metal rings and the latest absorbers based on the fractal-cross structure reported recently. The theoretical analysis indicated that the absorption mechanism is the coupling response of the enhanced electromagnetic field between metallic rings and the merging of the adjacent resonant peaks in the multi-resonators [12]. In the same year, J. Zhang, et al presented a new microstrip patch antenna with wideband (RCS) reduction. The RCS of the proposed antenna was reduced by subtracting the current-direction slots of the patch, with the radiation performance sustained not only for the current-direction subtraction, but also for the no modification in the ground plane. In the frequency band

from 3.9 to 8.1 GHz, the RCS of the modified antenna was reduced in the whole band compared with the RCS of the reference antenna. The maximum RCS reduction was 7 dB at a frequency of 6.7 GHz [13].

L. Ali, Q. Li, T. Ali Khan, J. Yi, and X. Chen in 2019 presented a radar cross-section (RCS) reduction technique by using the coding diffusion metasurface, which was optimised by a random optimization algorithm. It has a working frequency band from 8.6 GHz to 22.5 GHz, with more than 9 dB RCS reduction.[14] In the same year, F. Wang, K. Li, Y. Ren, and Y. Zhang proposed an active reconfigurable FSS with PIN diodes that was used as a reflector for the antenna to reduce RCS. The reconfigurable FSS reflector has a different performance by PIN diodes with or without DC bias. The design can switch between band-pass FSS and band-stop FSS, and thus can contribute to the switchable RCS reduction of dipole antenna without degrading its radiation performance [15].

In 2020, M. I. Hossain, N. N. Trong, K. H. Sayidmarie, and A. M. Abbosh presented an accurate equivalent-circuit (EC) design approach for wideband nonmagnetic absorbers operating at the low microwave frequency (1 – 10 GHz) utilizing the impedance matching method. Two simple and commonly used resistive frequency selective surfaces (FSS), i.e. square patch and single square loop, are taken into account in that study, compared to full-wave simulations, the proposed EC model showed more than 95% accuracy. Through the use of the suggested model and genetic algorithm-based optimization, several designs of broadband absorbers were demonstrated. The outcomes demonstrate the effectiveness of the suggested technique for building thin wideband absorbers with single-layer or double-layer FSS designs [16].

M. Nadi, S. H. Sedighy, and M. K. Amirhosseini in 2020 proposed a general strategy to design ultra-wideband radar cross section reduction

metasurface by employing non-resonant unit cells in chessboard arrangement. The proposed miniaturized artificial magnetic conductor unit cell is consisting of two layered non-resonant patches separated from one another by thin dielectric substrates. The genetic optimization algorithm was used to optimize the unit cell design parameters. The suggested approach was carried out to design three different RCSR metasurfaces, ideal, ROGERS and low-cost substrates. The low cost RCSR metasurface is composed of FR-4 substrate which reduced the RCS by more than 10-dB from 5.22 GHz to 30.85 GHz, 142% fractional bandwidth [17].

R. Jaiswar, et al, in 2020 presented a microwave absorber combining frequency-selective surfaces (FSSs) and dielectric layers. FSSs are printed on dielectric layers employing a carbon nanotube suspension-based resistive ink. The absorber exhibits a fractional bandwidth of 137%, corresponding to reflectivity lower than -15 dB and absorption upper than 90% from 7.30 till 41.95 GHz, meaning a 34 GHz bandwidth, for a thickness of only 0.13λ . This performance is obtained by tuning the number of printed layers, which fixes FSS resistivities [18].

S. Ünalı, H. Bodur, S. Çimen, and G. Çakir in 2020, presented a broadband reflectarray antenna with low RCS level. The RCS reduction is obtained with double layer FSS having variable-sized unit cell elements. The proposed reflectarray antenna with metallic grounded and FSS backed were designed, simulated, and fabricated. The measurement and simulation results for the designed FSS grounded reflectarray shows decreased RCS level effectively almost in the whole band (2-18 GHz) [19].

In 2021 J. Y. Jeong, et al suggested a manufacturing procedure for a wide-bandwidth microwave absorber. The manufactured microwave absorber includes 144 resistive double square designs that are not connected to one another. These patterns were precisely fabricated within a size error of 1% and

a flat surface having an average roughness under than 100 nm. The developed microwave absorber revealed that a performance of RCS reduction with reflectance less than -10 dB over 8 to 14.6 GHz frequency range. Further research is needed to improve the morphologies of resistive array patterns and the characteristics of the conductive carbon ink in order to expand the RCS reduction performance across the full Ku-band or higher frequencies and to make the performance more uniform throughout the frequency range [20].

Y. XI, et al in 2021 proposed a hybrid mechanism metasurface (HMM) that incorporates absorption, polarization conversion and phase cancellation mechanisms for wideband and wide-angle radar cross section (RCS) reduction. The polarization conversion absorber (PCA) is suggested by embedding the lumped resistors into the structure of polarization conversion, which integrates the absorption and polarization conversion mechanisms. Then, the phase cancellation mechanism is employed to redirect the scattering energy to the non-incident directions through the chessboard configuration [21].

In 2021 Y. Chen, et al proposed a coding metasurface antenna array, which combines the two concepts of digital coding metasurface and metasurface antenna. The resulting array has diversified reconfigurable scattering patterns. By controlling the states of PIN diodes, the scattering performance of the coding metasurface antenna array can be tuned dynamically without degrading the array radiation property. Using the concept of phase cancellation principle, a 8×8 antenna array was simulated and fabricated. Both simulated and measured results showed the feasibility of the proposed structure [22].

S. Huo, et al in 2022 presented a new method to suppress the electromagnetic radiation between the heatsink and packaging substrate in the system-in-package by using a resistance film absorber. The unit size of the

absorber is $0.14\lambda_L \times 0.14\lambda_L$ and the thickness is $0.049 \lambda_L$. It has an absorptivity of more than 90% in the frequency range of 21 GHz to 55 GHz with polarization insensitivity and angular stability [23]. Moreover, M. S. Patinavalasa, et al in 2022 presented a polarization-insensitive frequency-selective absorber (FSR) with wideband absorption and in-band transmission characteristics. The unit cell of the proposed FSR comprises one lossy and one lossless resonator both printed on FR-4 substrates and segregated by an air spacer. Resistive ink patterns were deposited on the top lossy layer to achieve a wideband absorption, displaying significant improvement over the existing FSR structures. The absorption bandwidths are obtained from 1.31 to 3.22 GHz and 4.88 to 6.69 GHz having fractional bandwidths of 84.32% and 31.28%, respectively [24].

In 2022, M. Abdul Shukoor, S. Dey, and S. K. Koul presented a simple broadband polarization-insensitive circuit analog absorber (CAA) with wide angular stability. It comprised of dual-cut square loop resonator loaded with eight lumped resistors as top patch and an inductive grid [25]. The inductive grid enhances the angular stability of the TM mode. The normal incidence reveals a 90% absorption bandwidth of 20.51 GHz (110% fractional bandwidth) covering the entire X to K-band.

Last, K. R. Jha, Z. A. Pandit Jibrán, and S. K. Sharma in 2022 present an ultrathin absorber for lower microwave frequency applications. The structure was designed using a thin dielectric substrate and a commercially available magnetic sheet superstrate. Due to its low thickness, it is suitable for both planar and conformal applications. For normally incident electromagnetic wave, the measured reflectivity (R) ≤ -10 dB extends from 1.75–3.4 and 1.7–3.36 GHz in the transverse electric (TE) and the transverse magnetic (TM) modes, respectively. The total thickness of the absorber was

$0.023\lambda_L$ where λ_L is the wavelength at the lowest operating frequency, and the structure was bent around a cylindrical base [26].

1.3 Aims of the Dissertation:

The dissertation aims to investigate the methods of radar cross-section (RCS) reduction through:

- 1- Studying the various techniques to reduce the radar cross-section (RCS) of planar surfaces.
- 2- The feasibility of using FSS techniques for RCS.
- 3- Creating and characterizing a sample of the proposed approach according to the desired design by testing different characteristics such as reflection and scattering over the frequency range of interest, which is also relevant to the frequency band of operation.
- 4- Optimizing the loss at the specified frequency using the material available. Because it is difficult to obtain materials with the necessary dielectric and magnetic characteristics to operate as an absorbent at any frequency bandwidth.

1.4 Dissertation Layout:

This dissertation first provides research and then details how to create a frequency-selective surface unit cell to minimize the radar cross section. The study is divided into five chapters. Chapter one presents an introduction and a literature review. The second chapter explains the background of radar cross section and discusses the methods that can be reduced, and chapter three presents the simulation results of the proposed FSS unit cell with copper case and ohmic sheet case to reduce the RCS, while chapter four presents an investigation and a design of FSS unit cell with copper and carbon paste cases. Chapter five gives the conclusions and some suggestions for future work.

CHAPTER TWO
BASICS OF RADAR
CROSS-SECTION
REDUCTION

CHAPTER TWO

BASICS OF RADAR CROSS-SECTION REDUCTION

2.1 Introduction

In many military and civil applications, a certain electromagnetic wave at some frequency is sent toward a region to explore the objects there to search for a certain object that is usually named a target. Therefore, the fraction of the sent power that is reflected back is a vital parameter in determining a reliable detection of the target. The ability of a target to reflect the incident E.M. wave is called the radar cross-section of the target. Radar cross-section (RCS) is defined as the comparison between the intensities of two radar signals. One is the radar beam's intensity when it hits a target, and the other is the strength of the reflected echo sensed by the receiver [3]. The Radar Cross Section is an object-specific number that is affected by many factors related to the shape and size of the object in terms of the wavelength. In practice, the RCS of a target is determined by: the physical geometry and external properties of the target, the direction of the incident wave, and the frequency of operation [27]. The RCS σ of a target is given by the following equation [2].

$$\sigma = \frac{4\pi R^2 S_r}{S_t} \dots\dots\dots(2.1)$$

Where; R = radar range,

S_r = Scattered power density (W/m^2)

S_t = Power density intercepted by target (W/m^2)

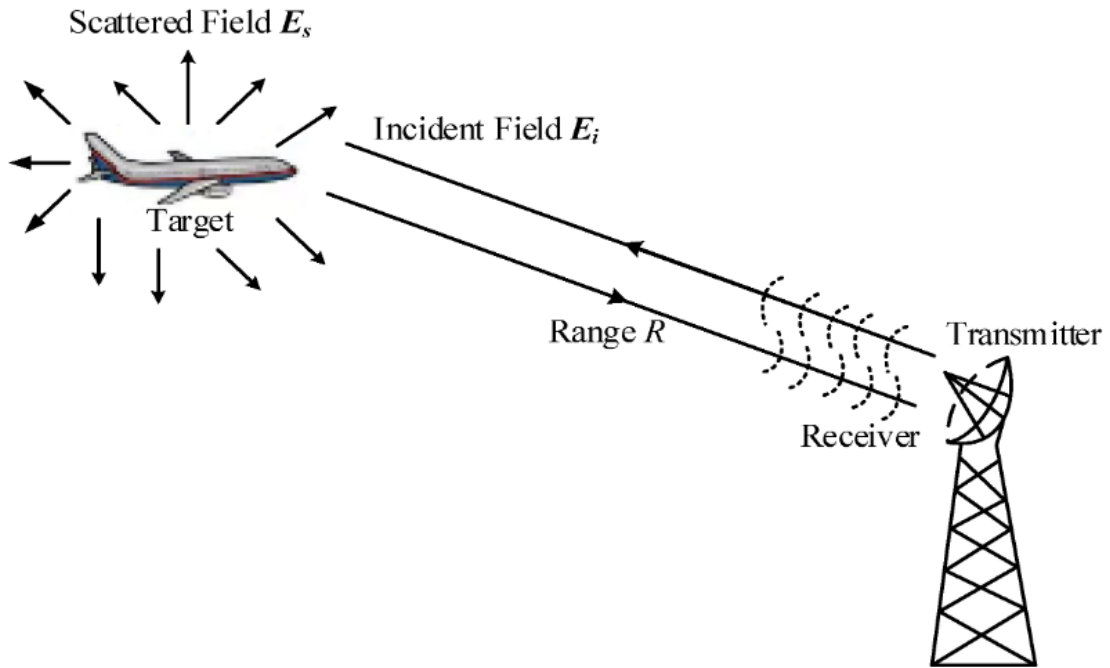


Figure 2.1 Radar Cross-Section notion [28].

As seen in Fig. 2.1 RCS concept represents the ratio between the power density due to the incident wave and total waves under the isotropic scattering situation. The definition of conventional RCS can be given as:

$$\sigma = \lim_{R \rightarrow \infty} 4\pi R^2 \frac{|E_s|^2}{|E_i|^2} \dots\dots\dots(2.2)$$

Where:

E_s (V/m) is the scattered electric field at the receiving antenna.

E_i (V/m) is the incident electric field.

2.2 Radar Cross-Section Reduction Concepts

Since World War II, the idea of the technology of stealth has been a challenging objective in various military applications and a topic that has raised increasing interest. The radar can detect a certain target only if the received backscattered signal is detectable. Building on this, various methods were proposed to reduce the RCS in [29], by either redirecting the wave that was reflected back away from the receiver or absorbing the incident wave by

the target. The various methods that were proposed for RCS reduction are discussed in the following sections.

2.2.1 Absorption

In the absorption process, part of the energy of the incident wave is transferred to the target. The energy transmitted by the radar antenna can be absorbed by one or more of several loss mechanisms, which are related to the dielectric or magnetic characteristics of the material of the target or a certain coating applied to the target. The lost E.M. energy is actually converted into heat that is too small to elevate the temperature of the target [3].

2.2.2 Scattering

Scattering is redirecting the incident energy on the objects to other directions away from the radar or the source of the electromagnetic energy so that less signal will be reflected to the radar receiver.

2.3 Classification of RCS Reduction Methods

There are a lot of techniques that have been proposed to achieve a desirable reduction in the RCS of the target [29]. These methods can be categorized into two main groups. Active RCSR, and Passive RCSR according to the method of reducing the RCS [30]. Figure (2.2) shows a flow chart of the RCS reduction techniques.

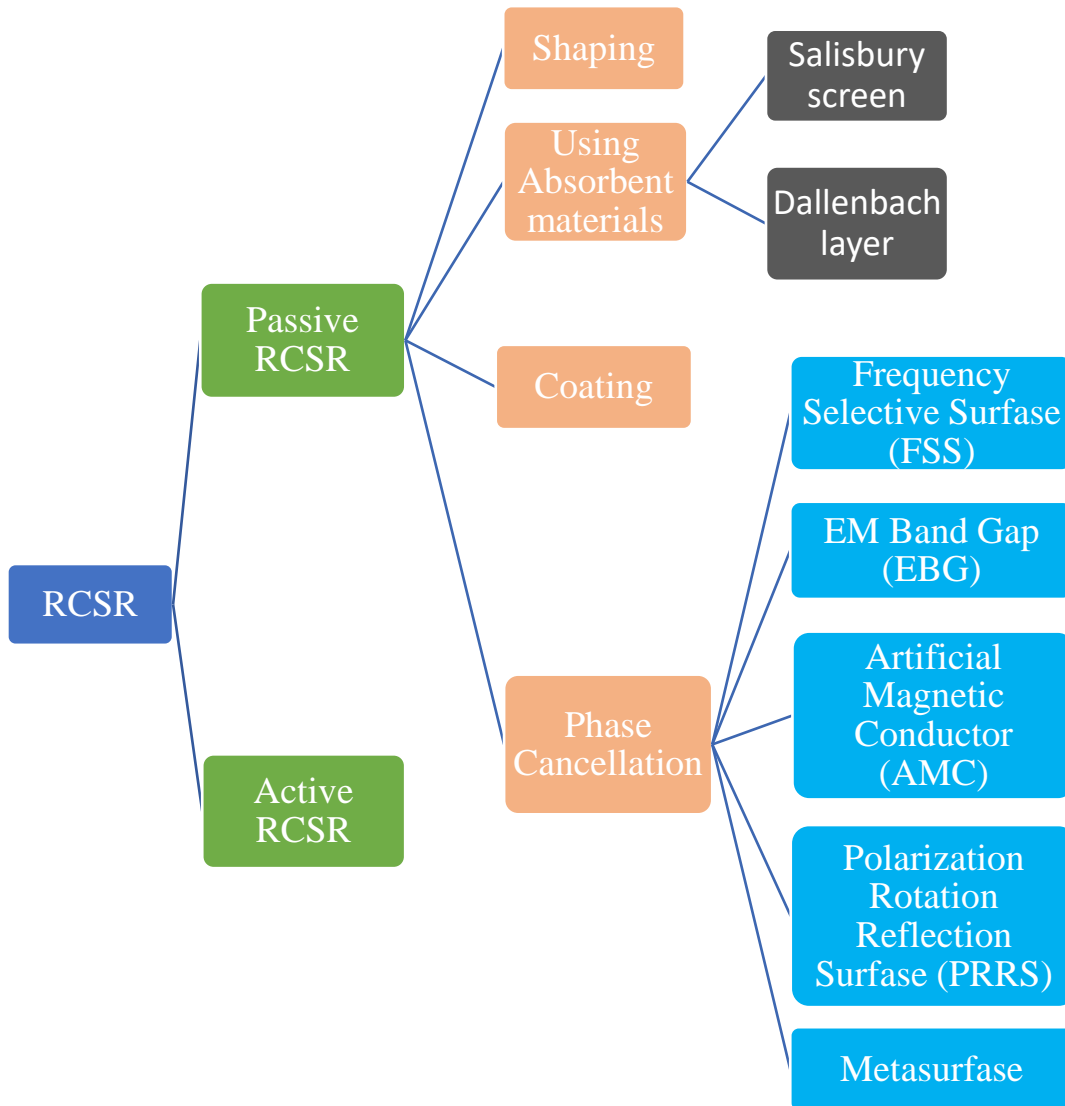


Figure 2.2 Classification of the RCS reduction techniques.

2.3.1 Active Radar Cross-Section Reduction

The concept behind the active RCS reduction is to minimize or control the energy received by the radar receiver. The target must have the means to detect and determine the various parameters of the incident wave such as the frequency, amplitude, phase, and angle of arrival. Then the target must radiate in synchronise with the incident pulse another pulse whose amplitude and phase are tailored to cancel the incident one so that the reflected energy is minimized [31-33]. In active RCSR or active cancellation, the target should

have the capability to transmit a signal which is similar to the echo of the radar but phase-shifted by 180° , so that it tries to cancel the actual reflected signal, and thus the radar detects no returns at all. This method uses very low power as compared to the conventional Electronic Warfare, which uses jamming by high power, and gives no idea about the target's presence [3]. In contrast to this advantage, this method requires very fast processing and complex circuits.

The active RCS reduction depends on the system parameters of the radar phased array, such as element size, inter-element spacing, load impedance, feed network, and the E.M. environment [34]. The active cancellation method can be considered as the most suitable for low-frequency RCSR applications, where using absorbers and employing shaping are difficult.

2.3.2 Passive Radar Cross-Section Reduction

The techniques of passive cancellation rely on loading the target with certain elements such as slots, rings, or dipoles to reduce the overall RCS. These techniques can be difficult to deploy practically and are limited in bandwidth [33]. In this method of cancellation, the basic idea is to add a reflecting element whose phase and amplitude can be adjusted to cancel the echo of the original target. This method is sometimes called impedance loading [35].

As seen in Fig 2.2, the passive RCSR methods follow three main approaches to reduce the scattered wave in the direction of the radar receiver. These ways are target shaping [36], using absorbent materials[37], and coating[38]. Apart from the above-mentioned passive techniques, other methods such as the use of artificial magnetic conductors (AMC) [39], frequency selective surfaces (FSS)[19][3], Electromagnetic Band Gap (EBG) [40-41], polarization rotation reflection surface (PRRS)[6][42][43], and

metasurface [44-45] all these methods fall within phase cancellation or destructive interference.

2.4 Techniques of RCS Reduction

In the last few decades, there have been tremendous efforts to reduce the radar cross-section of various objects ranging from airplanes to rockets, projectiles, and even antennas. Researchers have followed many procedures and proposed various methods aiming to reduce the radar cross-section. The proposed techniques differ from one application to the other, as well as the desired range of frequencies. The various adopted methods showed different performances, complexity, and cost. In the following sub-sections, various methods for RCS reduction are discussed.

2.4.1 Shaping

Target shaping can be considered as a special selection of target surface shapes that lead to minimize the reflected wave to the radar, by redirecting the scattered energy away from the direction of incidence. Shaping is a high-frequency technique that aims to design the geometrical shape of the target such that the backscattered wave from it in the radar direction is minimized [3]. The two distinct methods of shaping that were explained in [46], to minimize the target RCS are either implementing a compact, smooth, blended external geometry or using a faceted design to lessen reflections returning to the radar.

The process of shaping utilizes some angular sectors over which low radar cross section is less important compared to others [47]. In general, a forward cone is of primary interest for RCS reduction, hence, normally it is preferred to "shift" large cross sections out of the forward sector and toward the broadside.

2.4.2 Absorbing Materials

The radar absorber's objective is to absorb a certain fraction of the power in the incident wave and thus reduce the reflected wave to the radar receiver [1]. Also, the coating is considered as branch of absorbing technics by placing a layer on the object whose properties cause the reflected wave to be redirected or the incident wave is absorbed and thus the RCS is reduced. In order to obtain the stealth effect, Radar Absorbing Materials (RAM) are usually used to coat the surfaces of aircrafts, reducing their Radar Cross-Sections (RCS) [48].

There are two main methods for reducing the reflections from an object: absorption and cancellation, the energy transfer from the wave to the substance as it travels through is known as absorption [35]. Radar radiation is absorbed by one or more loss processes, which is related to the material's dielectric or magnetic characteristics.

In general, absorbers do not have to absorb enough energy to raise their temperature, since the incident radar energy is small [3]. The role of the radar absorption material design is to provide a layer (or layers) with a small thickness, and minimum reflection coefficient, across the desired frequency range, while being cheap, lightweight, and long lasting. Such layer or layers are called Radar Absorbing Material (RAM) [49]. The two earliest and most fundamental types of absorbers (Dallenbach layers and Salisbury screens) are described in the following:

Salisbury Screen

This type of absorber is made by laying a resistive sheet on top of the surface of the object so that it creates a resonant absorber. The covered conducting object forms a transmission line section that is short-circuited at the object side. If the thickness of the resistive sheet is a quarter-wavelength,

then it converts the conductor plate short circuit to an open circuit [50]. Figure (2.3) shows the diagram and transmission line equivalent circuit of the Salisbury screen.

$$\frac{1}{Z_{in}} = \frac{1}{R_s} + \frac{1}{\infty} = \frac{1}{R_s} \dots\dots\dots (2.3)$$

The reflection coefficient tends to be zero when $R_s=377\Omega$. When the line is quarter-wavelength, then a matched load is provided and there will be no reflection. Therefore, the Salisbury screen is most the effective RCS reduction method at normal incidence. However, at oblique incidence onto the absorber, the reflection coefficients magnitude for the parallel and perpendicular polarizations are expressed in terms of θ ,

$$|\Gamma_{\perp}| \simeq |\Gamma_{\parallel}| = \frac{1-\cos\theta}{1+\cos\theta} \dots\dots\dots (2.4)$$

In Fig.2.4, Equation (2.4) is displayed for angles up to 35° in Fig. (2.4), where θ is the off-normal angle. Performance is greater than 20 dB when the reflection coefficient is less than 0.1 [49].



Figure 2.3 (a) Diagram of the Salisbury screen (b) transmission line equivalent circuit [35].

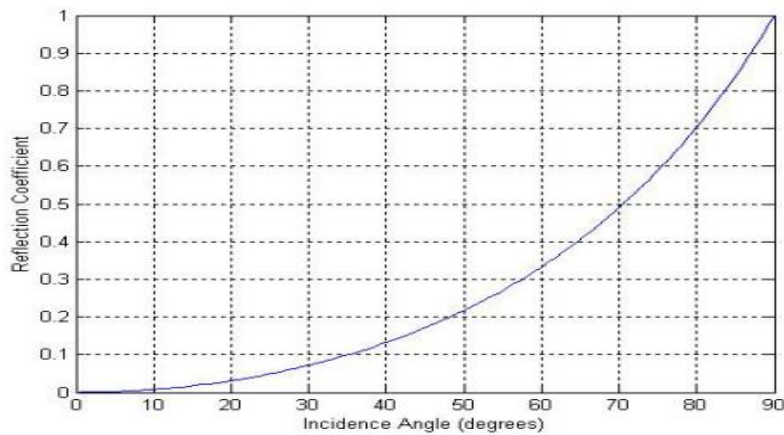


Figure 2.4: Variation of the reflection coefficient as a function of incidence angle [49].

Dallenbach Layer

The Dallenbach layer is formed of a layer of homogeneous lossy material that is backed by a metallic plate (the object). In this arrangement, the rear surface's reflection is cancelled out by the reflection from the outside surface (the metallic object). The lossy material is a blend of compounds designed to have a specified permittivity and permeability [51]. Figure 2.5 shows the geometry of the RCS reduction method, and a transmission line equivalent circuit of the Dallenbach layer. The reflection coefficient at the outer surface can be given by [35]:

$$\Gamma = \frac{Z_{in} - Z_0}{Z_{in} + Z_0} \dots\dots\dots (2.5)$$

Where,

$$Z_{in} = \frac{Z_{load} + jZ_0 \tanh(\gamma t)}{Z_0 + jZ_{load} \tanh(\gamma t)} \dots\dots\dots (2.6)$$

Where γ is the complex propagation constant.

$$\gamma = \alpha + j\omega\sqrt{\mu\varepsilon} \dots\dots\dots (2.7)$$

The Dallenbach Layer design usually includes lossy magnetic materials as well as carbon particles responsible for ohmic losses. Consequently, the

permeability and permittivity will have imaginary parts, leading in a complex index of refraction. The resulting propagation constant will have a real part that attenuates the wave passing through the material [51]. Figure 2.6 shows the variation of the reflection coefficient with the thickness of the layer for two values of permeability and permittivity [35]. The thickness of the layer should be as small as possible to reduce the size and weight of the added coating.

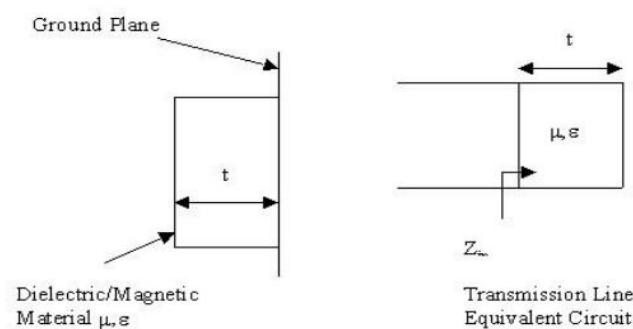


Figure 2.5 Dallenbach layer [35].

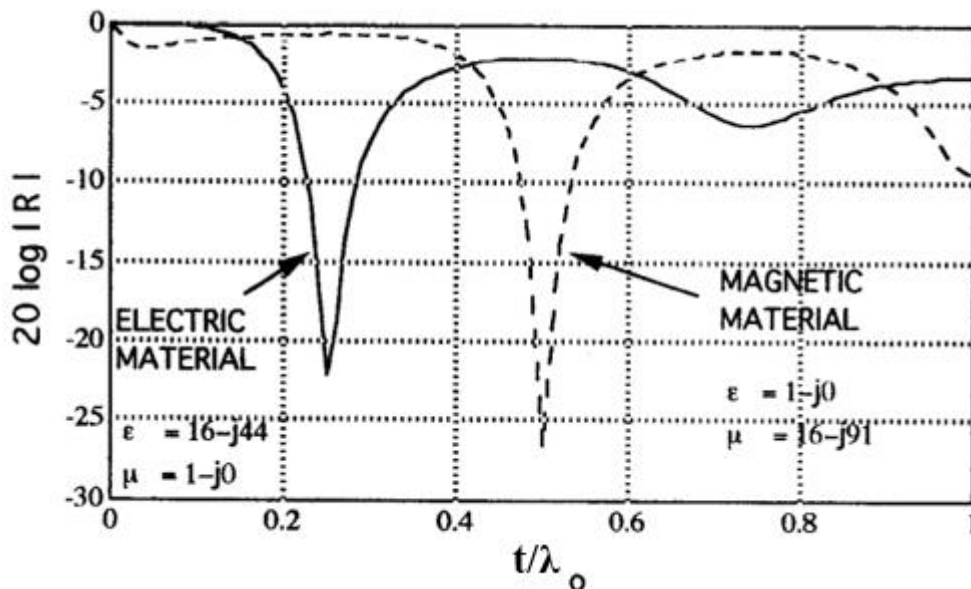


Figure 2.6. Performance of the Dallenbach Layers [35].

2.4.3 Frequency-Selective Surface (FSS)

A frequency-selective surface (FSS) is a periodic structure consisting of elements arranged in a two-dimensional layout, as shown in Fig.2.7 which

shows the most prevalent shapes of the FSS, including dipole, square and circular patches, cross-dipole, square loop, Jerusalem cross, and ring (or square aperture, circular loop, etc.). Such configuration exhibits reflection and transmission properties that vary with the frequency of the incident wave, in a similar manner to the filters in the conventional (RF) circuits. A periodic array of slots in a perfectly conducting plane behave like a bandpass filter, as they pass waves when the slots resonate while rejecting the passage of waves at other frequency bands. On the other hand, an array of conducting patches works as a band-reject filter, by reflecting waves at the resonant frequency of the patch but passing waves at other frequencies. Thus, the filtering behavior of an FSS made of patch elements and aperture FSS are perfectly complementary to each other due to these filtering properties, there are two main uses of the FSS. The first one is in reflector antennas, where FSS reflectors are employed to isolate the feeders of various bands. The second use is to use FSS as antenna radomes for flexible control of the transmitted and reflected E.M. waves [52-54]. As the FSS can be designed such that it has a small reflection coefficient, then the FSS can readily offer RCS reduction.

2.4.3.1 FSS used as reflectors

The FSS are usually used for selecting or filtering out E.M. waves at certain frequencies [53], [55], [56]. With this spatial filtering property, the FSS have been used to increase the operating bands of reflector antennas [57]. With the employment of proper FSS, the number of feeders in the reflector antenna is increased, and thus the number of operating bands can be increased. It was demonstrated that the transmission-line equivalent circuit can be utilized in the design of the FSS.

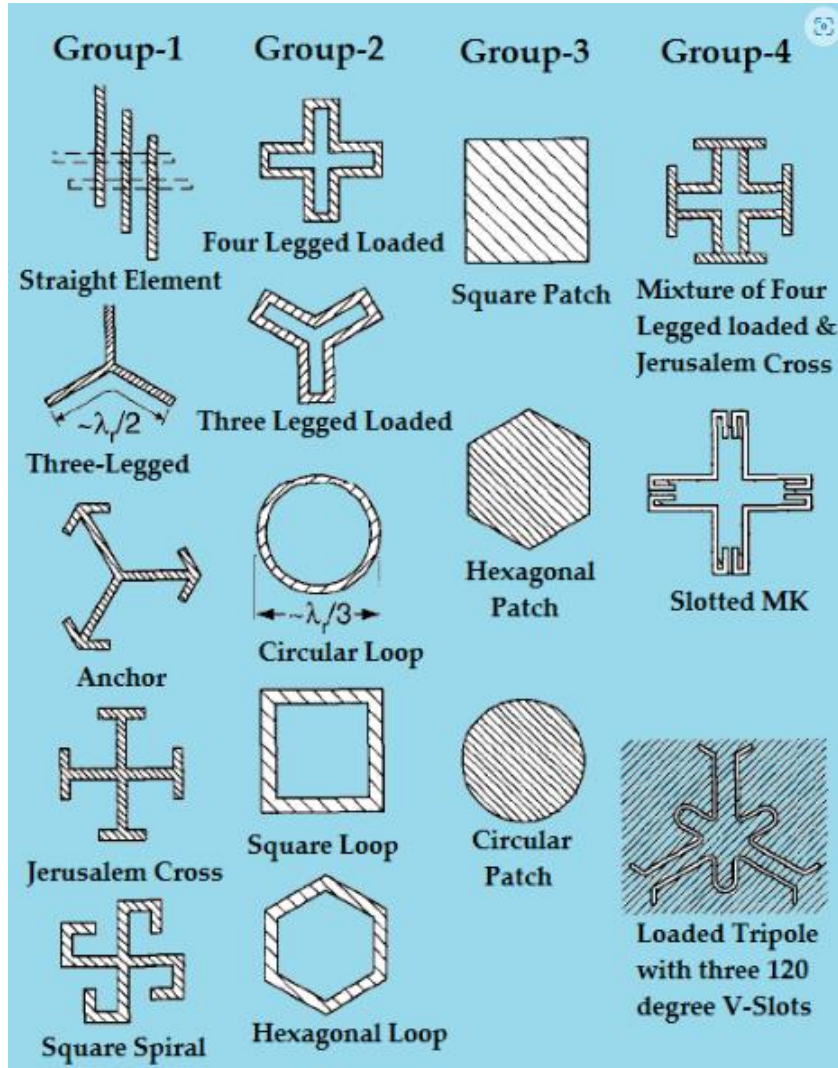


Figure 2.7 Some typical FSS element shapes [53].

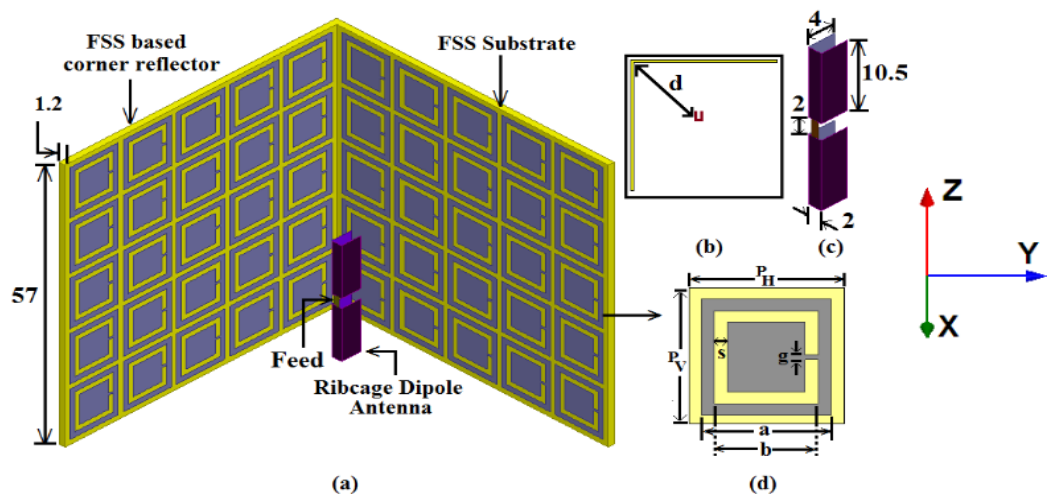


Fig. 2.8 (a) Dipole antenna with the FSS reflectors (b) Top view. (c) Ribcage dipole antenna (d) the FSS unit cell [58].

2.4.3.2 FSS used as antenna radomes

In many circumstances, the antenna is shielded from wind, rain, sunlight, rays, ice, and high temperatures by a Radome (derived from Radar+Dome). Radomes are also used in airplanes and missiles. The radome can be considered as a spatial filter that passes the wanted range of frequencies, while at the same time it should have a low RCS. The E.M. performance characteristics of radomes have been developed utilizing a variety of methodologies and techniques, including resonant, anisotropic constructions, metamaterials, and frequency selective services (FSS). One design example for the radome can be found in [59], as shown in Fig. (2.9).

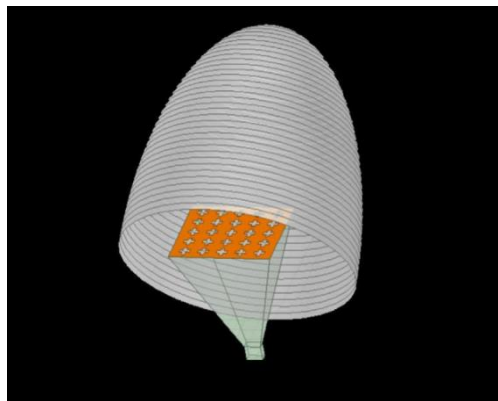


Figure 2.9: FSS-antenna-radome system [59].

2.4.4 Artificial Magnetic Conductors (AMC)

An Artificial Magnetic Conductor (AMC) is a type of metamaterial that is used in several antennas and microwave design applications. Figure 2.10 shows a typical design for a surface that offers metamaterial characteristics, among them zero or negative values of the equivalent permittivity and permeability. By careful deployment of the unique properties of the metamaterials, the performance of many microwave devices can be improved [60]. The AMC is a metamaterial that tries to mimic the properties of a perfect magnetic conductor (PMC). The useful property of the PMC that is mimicked

by AMC is its ability to offer zero-degree reflection phases at the resonance frequency [61]. Zero or minimum reflection coefficient means very small RCS values. The RCS can be reduced using AMC technology where the RCS of Perfect Electric conductor PEC (original object) is reduced by the addition of an AMC. Since the PEC surface has a reflection phase of 180° , then to satisfy the condition of phase cancellation a reflection phase of 0° is required for the added metasurface to reduce the RCS. For example, in Fig. 2.11, the reflection phase response of additional RCS reduction, AMC metasurface is shown which has a reflection phase of 0° at 10 GHz.

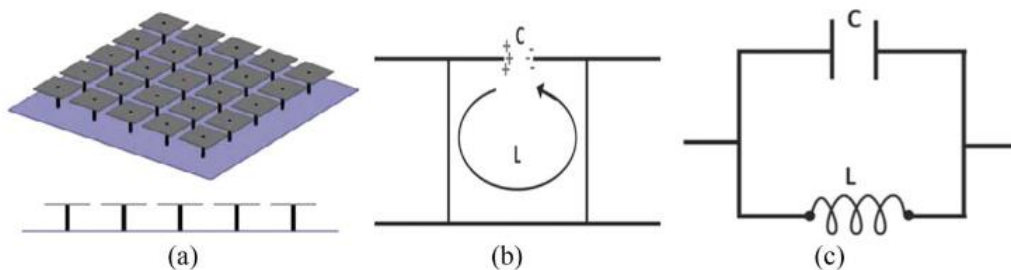


Figure 2.10 (a) An AMC formed of an array of unit cells. Each via is connected to the ground plane, (b) the equivalent LC circuit, and (c) the corresponding model [62].

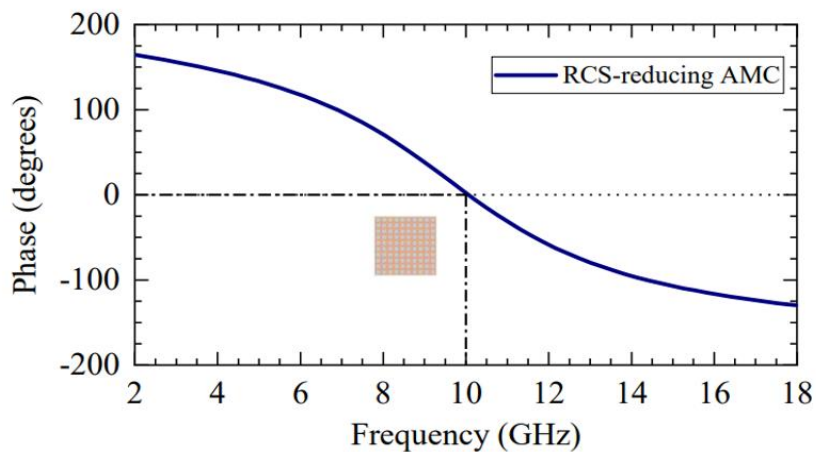


Figure 2.11: Reflection Phase of RCS-Reducing AMC[63].

2.4.5 Electromagnetic Band Gap (EBG)

This type of structure is synthesized from an array of elements so that it offers unique characteristics [64-65]. They were widely employed in antenna designs due to their in-phase reflection coefficients across certain frequencies. The reflection coefficient phase of the EBG surface varies smoothly between $+180^\circ$ and -180° with the frequency of the incident wave. The EBG structure is often called an artificial magnetic conductor (AMC) when the reflection phase is between $\pm 90^\circ$ [66], and this property leads to using the AMC instead of a PEC ground plane [67].

The (EBG) structures have favorable electromagnetic properties such as their phase response with frequency [40]. When combining two structures of a perfect electric conductor (PEC) and an EBG as a single unit, then the reflected wave from the unit will be altered due to the characteristics of EBG structures. The reflected fields are cancelled along the principal planes as the PEC and EBG structures have opposite phases at the resonant frequency. A square checkerboard surface can be designed to achieve destructive and constructive scattering patterns simultaneously leading to a reduction in the level of the scattered fields toward the observer, or a reduction in (RCS) of the target [10]. Figure (2.12) shows the square patch structure of EBG.

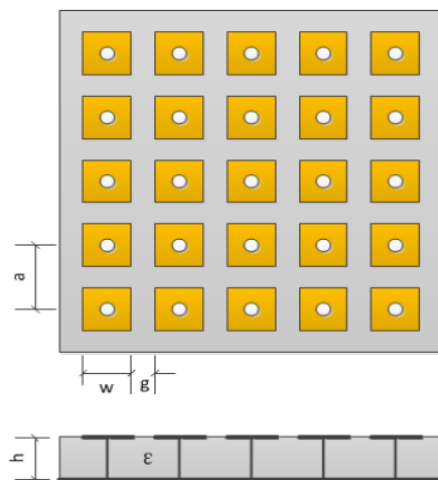


Figure 2.12: EBG structure with square patch [68].

2.4.6 Polarization Rotation Reflecting Surface (PRRS)

Polarization is a basic property of E.M. waves, defined as “the direction that an electric field is oscillating in perpendicular to the direction of propagation” [69]. Some surfaces change the direction of polarization of the wave passing through them, and thus they are called polarization rotators. The polarization rotators are classified into two types: transmission and reflection, when these rotators and reflectors are combined, they form a single component known as polarization rotating reflective surfaces (PRRS). RCSR is one of the important applications of PRRS. The PRRS structure employed in this application may reflect the incoming wave with a 90-degree polarization rotation.

A sample unit cell of PRRS structure is shown in Fig.2.13-a which shows the reflector as a square patch in the center and the rotators as at the corners of the unit cell. Unlike the AMC/EBG/FSS designs in which many types of unit cells are used for RCSR [70], only one type of PRRS unit cell is used in this method to form a checkerboard structure for the reduction of the RCS.

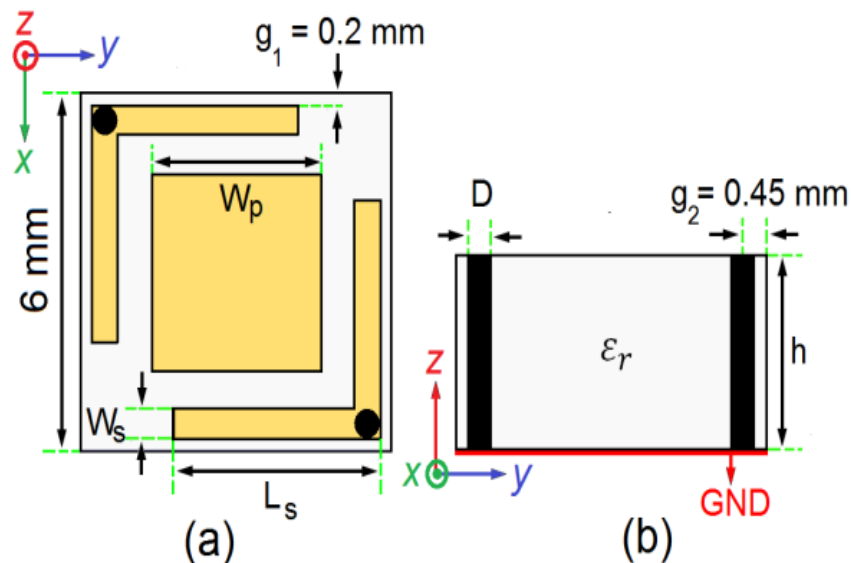


Figure 2.13: The PRRS unit cell design (a) top view (b) Side view [71].

2.4.7 Metasurface

The metasurface is a 2D metamaterial structure typically made of inhomogeneous arrays of subwavelength elements [72], and they have been extensively used for radar cross-section reduction in the past decade. Diffusion metasurfaces have been used to backscatter energy randomly in many directions. Such metasurfaces have been prepared by assembling meta-particles with various sizes and/or orientations so that a broadband and wide-angle RCSR can be obtained. The diffusion metasurfaces [73-74] can be categorized into different groups realizing and focusing on some interesting functions and applications of them, such as polarization conversion metasurfaces [75-76] checkerboard metasurfaces based on phase cancelation [77-78] coding and digital metasurfaces, [45], [79-80] phase gradient metasurfaces [81], and hybrid metasurfaces [82]. Figure 2.14 shows schematics of metasurface comprised of 10×10 subarrays. The subarrays have been randomly organized to acquire a random backscattering pattern. Each subarray become set as 3×3 meta-atoms.

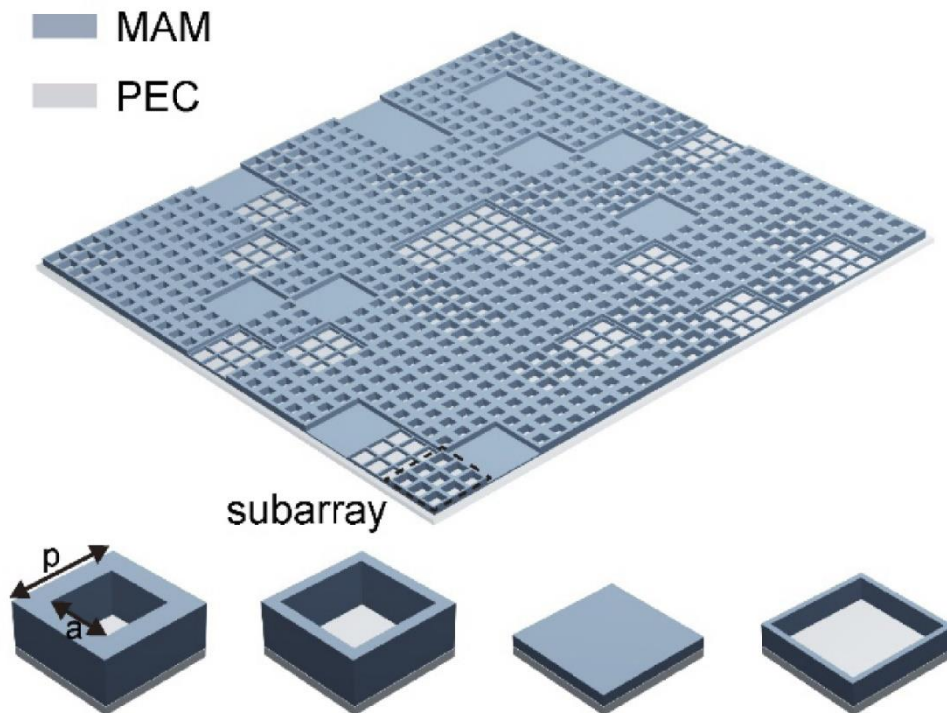


Figure 2.14: Schematics of an absorptive array metasurface [83].

2.4.8 Opposite Phase Cancellation (OPC)

The last method is opposite phase cancellation (OPC). It was widely employed in many disciplines of optics, electromagnetics, and acoustics as an efficient means of suppressing vector fields [84]-[87]. Opposite phase cancellation (OPC) is a conventional approach for reducing RCS. The fundamental concept is to take use of the cancelling effects caused by the well-known 180° phase difference between the matching reflection coefficients. Because the direction and frequency of incident wave is unpredictable in practice, stealth technology relies heavily on bandwidth and oblique incidence performance.

In 2007, Paquay et al. proposed a RCS reduction method that uses planar structure. It supported a mix of artificial magnetic conductors (AMC) and perfect electrical conductors (PEC) in a checkerboard-like configuration, [88] as shown in Fig. 2.15. The backscattered field is effectively canceled by rerouting it to various angles. However, the slender reflection phase of the AMC restricts the RCS reduction frequency range. In [89], An outline of a planar monolayer chessboard is presented as a broadband RCS reduction AMC technology. Fragmentary bandwidth (FBW) of quite 40% is acquired by a monostatic RCS reduction greater than 10 dB. These rectangular board surfaces of periodic phase arrangement produce four scattering beams and bistatic RCS reduction of concerning 8.1 dB [88]– [91].

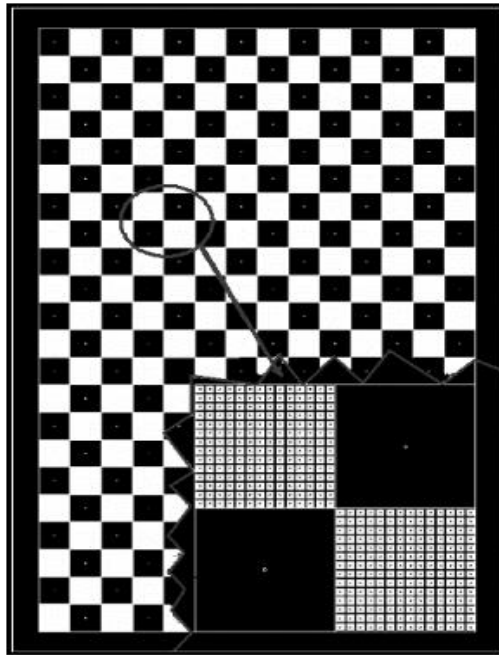


Figure 2.15. Chessboard structure. The black squares represent the PEC elements and the white squares the AMC elements. The inset shows the unit cell [88].

Balanis et al, in 2015 suggested the use of a hexagonal checkerboard surface with periodicity phase arrangement [92] as shown in Fig. 2.16, which offered a 10-dB RCS reduction bandwidth of around 61%. This can form six bistatic RCS lobes, resulting in additional bistatic RCS reduction. A chessboard AMC surface made up of saltire arrow and four-E-shaped unit cells offers an 85 % bandwidth for a 10 dB RCS reduction [93]. subsequently supplied in the dual wideband checkerboard surfaces [94], and showed a 10 dB RCS reduction in the frequency bands of 3.94-7.40 GHz and 8.41-10.72 GHz. They employed two dual-band electromagnetic bandgap (EBG) structures.

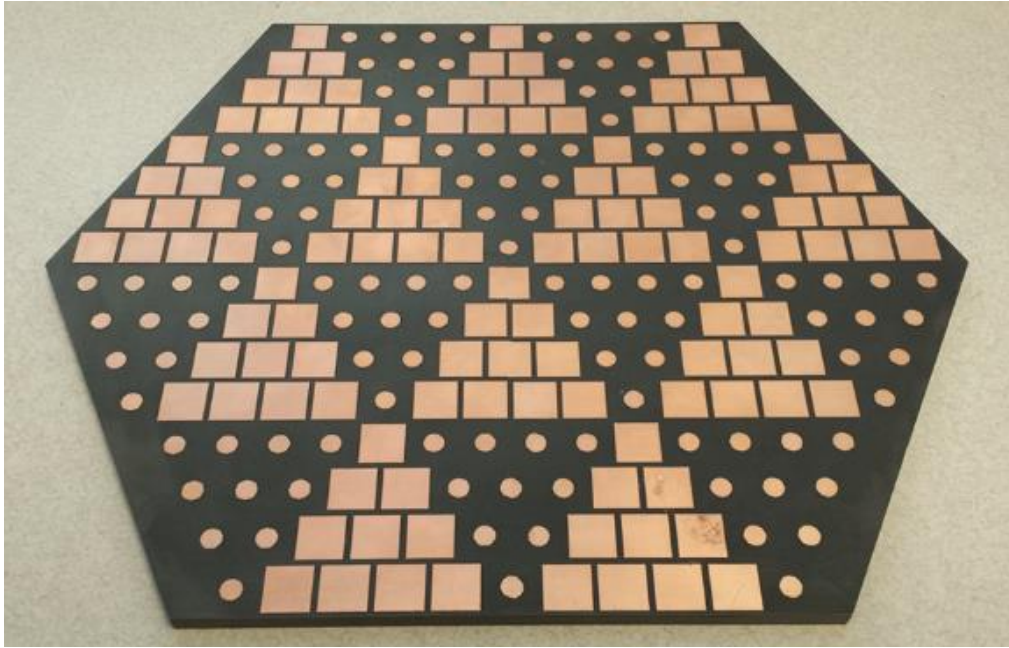


Figure 2.16. The fabricated hexagonal checkerboard ground plane combining EBG1 and EBG2 structures [92].

CHAPTER THREE

RADAR CROSS-SECTION

REDUCTION USING FSS

WITH CONDUCTIVE

UNIT CELLS

CHAPTER THREE

RADAR CROSS-SECTION REDUCTION USING FSS WITH CONDUCTIVE UNIT CELLS

3.1 Introduction

This section investigates the use of Frequency-Selective Surfaces FSS for the reduction of the radar cross-section of objects. The objects whose radar cross-section is to be reduced are in general conductive ones. The frequency of the radio waves used depends on the radar applications. Radar systems are often designated by the wavelength or frequency band in which they operate and it ranges from (0.3-100) GHz in this dissertation focused on the range of s band (2-4) GHz. Therefore, the FSS surfaces suitable for the cross-section reduction of these objects should have a conductive ground plane. Thus, the aim of this chapter is to design FSS unit cells that can offer a small reflection coefficient so that it can be utilized in reducing the radar cross-section. The CST Microwave Studio was used in the simulations.

3.2 Design of the FSS Unit Cell

In this chapter, the absorbing properties of various designs for FSS unit cells are investigated. The approach is to use the single ring design and also double ring design to obtain wide band property while keeping the FSS thickness at minimal without any air spacing between the resonating rings and the ground plane. Various designs are investigated to merge the two bands due to the two rings into a single wideband. This chapter is organized as follow, subsection (3.3.1) presents the basic design of the single ring FSS unit cell with various size of ring, subsection (3.3.2) presents the basic design of the double ring FSS unit cell with various size of the inner ring, while subsection (3.3.3) aims to meander the inner ring to obtain longer circumference approaching that of the outer ring. Subsection (3.3.4) investigates another

approach by using an opened inner ring to reduce the frequency of the second band. The characteristics of the three proposed designs are compared in subsection (3.3.5).

3.3 Copper Unit Cell

The proposed FSS unit cells in this section include the ground plane made of copper and a ring also made of copper printed on one side of the FR-4 substrate, for all the investigated designs (single ring, double rings, meander ring, and open ring).

3.3.1 Single Square Ring

The simulations started with a single square ring as shown in Fig. 3.1. The unit cell includes a ground plane of copper, Fr-4 substrate with relative permittivity $\epsilon_r=4.3$, substrate thickness $h=1.6$ mm and copper thickness of the ground plane and the ring is 0.035 mm. With a single ring of copper, the unit cell dimensions $L=19\text{mm}\times 19\text{mm}$, the outer side length of ring $L_1 = 15.6$ mm, and width of the ring $W=2\text{mm}$ were chosen. The inner side length of ring $L_2 = L_1 - 2 \times w = 11.6$ mm. Figure 3.1 also shows the direction of the electric field of the incident wave.

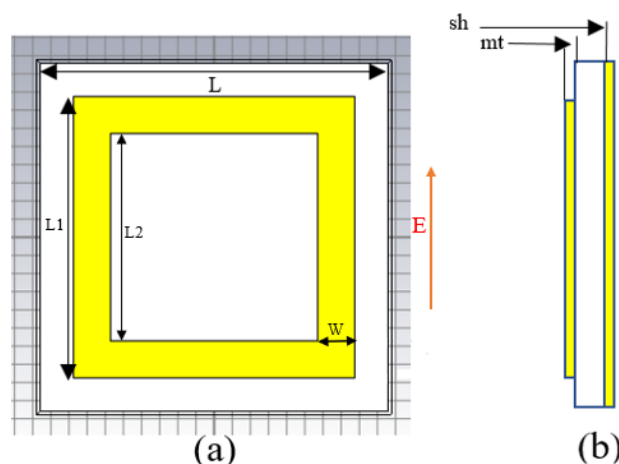


Figure 3.1 The FSS unit cell geometry of single ring (a) "front view" (b) "side view".

To measure the reflection coefficient of the proposed unit cell in the CST Microwave Studio a linear polarization using waveguide port to simulate the normally incident wave (toward the negative direction of z-axis or w-axis) is used. Fig. 3.2 shows the unit cell with waveguide port that was used in the simulation.

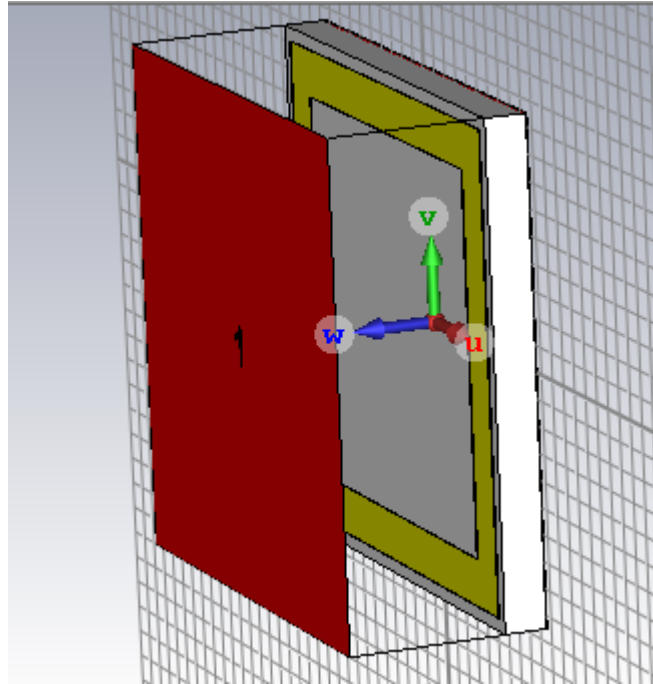


Figure 3.2 The unit cell with waveguide port for simulation using the CST Microwave studio.

The most important factors connected to the unit cell and its relation to the resonant frequency and average circumference can be calculated from the following equations where

$$\lambda_e = \frac{\lambda_0}{\sqrt{\epsilon_{eff}}} \dots\dots\dots(3.1)$$

Where λ_0 is the wavelength in air, and ϵ_{eff} is the effective relative dielectric constant of the FR-4 substrate that is given by [95]:

$$\epsilon_{eff} = \frac{\epsilon_r + 1}{2} + \frac{\epsilon_r - 1}{2} \left(1 + 12 \frac{h1}{w}\right)^{-0.5} \dots\dots\dots(3.2)$$

When ϵ_r is the relative dielectric constant, (h1) or is substrate height, and W = ring width. The wavelength λ_0 is given by:

$$\lambda_o = c/f \dots\dots\dots(3.3)$$

When c is the speed of light, and f is resonance frequency.

From the geometry of Fig.1, the average circumference of the outer ring are given by

$$CR_{av} = 4(L1-W) \dots\dots\dots(3.4)$$

The ring resonates at frequencies when its average circumference is equal to the effective wavelength as given below

$$CR_{av} = \lambda_e \dots\dots\dots(3.5)$$

$$\text{the average circumference of the ring} = 4 * \frac{(L1+L2)}{2} \dots\dots\dots(3.6)$$

$$= 4*(L1-w) = 4*(L2+w)$$

The results of the simulations for the reflection coefficient (S_{11}) of the single ring FSS is illustrated in Fig. 3.3, for various of the ring side length L1.

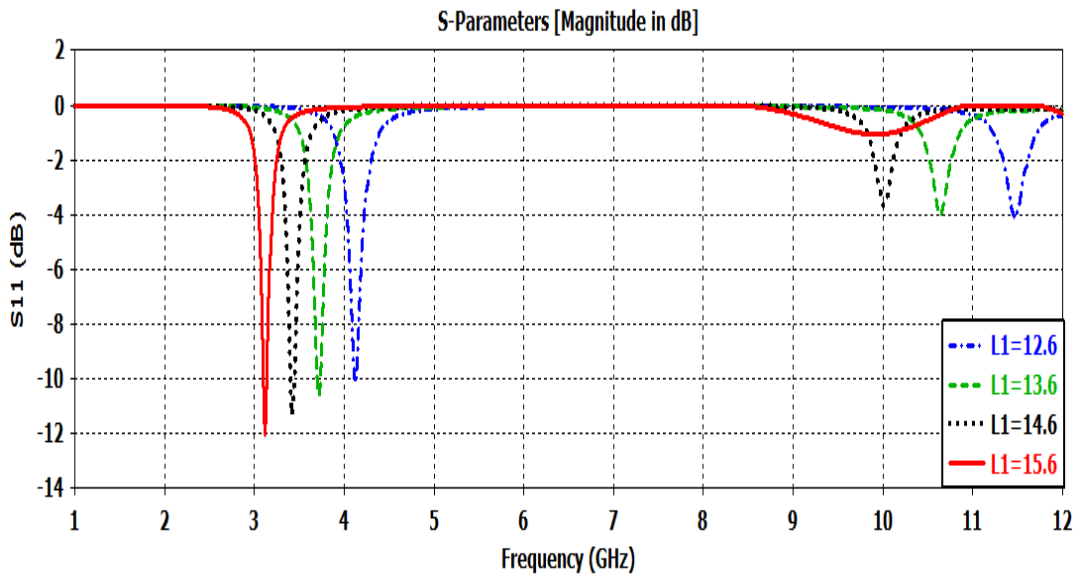


Figure 3.3 The reflection coefficient (S_{11}) of the single ring FSS.

From Fig.3.2, it can be seen that the minimum value of reflection coefficient S_{11} is -12 dB occurs at about 3.2 GHz and the bandwidth is (39 MHz) and by decreasing the ring side length the resonance frequency will increase.

Table (3.1) shows the results of using various values for inner ring side length. The right column of the Table shows the calculated ratio of the ring circumference to the effective wavelength at the resonance frequency (the frequency at which S_{11} is minimum). It can be seen that this ratio is always unity, indicating that at resonance the wavelength is equal to the average circumference of the ring, as predicted by Eq. 3.5.

Table 3.1: The simulations of the single ring FSS with various ring length with $\epsilon_e=3.1568$.

case	L mm	W mm	Freq GHz	λ_o mm	λ_e mm	S11 dB	Circumference/ λ_e
Case1	15.6	2	3.122	96.1	54	-12.04	1.007
Case2	14.6	2	3.42	87.7	49.36	-11.3	1.02
Case3	13.6	2	3.72	80.65	45.39	-10.6	1.02
Case4	12.6	2	4.122	72.78	40.96	-10.15	1.035

The surface current distribution on the square ring at the frequency of 3.2 GHz is illustrated in Fig.3.4, when the ring side length is equal to 15.6 mm. The current variation shows two peaks and two nulls indicating a complete one cycle along the ring circumference. This is a spatial verification of the relation predicted by Eq. 3.5.

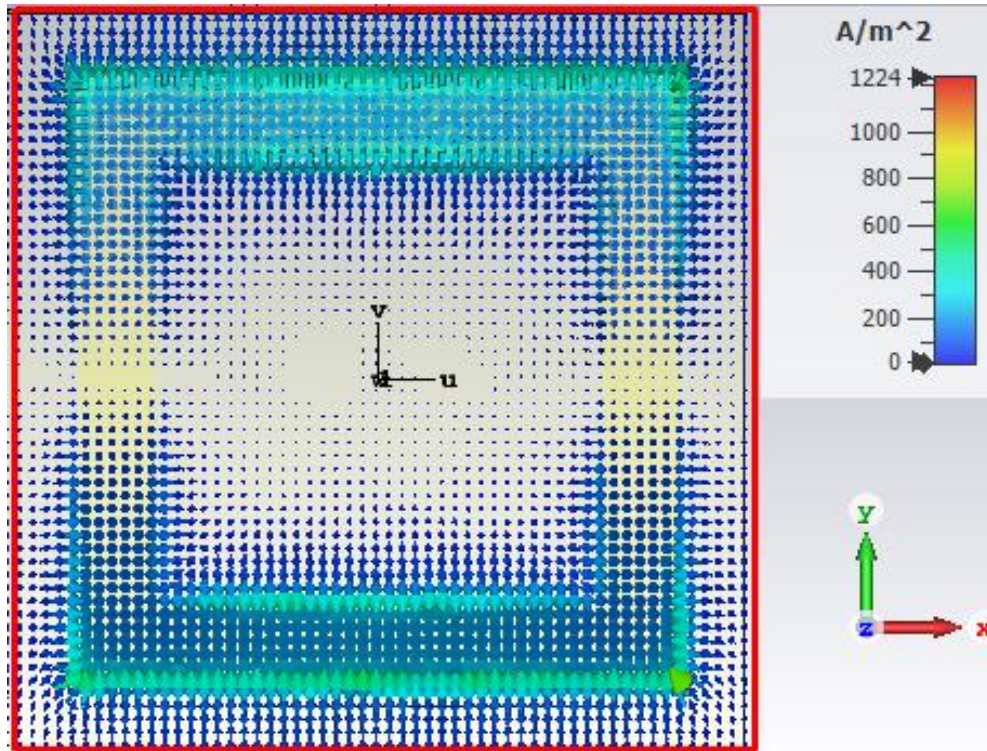


Figure 3.4 The surface current distribution on a single square ring at 3.2 GHz frequency.

3.3.2 Double Square Closed Ring

The square shape is used as it offers similar responses to the incident vertical and horizontal polarizations, as well as more stability for the incidence angles [96]. To increase the bandwidth of the absorber, it was suggested to use another ring of a smaller size so that the obtained two bands can be joined together to obtain a wider band. Figure 3.5 shows the proposed Unit cell, where the FR-4 substrate with relative permittivity $\epsilon_r=4.3$, thickness of $h=1.6$ mm and copper thickness of 0.035 mm is used. The unit cell dimensions $L=19\text{mm}\times 19\text{mm}$, outer ring side length $L_1=15.6$ mm, and width of ring $W=2\text{mm}$, and the inner ring size $L_2=0.65*L_1=10.14\text{mm}$.

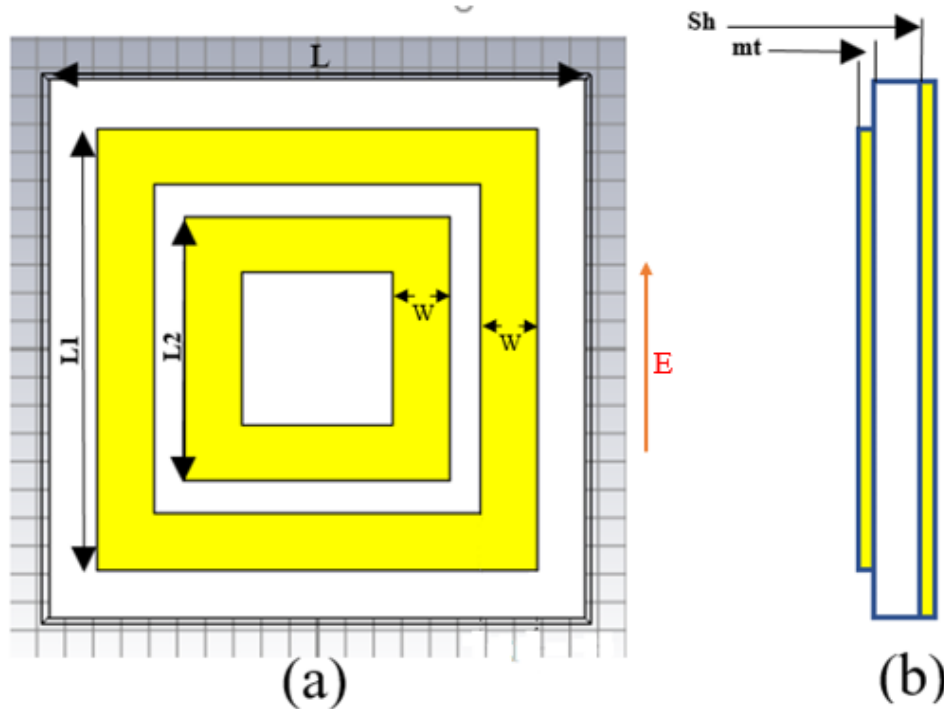


Figure 3.5 Double ring unit cell geometry (a) "front view" (b) "side view".

The results of the simulations for the reflection coefficient (S_{11}) of the double ring unit cell is illustrated in Fig. 3.6, which show that there are two bands of low reflection, the first at about 3.2 GHz, while the frequency of the second band at 5.5 GHz, each ring of the unit cell is responsible for one of the low reflection band.

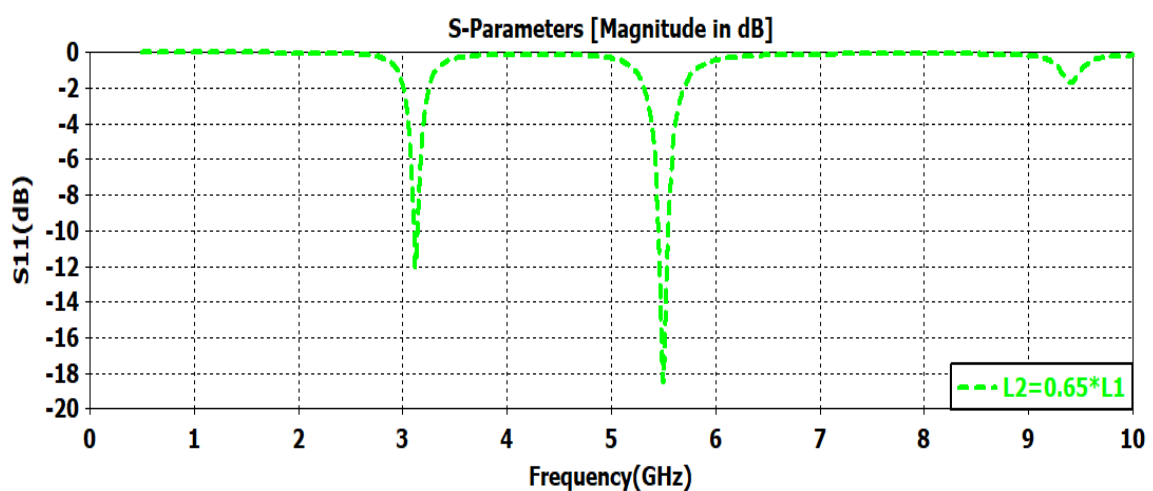


Figure 3.6 The reflection coefficient (S_{11}) of double ring unit cell.

In this design, two closed square rings are employed. The size of the inner ring was considered a design parameter as it was chosen to be a fraction of that of the outer ring ($L_2 = S \cdot L_1$), where ($0 < s < 1$). Figure 3.7 shows the variation of the reflection coefficient (S_{11}) of double rings unit cell with frequency for different values of the inner ring. The results show two bands the first at about 3.2 GHz, and the second one at a higher frequency corresponding to size of the inner ring. The frequency of the upper band decreases as its size is increased.

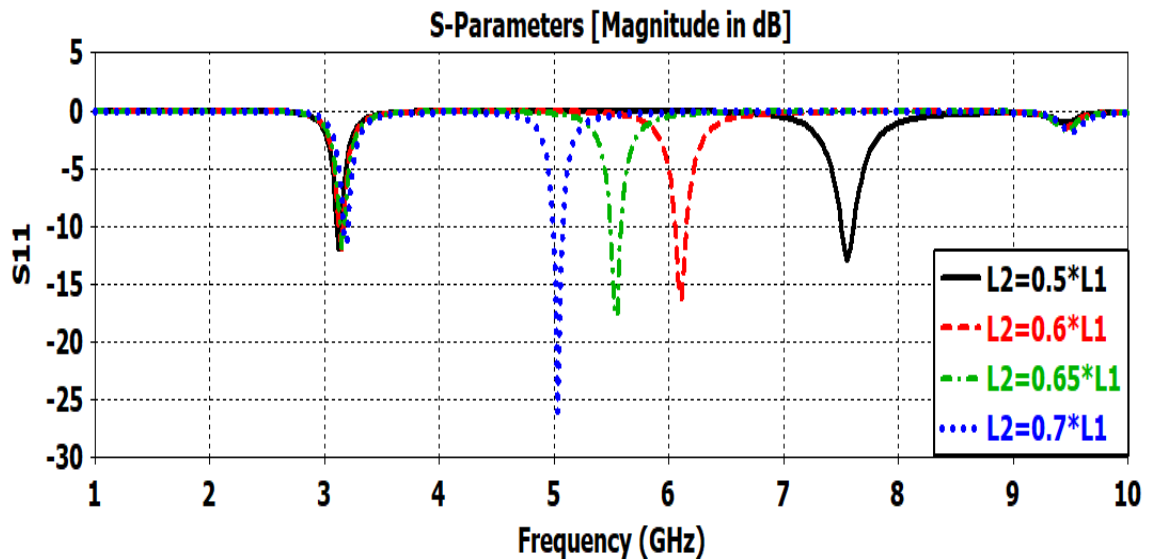


Figure 3.7 S_{11} of different values of the inner ring.

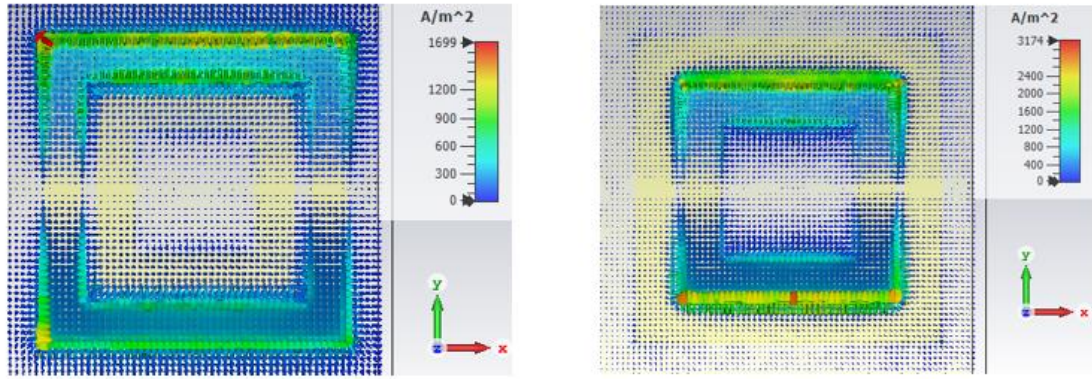
To reduce the spacing between two band aiming to attain a single wide band, the inner ring side length was increased. However, the two rings overlap physically before the two band can be merged together. Table 3.2 shows the results of the simulations, where the right column confirms that the resonance occurs when the effective wavelength is equal to the circumference of the ring, and this is applicable for each of the two rings. The table also shows that the reflection coefficient can be reduced to below -11 dB.

The results of the Table show that there are two bands of low reflection, the first at about 3.2 GHz, while the frequency of the second band depends on the side length of the inner ring (L2). As the side length of the inner ring was increased from $0.5*L1$ to $0.7*L1$, the frequency of the upper band decreased from 7.6 GHz to 5.03 GHz. However, the frequency of the lower band was essentially unchanged.

In Figures 3.8-a and 3.8-b, the surface current distribution on the double square ring is shown for frequencies of 3.2 GHz and 5 GHz, respectively, with using side lengths of 15.6 mm and 10.92 mm, respectively. Indicating a full one cycle around the ring's circumference, the present variation has two peaks and two nulls. A geographic verification of the relationship anticipated by Eq. 3.5 is provided by this.

Table 3.2: The simulation results of the double ring FSS with various dimensions with $\epsilon\epsilon= 3.1568$

case	L mm	W mm	λ_0 mm	Freq GHz	λ_e mm	S ₁₁ dB	Circumference / λ_e
Outer ring	15.6	2	95.23	3.15	53.598	-11.3	1.014
1-inner ring 0.5*L1	7.8	2	39.73	7.55	22.36	-12.9	1.037
2-inner ring 0.6*L1	9.36	2	49	6.11	27.578	-16.2	1.067
3-inner ring 0.65*L1	10.14	2	55	5.45	30.95	-17.5	1.052
4-inner ring 0.7*L1	10.92	2	59.6	5.0325	33.54	-26	1.063



(a)

(b)

Figure 3.8: The surface current on the double square ring (a) at 3.2 GHz (b) at 5 GHz.

3.3.3 Double Ring Unit Cell with Meander Inner Ring

The results of the last section show that it was not possible to eliminate the spacing between the upper and the lower bands, because increasing the circumference of the inner ring will lead to an overlap in between. Then, to increase the circumference of the inner one without increasing its overall size, it is suggested to meander the sides of the inner ring. Figure 3.9 shows the geometry of the proposed double ring unit cell, where two sides of the inner ring have been meandered. The path of meandering can be designed in two configurations, either meandering horizontal sides (Fig. 3.9-a) or meandering the vertical sides (Fig. 3.9-b). The unit cell dimensions used here were the same as of the previous case $L=19*19$ mm, $w=2$ mm, $L_1=15.6$ mm and the inner ring side length was set at $0.65*L_1= 10.14$ mm, but the average circumference of inner ring after meandering is 47.78 mm. The incident wave is assumed to linear polarization whose electric field is along the vertical direction (V-axis).

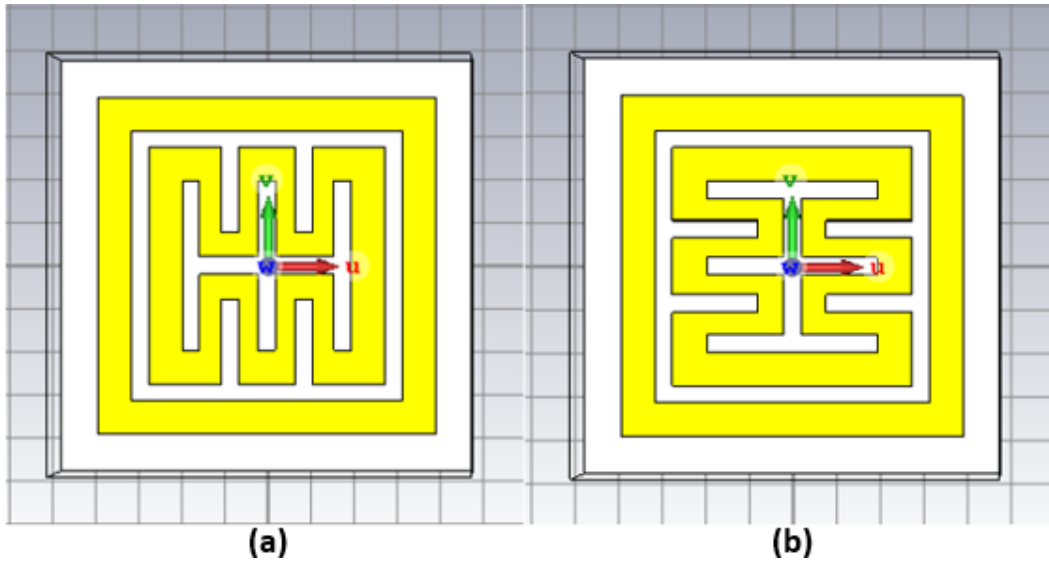


Figure 3.9 Double rings unit cell with meandered rings (a) meandering the horizontal sides, (b) meandering the vertical sides.

Figure 3.10 shows the variation of the reflection coefficient (S_{11}) of the double ring's unit cell for both of the configurations that are depicted in Fig. 3.9. For the case shown in Fig. 3.9-a, where the horizontal sides of the inner rings are meandered, the reflection coefficient shows resonance at 3 GHz, with a minimum of -15 dB. There is also another resonance at 8.17 GHz, with higher reflection coefficient of -15 dB. However, for the other design of the FSS, where the meandering is along the vertical sides of the inner ring (Fig.3.9-b), the behavior is different. In this case, there are two close resonances at 3 GHz, and 3.53 GHz, that correspond to the outer and inner rings respectively. The values of the reflection coefficients are better than -20 dB for both bands.

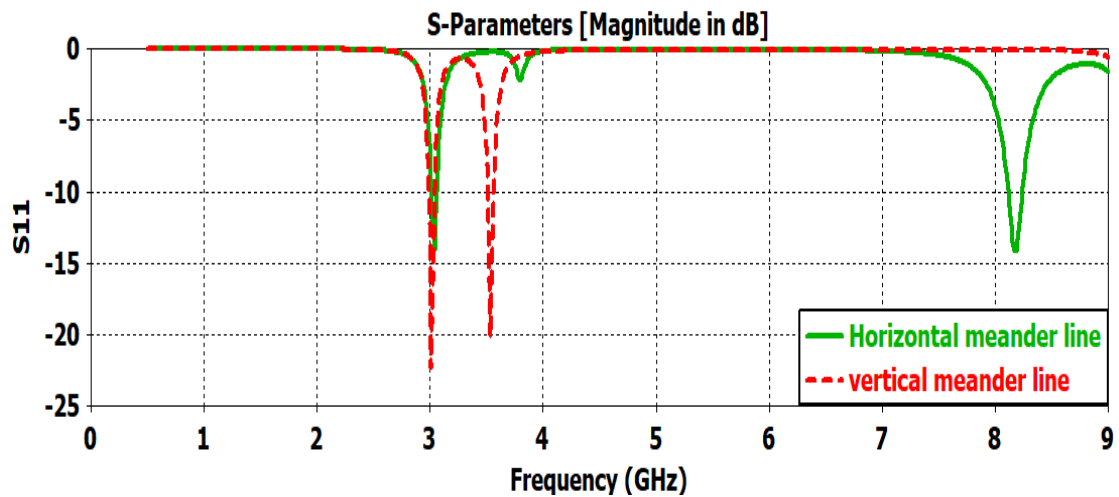


Figure 3.10 The reflection coefficient S_{11} of double rings unit cell (inner ring is meandered).

It can be said that when the meandering is in the same direction of the electric field, the extension in the length of the inner ring is effective. The meandering can be used to get longer circumference that helps to bring the second band nearer to the first one. However, with meandering applied only to one side pair, the orthogonal symmetry is lost, and the FSS unit cell will be sensitive to the direction of polarization.

3.3.4 Double Ring Unit Cell with Open Inner Ring

To reduce the resonance frequency of the inner ring and make it coincide with that of the outer ring, it is suggested here to use an open inner ring instead of the closed one as shown in Fig. 3.11. The idea behind that comes from the fact that an open ring resonates when its circumference is equal to half the effective wavelength. Moreover, the length of the gap opening also affect the resonance frequency and can be used to tune the resonance frequency.

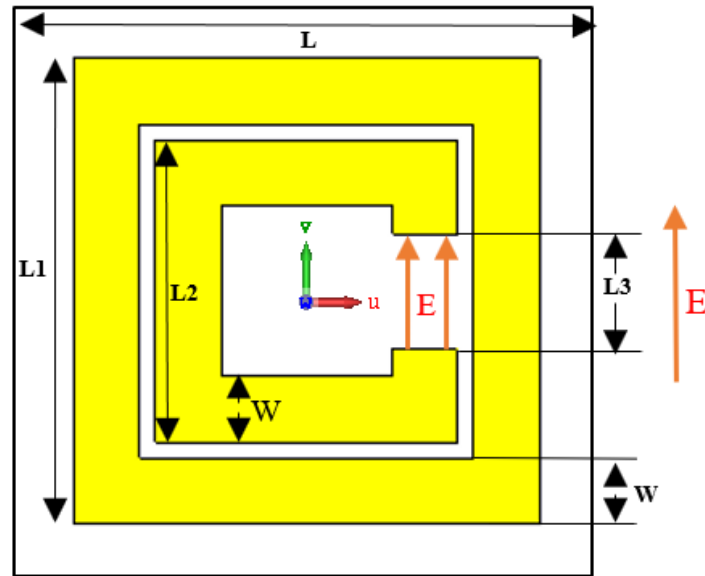


Figure 3.11 Geometry of double rings unit cell (open inner ring).

In the simulation for this FSS unit cell, the same dimensions of the previous two cases were used, with the exception of the inner ring. The inner ring side length of $L_2=0.65*L_1$ was used and the opening gap L_3 was assumed as a design parameter. In the first investigated case, the gap was placed on the right side of the ring and the incident wave was linearly polarized in the X-axis. The variation of the reflection coefficient with frequency is shown in Fig. 3.12 for various values of the gap. The results show that the two frequency bands have been joined together to yield a wider band. The value of the gap distance can be used to optimize the width of the band and the value of minimum reflection. It can be shown that the gap distance ($L_3= 4$ mm) has achieved a bandwidth of (132 MHz) for a reflection coefficient of better than -10 dB.

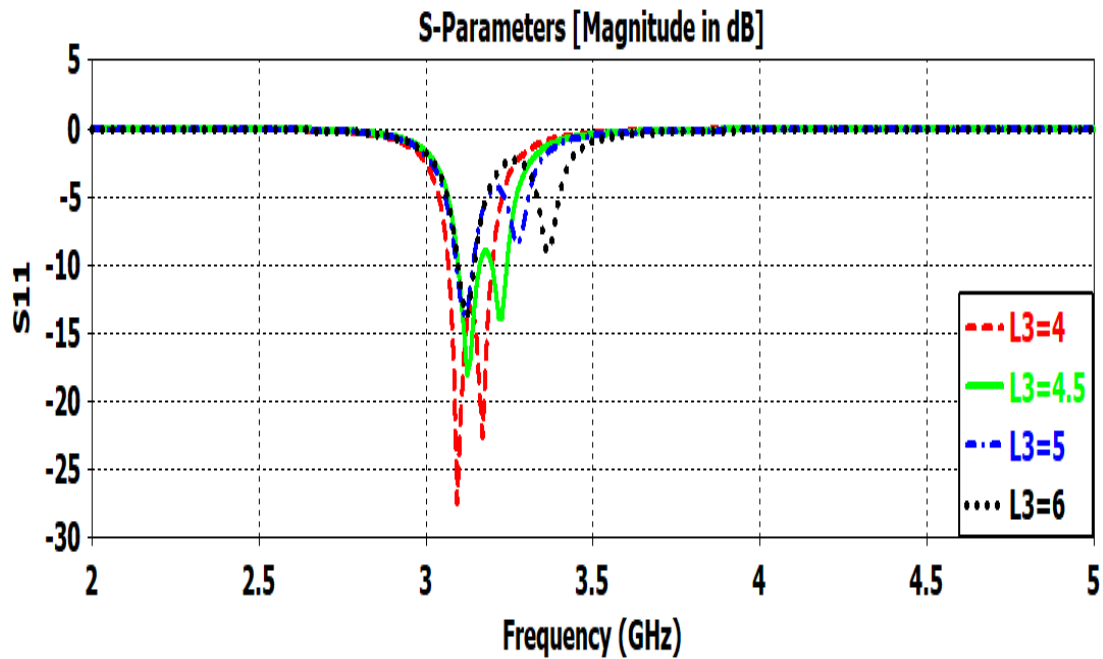


Figure 3.12 Reflection coefficient S_{11} of double rings unit cell (open inner ring).

As seen in Fig. (3.11) the space between the two ends of the inner ring, $L3$ value will change from (4, 4.5, 5, and 6) mm to get the best result among them. Figure (3.12) shows the reflection coefficient S_{11} results of double rings unit cell with an open inner ring by changing the length of inner ring (or space between the two ends of open ring). Table 3.3 shows the results of changing the value of $L3$ according to Fig. (3.12). The response displays two neighboring minima that led to a 0.064 GHz bandwidth for the case of ($L3=4.5$ mm) which is considered as best results after $L3 = 4$ mm.

The relationship between the two minima and the two resonance frequencies that relate to the rings' diameter is as follows:

The outer ring's circumference is equal to λ_e at its resonance frequency. At the ring's resonance frequency, the inner ring's circumference equals one-half of an λ_e .

Table 3.3 Simulation results of the double ring (open inner ring) with various lengths of L3

Space between two ends	Freq. of Lower Band (GHz)	Freq. of Upper Band (GHz)	BW of minima S ₁₁ (MHz)	Min S ₁₁ dB
L3=4	3.1	3.17	132	-27.4
L3=4.5	3.12	3.22	64	-17.6
L3=5	3.11	3.27	49	-13.5
L3=6	3.12	3.36	46	-13.76

To explain the effect of changing the polarization of the incident wave on the response of the reflection coefficient, the inner ring was rotated to direct its gap upwards as shown in Fig. 3.13. For this configuration, the electric field of the incident wave, is perpendicular to the gap spacing. Figure 3.14 shows the variation of the reflection coefficient with frequency for the FSS unit cell, for various spacing of the gap. The results show a very small effect of the gap spacing. The reason for the results shown in Fig. 3.12 and Fig. 3.14 can be explained by considering the gap as a capacitor, and the E-field of the incident wave is either along the gap (in Fig.3.11), or perpendicular to the gap (Fig. 3.13). The value of the capacitance is not the same for the two cases.

Figure 3.14 shows that when the space between the two ends of open ring toward the X-axis the reflection coefficient and bandwidth (BW) are changed by changing the value of the space but when the space between the two ends of open ring is toward the Y-axis, the changing of the value of the space does not affect the reflection coefficient and bandwidth of the 1st resonance frequency at 3.2GHz, but caused a small shifting in the 2nd resonance.

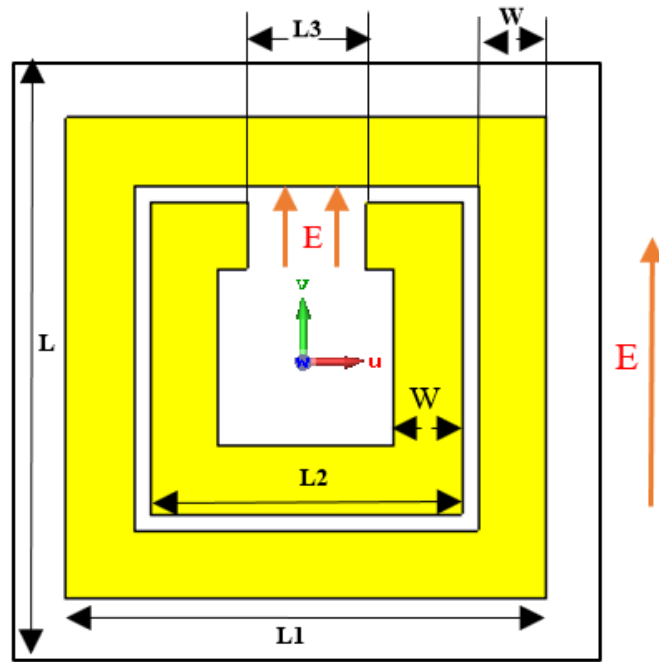


Figure 3.13 Geometry of double rings unit cell (open inner ring).

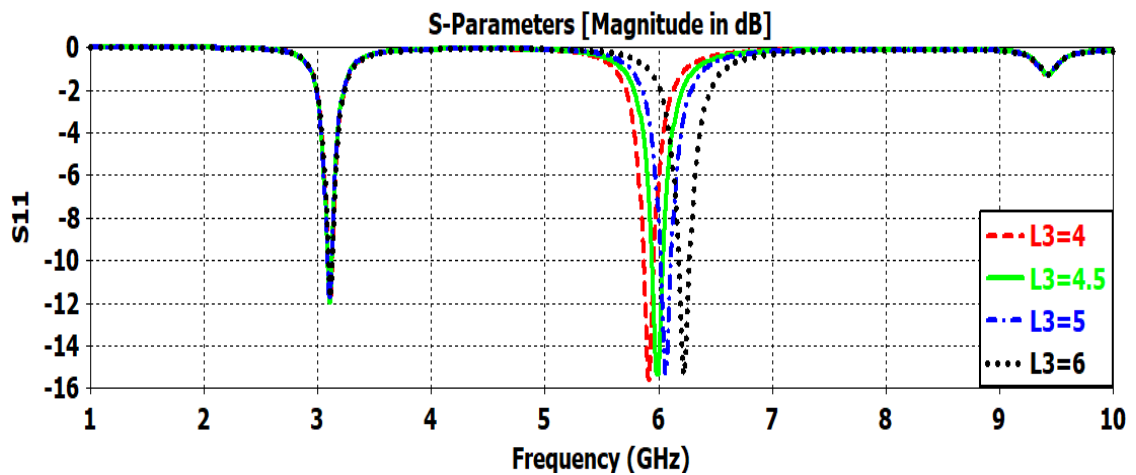


Figure 3.14: Reflection coefficient S_{11} of double rings (open inner ring) with changed the polarization.

3.3.5 Comparing the Performance of the Proposed Designs

The obtained results of the former sections are tabulated in Table 3.4 for comparison. It can be seen that the FSS unit cell of the double ring with an open inner ring has the best results as it offered a minimum reflection coefficient $S_{11} = -27.4$ dB, and the largest bandwidth of about 132 MHz. However, this configuration is sensitive to the direction of the polarization.

Table 3.4: Comparing the obtained results.

Type of cell	Freq. of Lower Band (GHz)	Freq. of Upper Band (GHz)	BW of minima S ₁₁ (MHz)	Min S ₁₁ (dB)
Single ring	3.2	9.6	93	-11
Two square rings	3.15	5.0325	86	-26
Square ring + meandered	3.01	3.53	51	-22.3
Closed + open rings	3.03935	3.17	132	-27.4

3.4 The Ohmic Sheet or Resistive Sheet Unit Cell

In the former sections, the rings and ground plane were assumed of a very good conductor (copper with conductivity of $5.8 \times 10^7 \text{S/m}$). As the aim of these investigations is to reduce the radar cross-section by either reducing reflection from the FSS surface or absorbing some of the power in the incident wave, in this section the use of metals with lower conductivity than copper is investigated. The measure of conducting is expressed through the definition of the sheet resistance.

The term sheet resistance is a measure of the resistance of thin films that are nominally uniform in thickness. It is commonly used to characterize materials made by semiconductor doping, metal deposition, resistive paste printing, and glass coating. Sheet resistance is applicable to two-dimensional systems in which thin films are considered two-dimensional entities. When the term sheet resistance is used, it is implied that the current is passing along the plane of the sheet, not perpendicular to it. In a regular three-dimensional conductor, the resistance can be written as

$$R = \rho \frac{L}{A} = \rho \frac{L}{wt} \dots\dots\dots(3.7)$$

Where ρ is the resistivity of the sheet material, A is the cross-sectional area, L is the length. The cross-sectional area can be split into the width W , and the sheet thickness t . Upon combining the resistivity with the thickness, the resistance can then be written as:

$$R = \frac{\rho L}{t W} = R_s \frac{L}{W} \dots\dots\dots(3.8)$$

Where R_s is the sheet resistance, whose unit is referred to as "ohms per square" (denoted " Ω/sq " or " Ω/\square "). The geometry for defining resistivity and sheet resistance shows in Fig 3.15 but in both cases the current is parallel to the L direction.

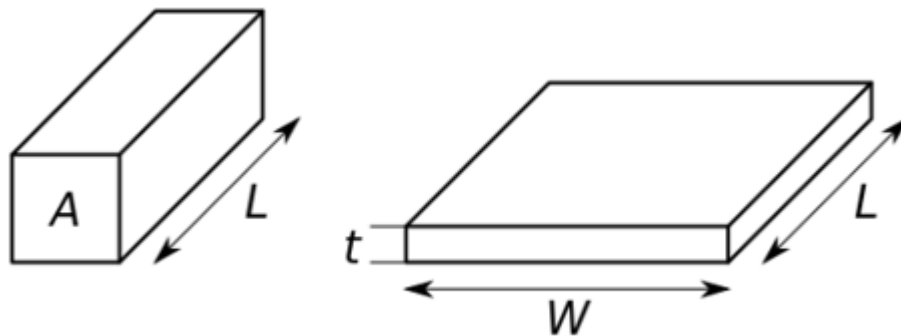


Figure 3.15 Geometry for defining resistivity (left) and sheet resistance (right).

3.4.1 Double ring unit cell

In this case, the unit cell consists of an ohmic sheet ground plane, Fr-4 substrate with relative permittivity $\epsilon_r=4.3$, and double ring of ohmic sheet also, as seen in Fig. (3.16-a). The unit cell dimensions are: $L=19 \text{ mm} \times 19 \text{ mm}$, outer ring side length $L_1 = 15.6 \text{ mm}$, and width of ring $W=2 \text{ mm}$ the substrate height $h=1.6 \text{ mm}$, the ground plane thickness $=0.035 \text{ mm}$, the resistive sheet ring thickness $mt=0.035 \text{ mm}$, and the inner ring $L_2= 0.65 \times L_1=10.14 \text{ mm}$.

The results of the simulations for the reflection coefficient (S_{11}) variation with frequency, when using sheet resistivity of (0.1, 10, 15 and 50) Ω/sq are shown in Fig. 3.17. These results are compared with those obtained

when copper was used. According to Fig. 3.17, when the sheet resistance is less than ($0.1 \Omega/\text{sq}$), the reflection coefficient (S_{11}) value approaches that of the copper example. The results also show that increasing the sheet resistance above ($3 \Omega/\text{sq}$), the reflection coefficient start to increase for all frequencies, and the deep nulls start to disappear.

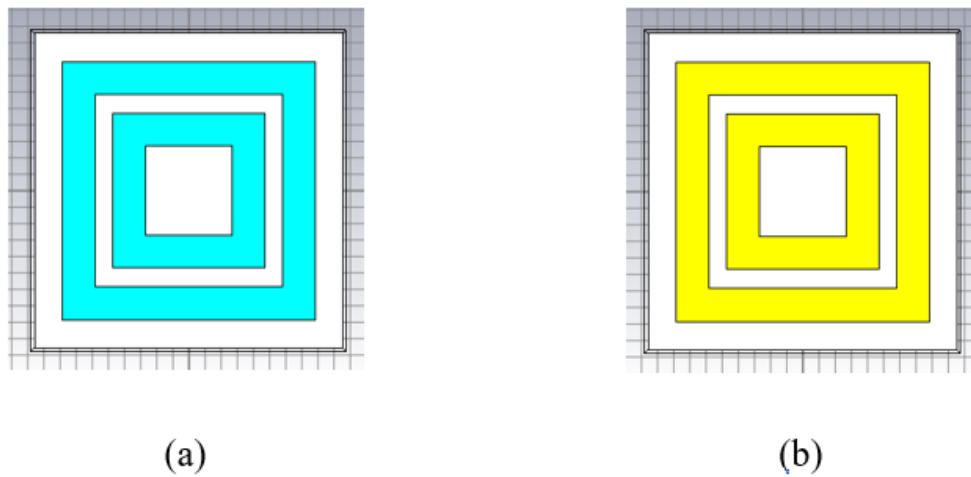


Figure 3.16 Geometry of the unit cell (a) Ohmic sheet case (b) Copper case.

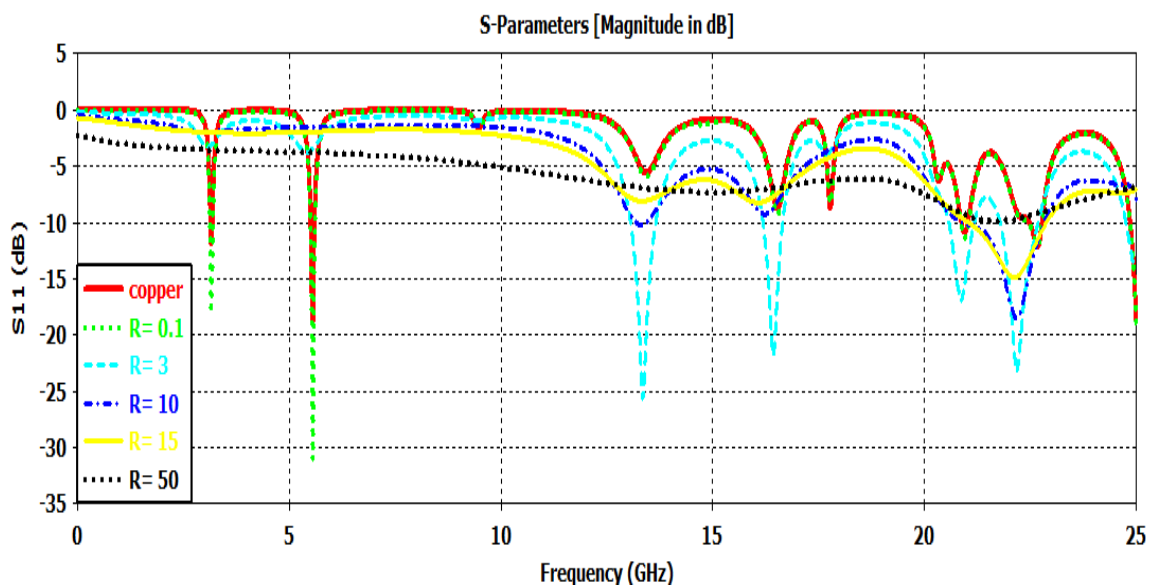


Figure 3.17 Reflection coefficient response of the double ring ohmic sheet compared to that for using copper.

3.4.2 Double Ring with Open Inner Ring Unit Cell

In this case, the inner ring was opened, and the unit cell consists of a resistive sheet ground plane and rings, while the same Fr-4 substrate with relative permittivity $\epsilon_r=4.3$, are taken as seen in Fig. (3.18). In the case of double ring unit cell with an open inner ring to optimize the results with minimum size of unit cell its dimensions will be taken as: $L=18\text{ mm}\times 18\text{ mm}$, outer ring side length $L_1=14.15\text{ mm}$, and width of ring $W=2\text{ mm}$ the substrate height $h=1.6\text{ mm}$ and ground plane thickness $=0.035\text{ mm}$ and resistive sheet ring thickness $mt=0.035\text{ mm}$, and the inner ring $L_2=0.65*L_1=9.1975\text{ mm}$. The simulations' results for the reflection coefficient (S_{11}) for various values of sheet resistivity are shown in Fig. 3.19, which shows that the sheet resistance increases other than that of copper, the reflection coefficient at the first and second frequencies start to increase from there minimum values that were achieved for copper. However, a region of low reflection starts to be obtained around the frequency of 14 GHz. This region has two local minima at (14.25 GHz, and 17.17 GHz).

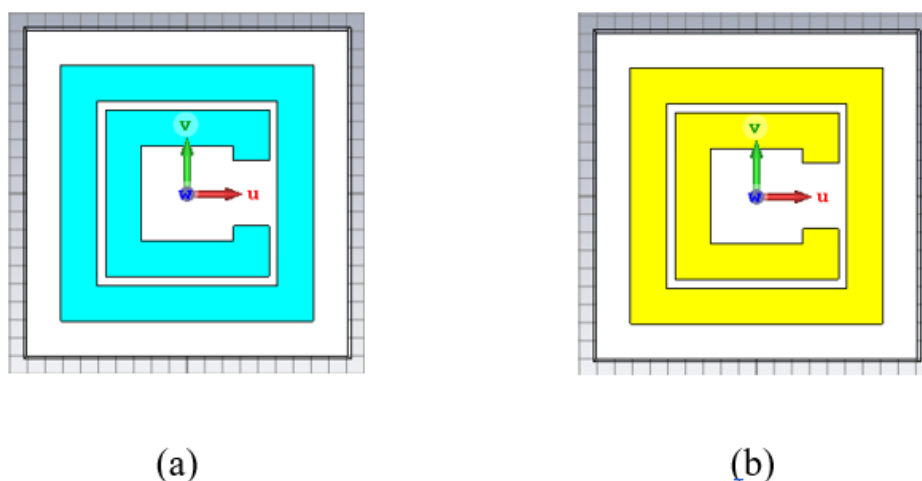


Figure 3.18: Geometry of the double ring with open inner ring unit cell
(a) ohmic sheet case (b) copper case.

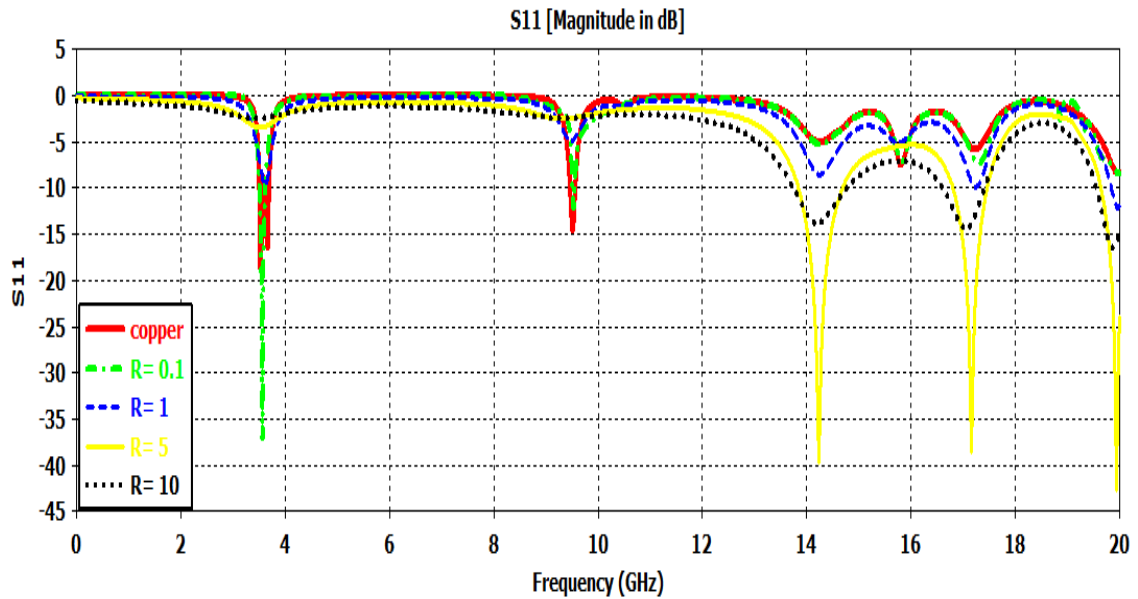


Figure 3.19 Reflection coefficient response of the double ring (open inner ring) ohmic sheet compared with the copper case.

Although the Ohmic loss increases with frequency in general, the resonances at these two frequencies have a pronounced effect. Moreover, at higher frequencies, the loss due to the substrate starts to show its effect. Table 3.5 shows the 1st and 2nd minima frequency for each resistive value at double ring (open inner ring) unit cell.

Table 3.5 1st and 2nd minima frequency for each resistive value.

Resistive (Ω/sq)	1st minima Frequency (GHz)	S11 (dB)	2nd minima Frequency (GHz)	S11 (dB)
0.1	3.56	-37.12	9.52	-12.12
1	3.62	-4.95	9.48	-8.56
5	14.2	-39.68	17.05	-38.45
10	14.24	-13.82	17.16	-14.4

Table 3.6 displays the simulation results for Fig. 3.18, when the resistivity of the sheet is changed. This confirms that at low resistivity, the resonance occurs when the effective wavelength is equal to the circumference of the ring, but at higher frequencies, it loses this characteristic, and this is true for both rings. Additionally, the Table demonstrates that the reflection coefficient may be lowered to below -39 dB.

For more insight into the effect of the sheet resistivity on the reflection coefficient, the sheet resistance was further increased in comparison with the values used in Fig. 3.19. As can be seen, when the sheet resistance is increased from that of copper, the nulls at the first two frequencies disappeared, and a sort of wide frequency response is achieved. The level of the reflection coefficient goes to less than -10 dB at sheet resistance of 100 Ω/sq and larger as illustrated in Fig. 3.21 which shows the results of the simulations for the reflection coefficient (S_{11}) at resistivity of (0.1 ,15 ,50 and 150) Ω/sq . The reason for the results displayed in the Fig. 3.19 and Fig. 3.20 can be attributed to the fact that as the resistance increases the quality factor of any of the resonating rings decreases leading to a lower reflection coefficient at a wider frequency response.

Table 3.6 The simulations result of the unit cell with various values of resistivity, ring width=2mm, and $\epsilon_r = 3.157$.

case	L (mm)	λ_0 (mm)	Freq (GHz)	λ_e (mm)	S11 (dB)	Circumference/ λ_e
1-outer ring 0.1 Ω/sq	14.15	84.269	3.56	47.429	-37.12	1.024
2-inner ring 0.1 Ω/sq	9.1975	31.51	9.52	17.73	-12.12	1.424
1-outer ring 1 Ω/sq	14.15	82.87	3.62	46.64	-4.95	1.042
2-inner ring 1 Ω/sq	9.1975	31.6	9.48	17.78	-8.56	1.422
1-outer ring 5 Ω/sq	14.15	21.12	14.2	11.88	-39.68	1.224
2-inner ring 5 Ω/sq	9.1975	17.59	17.05	9.9	-38.45	2.55
1-outer ring 10 Ω/sq	14.15	21	14.24	11.82	-13.82	4.11
2-inner ring 10 Ω/sq	9.1975	17.48	17.16	9.8	-14.4	2.58

Other simulations were performed using the ground plane and the substrate without the rings, so that any resonance effect due to the rings are excluded. The obtained results are shown in Fig. 3.21. The figure shows that by increasing the sheet resistivity, the reflection coefficient increases, and at (100 Ω/sq) the reflection coefficient approached to -23 dB at high frequencies.

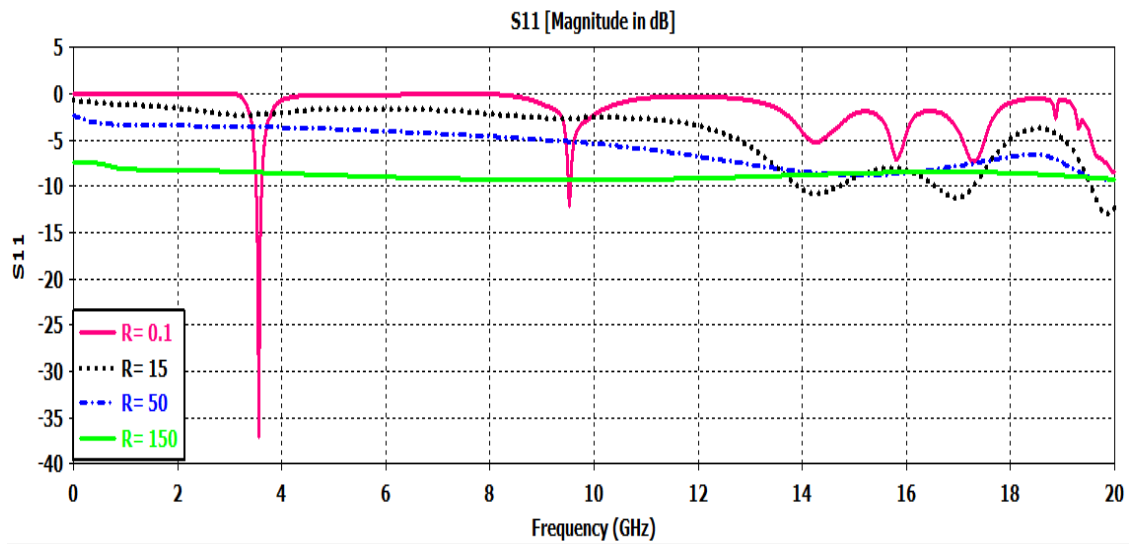


Fig. 3.20 Reflection coefficient response for variable sheet resistivity.

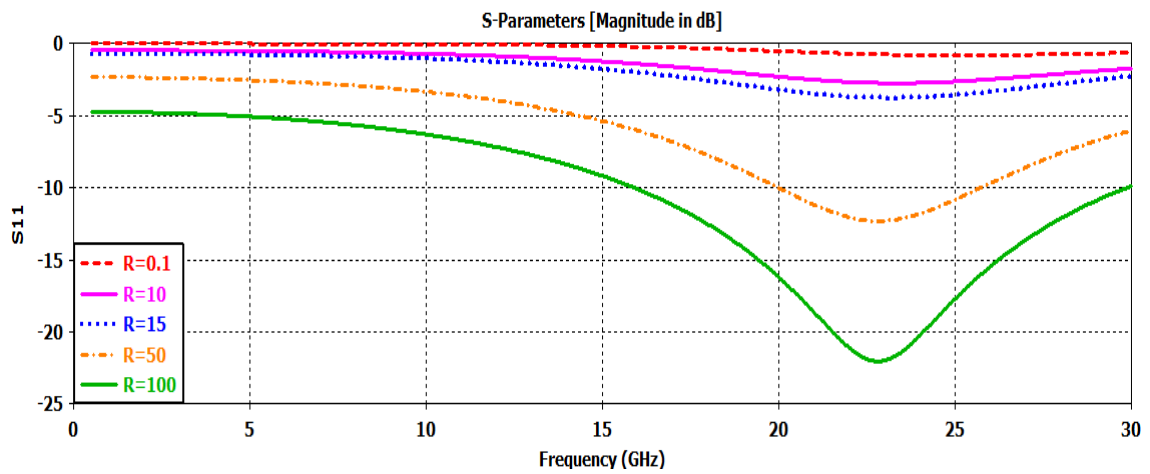


Figure 3.21 Reflection coefficient response of GP and substrate without the of rings.

CHAPTER FOUR

RADAR CROSS-SECTION

REDUCTION USING

RESISTIVE FSS UNIT

CELLS

CHAPTER FOUR

RADAR CROSS-SECTION REDUCTION USING RESISTIVE FSS UNIT CELLS

4.1 Introduction

A search in the literature related to the FSS and their use for the reduction of the RCS have shown that the majority of the published papers have used conducting elements in the investigated unit cells. It is well-known that conductors perform as very good reflectors at a wide range of frequencies. The FSS elements were printed on available substrates that usually have low loss, as required by the majority of applications. Therefore, if the FSS unit cell is to offer low reflection, and consequently a reduction in the radar cross-section, the mechanism of reduction should be through a cancellation of various reflections from the FSS unit cell.

The results of chapter three show moderate improvements in the performance of the FSS cell as an absorber to reduce the radar cross-section. In the following sections of this chapter, the feasibility of achieving improved reduction is investigated by employing resistive sheets or rings in addition to the conducting elements. The idea behind this is to provide power-absorbing elements that can help to reduce the reflected power from the FSS surface. The investigated FSS unit cells are the double closed rings, double rings with an open inner ring with the insertion of the carbon paste. The proposed FSS unit cells are investigated by various combinations of elements in the region of carbon paste insertion, changing dimensions of the rings, the conductivity, and thickness of paste for proposed shapes of unit cells.

4.2 Double Closed Copper Rings with Carbon Paste

In this section, the proposed FSS unit cell includes a copper ground plane, and copper rings printed on one side of the FR-4 substrate. Two designs are investigated; the first one has double closed copper rings with inserted a carbon paste layer in between the rings and at the center of the unit cell. The second case is a double copper rings with an open inner ring, and with inserting the carbon paste layer at various places on the surface of the FSS unit cell.

In this case, the proposed unit cell includes double rings of copper printed on FR-4 substrate with relative permittivity $\epsilon_r=4.3$, a thickness of $h=1.6$ mm and copper thickness of 0.035 mm, as shown in Fig. 4.1. The unit cell dimensions are $L=19$ mm \times 19 mm, outer ring side length $L_1=15.6$ mm, width of ring $W=0.1*L_1=1.56$ mm, and the inner ring size $L_2=0.65*L_1=10.14$ mm.

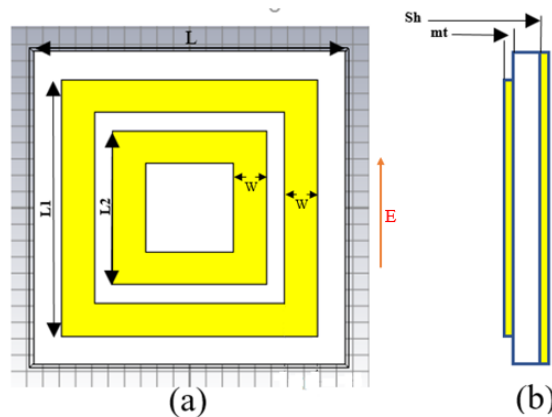


Figure 4.1 Double ring unit cell geometry (a) "front view" (b) "side view".

The simulation results for the reflection coefficient (S_{11}) of the double ring unit cell are shown in Fig. 4.3. They demonstrate the existence of two low reflection bands, one at a frequency of about 3.2 GHz and the other at about 5.3 GHz, with each ring of the unit cell being in charge of a separate low reflection band.

4.2.1 Double Closed Copper Rings with a Carbon Ring

To increase the losses in the unit cell, and thus reduce the power of the reflected wave, a layer of carbon paste was placed between the two rings without changing the dimensions to get more absorption. The geometry of the proposed unit cell is shown in Fig. 4.2, where the carbon layer is marked in black. The properties of the carbon paste are electric conductivity $\delta = 1.2$ s/m, density $\text{Rho} = 1070$ kg/m³, and carbon thickness is 0.035 mm, the thickness of the carbon layer used in sections 4.1, 4.2, and 4.4 was 0.035mm. The effect of the thickness of the carbon layer of the obtained results will be presented in section 4.5.

The proposed unit cell was simulated using the CST microwave suit as it was used in chapter 3, and the obtained results are shown in Fig. 4.3. The figure shows that the minimum reflection coefficient is about -23 dB at a resonance of 3.5 GHz frequency.

Figure 4.3 shows the variation of the reflection coefficient (S_{11}) of the double ring unit cell for the two cases with and without carbon paste. The effect of the carbon paste layer is seen to shift the frequency of minimum reflection from 3 GHz to 3.5 GHz, and the bandwidth has changed from 47.115 MHz to about 190 MHz.

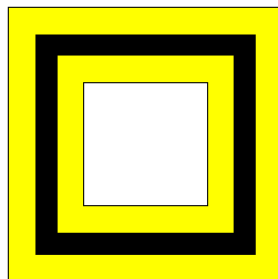


Figure 4.2 Double ring unit cell geometry with carbon paste layer placed in between the two rings.

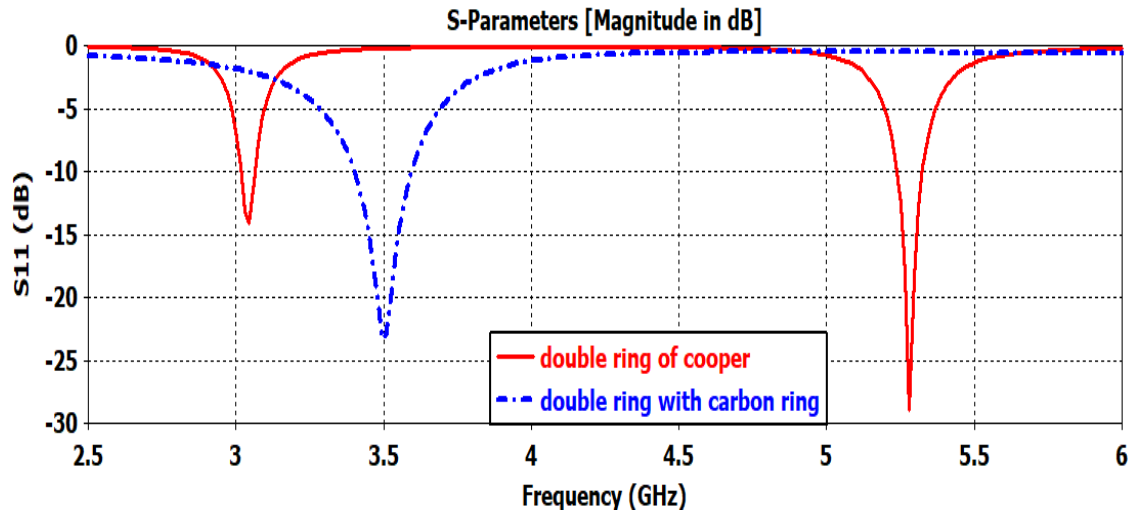


Figure 4.3 Variation of the reflection coefficient with frequency for the double ring unit cell with and without carbon paste.

To increase the bandwidth, it was decided to make some changes to the unit cell like increasing the carbon ring by decreasing the size of the inner ring so the inner ring side length $L_2 = 0.6 * L_1 = 9.36$ mm was used instead of $0.65 * L_1$ and the other parameters stay at the same values. Figure 4.4 shows that bandwidth is increased to 247.69 MHz but the resonance frequency is slightly shifted.

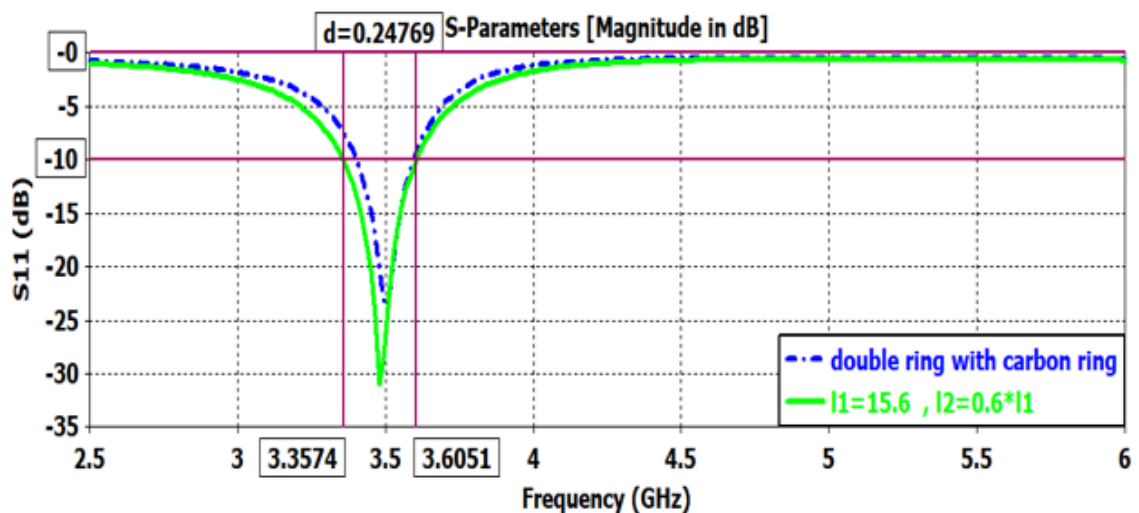


Figure 4.4 Variation of the reflection coefficient with frequency for the double ring unit cell with carbon paste after decreasing the size of the inner ring.

4.2.2 Double Closed Copper Rings with a Carbon Ring and a Patch

For further improvement in the response of the proposed unit cell, more carbon paste was added, by filling the square region inside the inner ring as shown in Fig. 4.5. The results of the simulations for the reflection coefficient (S_{11}) of the unit cell are illustrated in Fig 4.6. It can be noticed that the frequency of minimum reflection is now 3.44 GHz compared to the case before adding the carbon layer at the center of the inner ring. The bandwidth was also increased to 311.97 MHz from 247.69 MHz. The reason for these changes can be attributed to the increase in the regions of carbon paste at the unit cell.

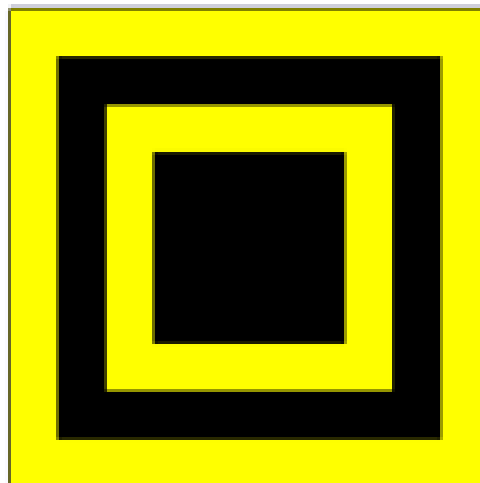


Figure 4.5 Double ring unit cell geometry with carbon paste ring and patch.

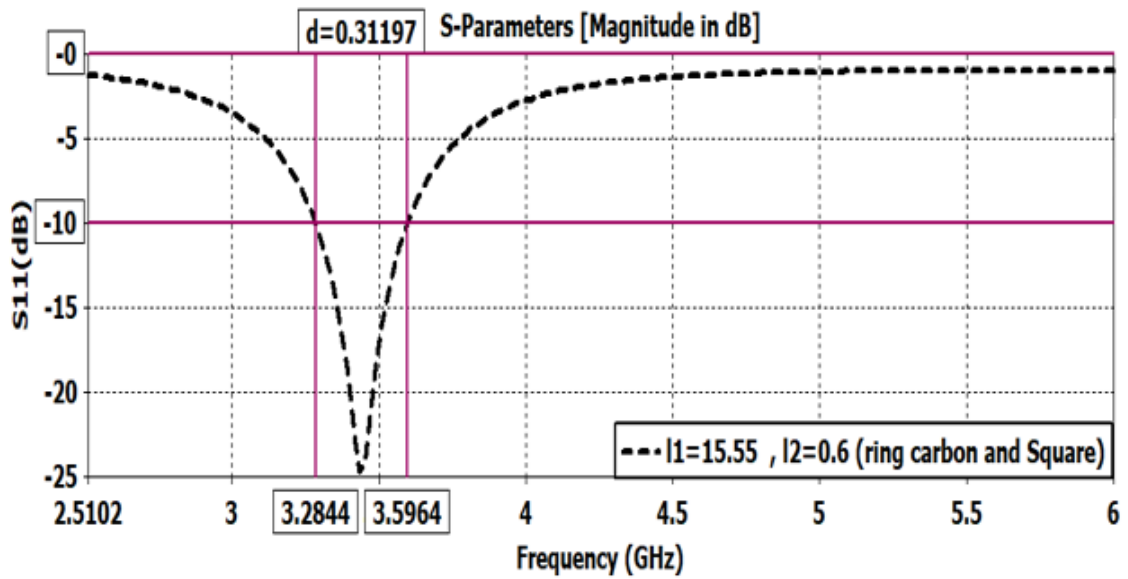


Figure 4.6 Reflection coefficient responses (S_{11}) of the double ring with carbon layers between the rings and at the center of the inner ring.

To reset the resonance frequency to 3.5 GHz, the length of the outer ring has been decreased to $L_1 = 15.4$ mm. The side length of rings is decreased to increase the resonance frequency from (3.35 to 3.5) GHz. Figure 4.7 shows the reflection coefficient (S_{11}) after resetting the frequency to 3.5 GHz.

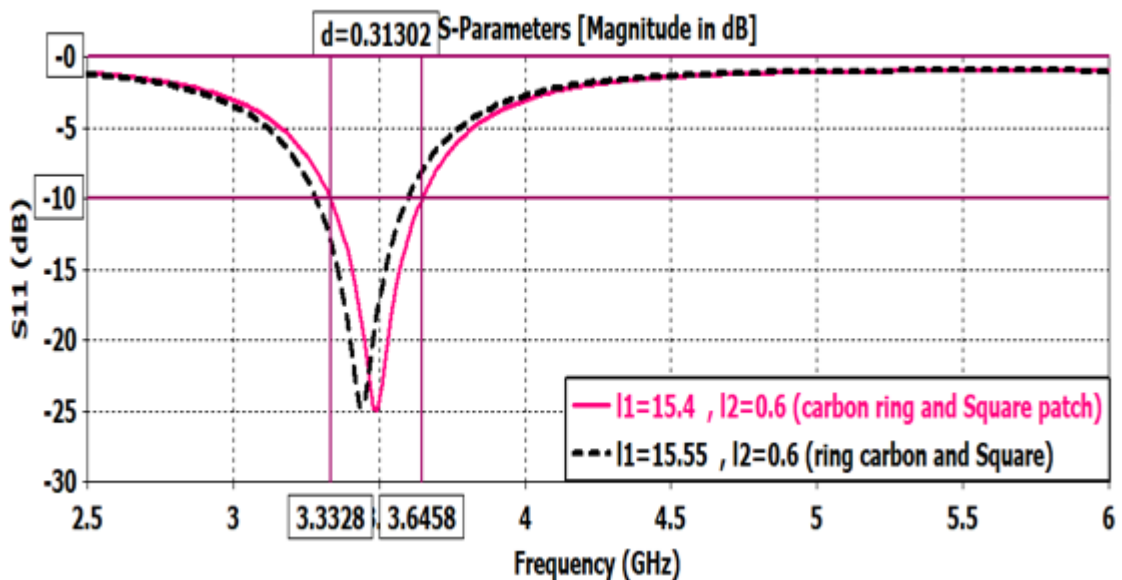


Figure 4.7 Reflection coefficient of double ring unit cell with carbon ring and patch after decreasing the outer ring size.

To draw comparisons among the three previous cases of unit cells, Fig. 4.8 and Fig. 4.9 show the geometry of the three cases of unit cells and their reflection coefficient S_{11} response, respectively. By comparing the three cases, it appears that the addition of the carbon paste to the unit cell causes an increase in the bandwidth of the reflection coefficient but it affected the resonance frequency.

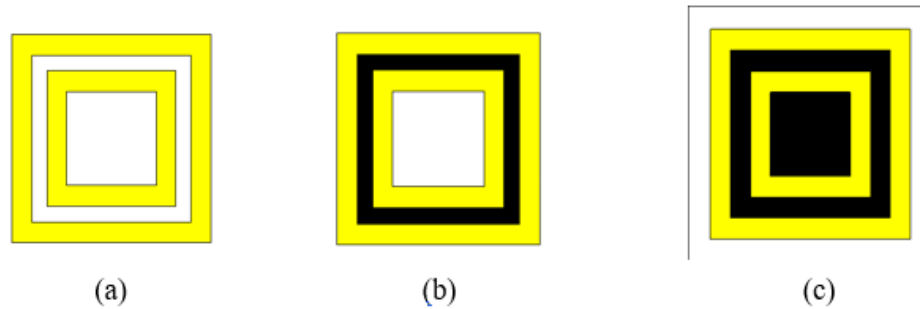


Figure 4.8 Geometry of unit cell (a) copper rings (b) adding carbon ring (c) adding carbon ring and patch at the center.

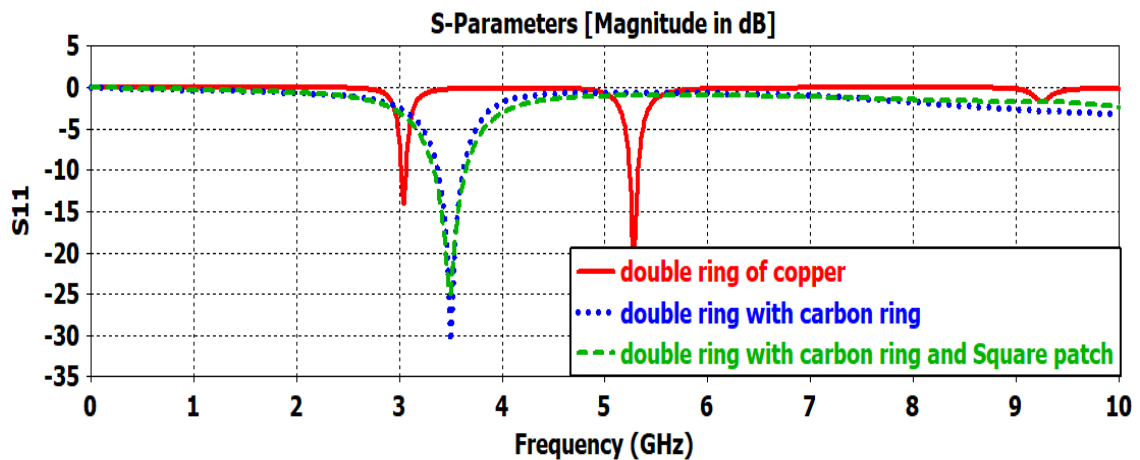


Figure 4.9 Reflection coefficient results of the (copper rings, adding a carbon ring, and adding a carbon ring and path at the center).

4.3 Double Rings with Opened Inner Ring

The suggested unit cell in this section uses a double ring (with an open inner ring) of copper, and the same substrate of FR-4 substrate with relative permittivity $\epsilon_r=4.3$, and a copper thickness of 0.035 mm. As shown in Fig. 4.10, the unit cell's dimensions are $L=18\text{mm}\times 18\text{mm}$, the outer ring side length

L_1 is 14.15 mm, the ring's width $W = 0.1 * L_1 = 1.56$ mm, and the inner ring size $L_2 = 0.65 * L_1 = 9.1975$ mm.

Figure 4.11 displays the simulation results for the reflection coefficient (S_{11}) of the double ring unit cell (with an open inner ring). The response shows two adjacent minima that resulted in increased bandwidth of 172 MHz. The two minima correspond to two resonance frequencies that are related to the circumference of the rings by the following relation;

Circumference of the outer ring = λ_e at the resonance frequency of the ring,

Circumference of the inner ring = $\frac{1}{2} \lambda_e$ at the resonance frequency of the ring,

As it was discussed in chapter 3.

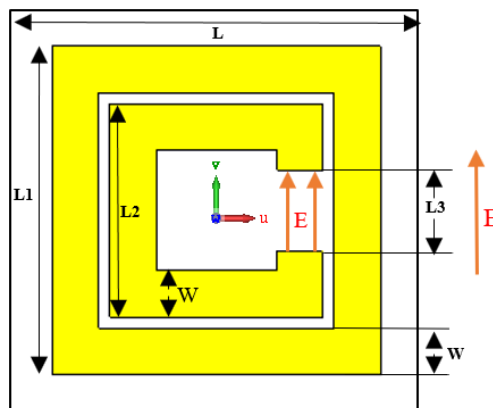


Figure 4.10 Geometry of double rings unit cell (open inner ring).

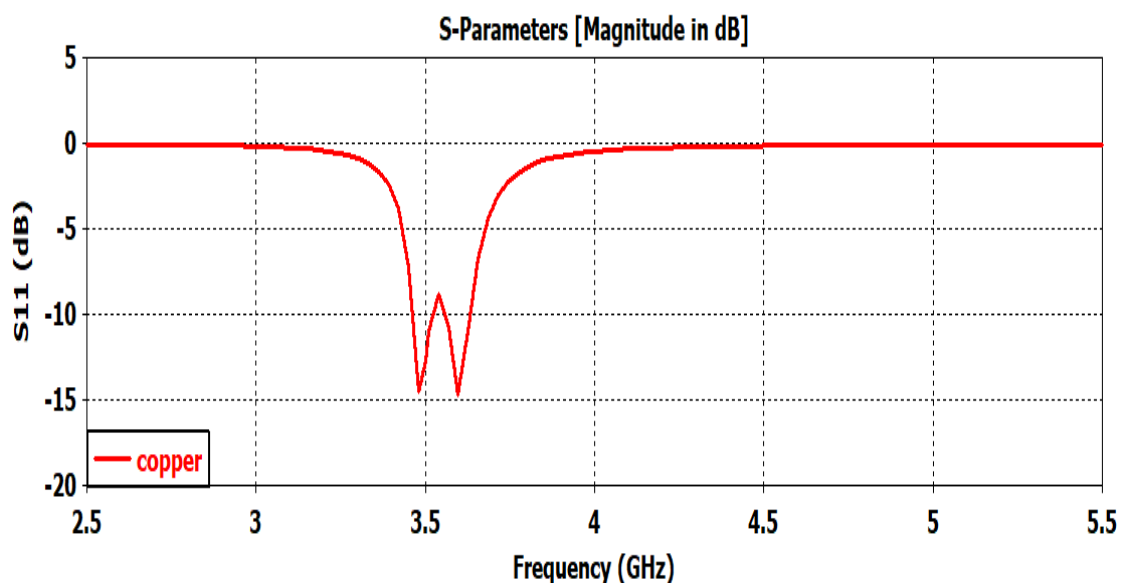


Figure 4.11 Reflection coefficient of the double ring with open inner ring unit cell.

4.3.1 Double Rings with Opened Inner Ring and Carbon Patch

In this section, the carbon paste is inserted at the center of the inner ring forming a square patch as shown in Fig.4.12. The same carbon paste ($\delta = 1.2$ s/m, $\rho = 1070$ kg/m³) was used, and the unit cell dimensions were 18 mm \times 18 mm, $L_1 = 14.15$ mm $L_2 = 0.65 * L_1 = 9.1975$, $w = 2$ mm.

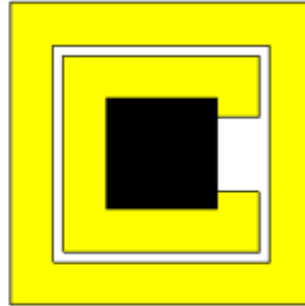


Figure 4.12 Double ring (open inner ring) with carbon square patch.

The simulation results of the reflection coefficient (S_{11}) of the double ring unit cell (open inner ring) with carbon square patch that is shown in Fig. 4.13 which shows that the bandwidth is about 51 MHz, and minimum value of reflection coefficient is achieved at 3.53 GHz. This value of the bandwidth is smaller than that (172 MHz) before adding the carbon paste.

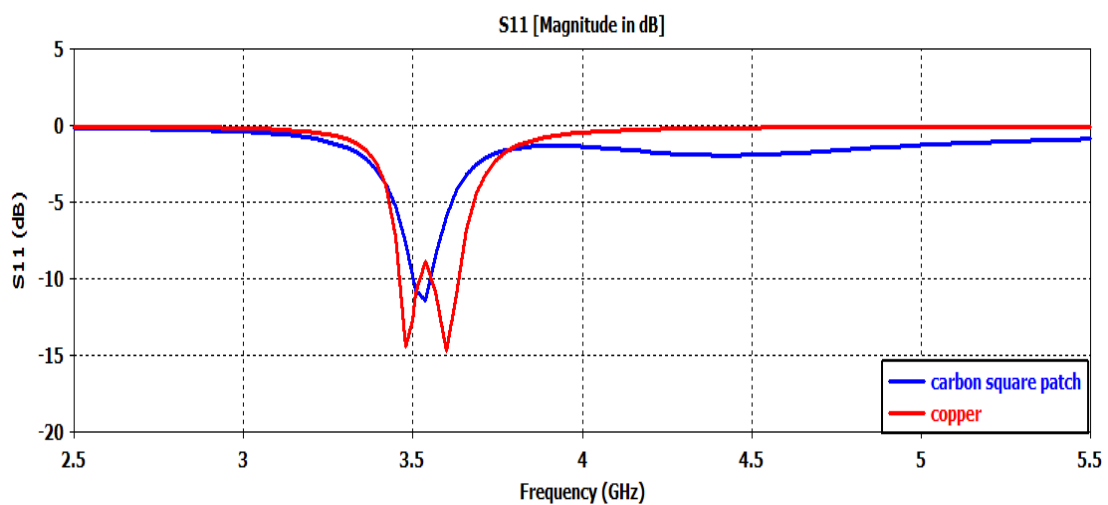


Figure 4.13 S_{11} of the double ring unit cell (with open inner ring) when adding a carbon square patch at the center.

4.3.2 Double Rings with Opened Inner and Carbon Paste at the Inner Ring Opening

The unit cell shape for the second case is shown in Fig. 4.14, which uses a double rings unit cell with an open inner ring and carbon paste inserted in the gap between the two ends of the inner ring.

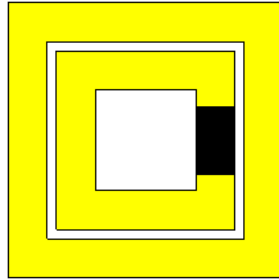


Figure 4.14 Double ring (open inner ring) unit cell with carbon in the internal ring opening.

Figure 4.15 exhibits the reflection coefficient's simulation results (S_{11}) of the double ring unit cell (open inner ring) with carbon paste in the internal ring opening. It shows that the bandwidth is around 47 MHz, and the minimum value of the reflection coefficient is obtained at 3.56 GHz. This value of bandwidth (172 MHz) is also smaller than that before adding the carbon paste.

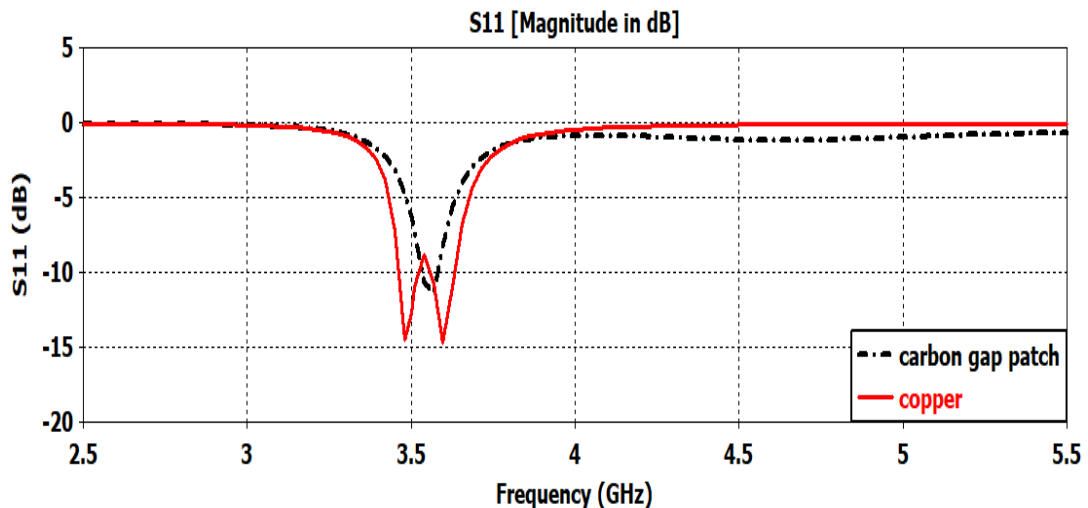


Figure 4.15 S_{11} of the double ring unit cell (with open inner ring) with carbon in the internal ring opening.

4.3.3 Double Rings with Opened Inner and Carbon Ring

The unit cell shape for the third case, which uses a double rings unit cell (open inner ring) and the carbon paste was placed in the space between the two rings as a carbon ring, is shown in Fig. 4.16.

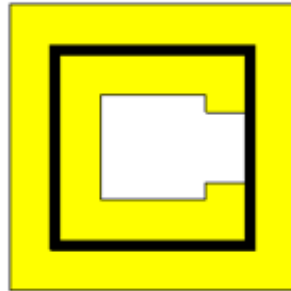


Figure 4.16 Double ring unit cell (open inner ring) with carbon ring.

The bandwidth is 175 MHz, and the minimum value of the reflection coefficient at 3.8 GHz, according to Fig. 4.17. This figure also shows the simulation results for the reflection coefficient (S_{11}) of the double ring unit cell (open inner ring) with a carbon ring compared to the initial case before adding a carbon ring. The carbon ring has led to a 3 MHz increase in the bandwidth.

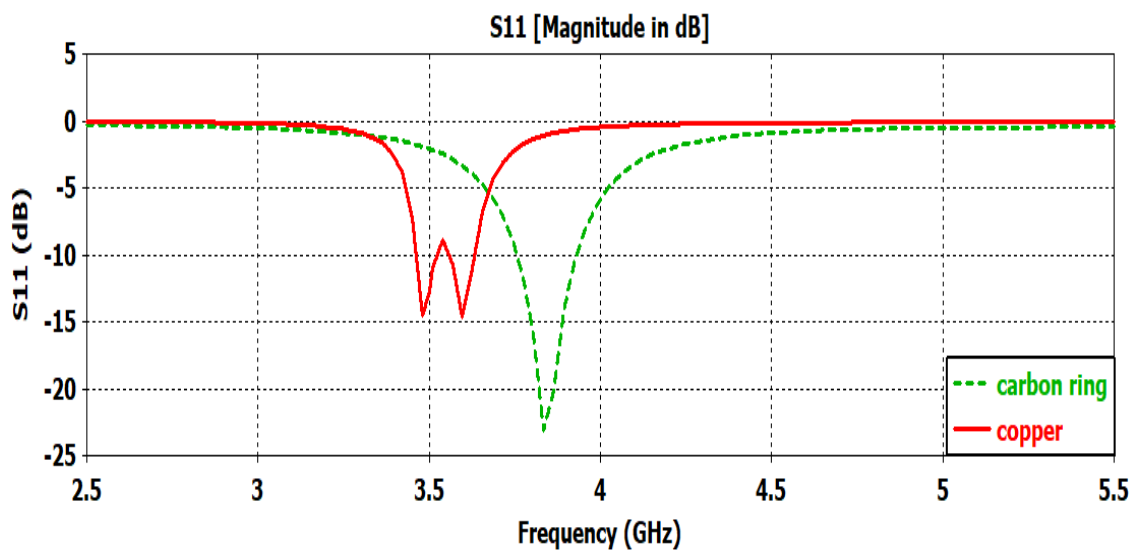


Figure 4.17 S_{11} of the double ring unit cell (open inner ring) with carbon ring.

The geometry of the double rings unit cells (open inner ring) for the cases of insertion of a carbon paste at one region at different places for each case of previous efforts are shown in Fig. 4.18.

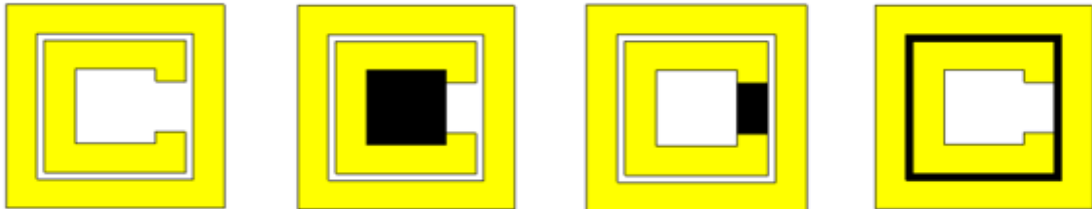


Figure 4.18 Geometry of the double ring unit cells (open inner ring) cases with carbon in one region of unit cell.

The variation of the reflection coefficient with frequency for the cases of inserting carbon paste into one region are shown in Fig. 4.19. The figure illustrates that the insertion of carbon as a ring in the space between two copper rings leads to an increase in the bandwidth to about 175 MHz, which is considered as the best result among the other cases but with changing the resonance frequency to about 3.8 GHz. The shift in the resonance frequency to a slightly higher value can be compensated for by a slight increase in the size of the rings.

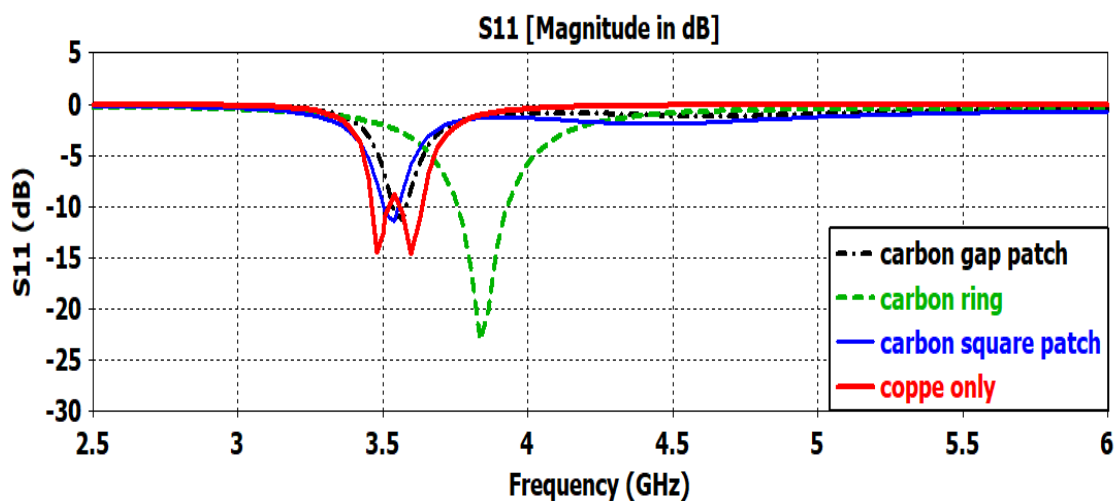


Figure 4.19 Reflection coefficient comparison of cases of unit cells with carbon in one region.

4.3.4 Double Rings with Opened Inner Ring Filled with Carbon Paste

This section investigates the case when using a carbon paste in two regions; inside the inner ring and in its opening as illustrated in Fig. 4.20. The unit cell dimensions are 18 mm×18 mm, $L1 = 14.15$ mm $L2 = 0.65 * L1 = 9.1975$ mm, and $w = 2$ mm.

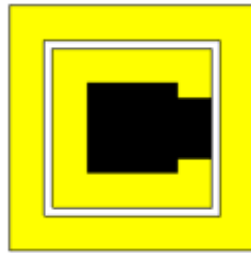


Figure 4.20 Double ring unit cell (open inner ring) with carbon in the square patch and at the inner ring opening.

Figure 4.21 displays the simulation results for the reflection coefficient (S_{11}) of the double ring unit cell, with the open inner ring filled with carbon paste. The obtained result is compared to that without using the carbon paste. The bandwidth is approximately 82 MHz, and the minimum value of the reflection coefficient is at 3.5 GHz. The placement of the carbon paste did not improve the performance.

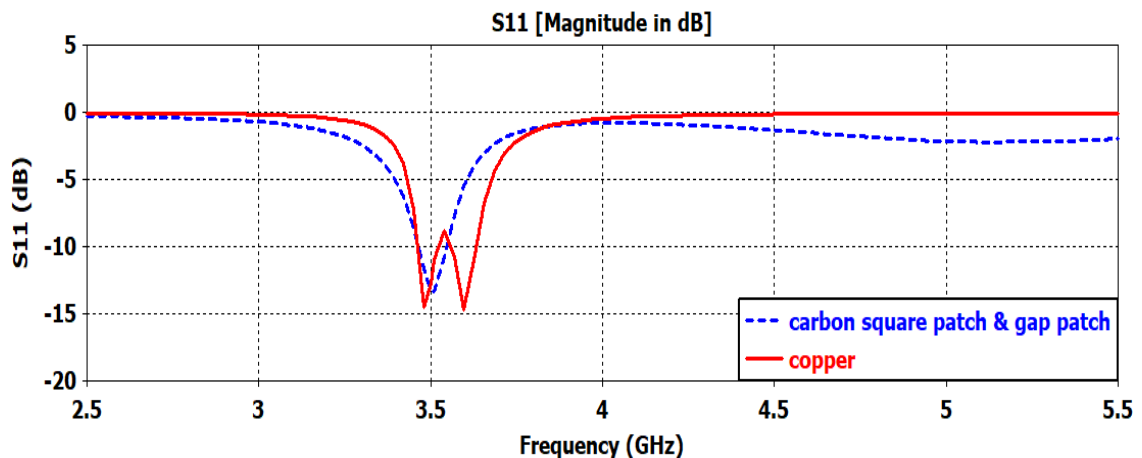


Figure 4.21 S_{11} of the double ring unit cell (open inner ring) with carbon in the square patch and at the space between two ends of the inner ring.

4.3.5 Double rings with opened inner ring, carbon ring and carbon patch

In this section, a double rings unit cell with an open inner ring and carbon paste placed at the square patch, and in between the two rings, as shown in Fig. 4.22, is investigated. The simulation results for the reflection coefficient (S_{11}) are shown in Fig. 4.23, which reveal that at 3.9 GHz the minimum value of the reflection coefficient is -20 dB, and the bandwidth is 282 MHz. Compared to the case without the carbon paste, the achieved bandwidth is larger and the minimum value of the reflection coefficient is smaller. Again, the shift in the frequency of minimum reflection can be compensated by an increase in the size of the ring.

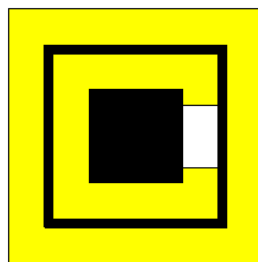


Figure 4.22 Double ring unit cell (open inner ring) with carbon ring and patch.

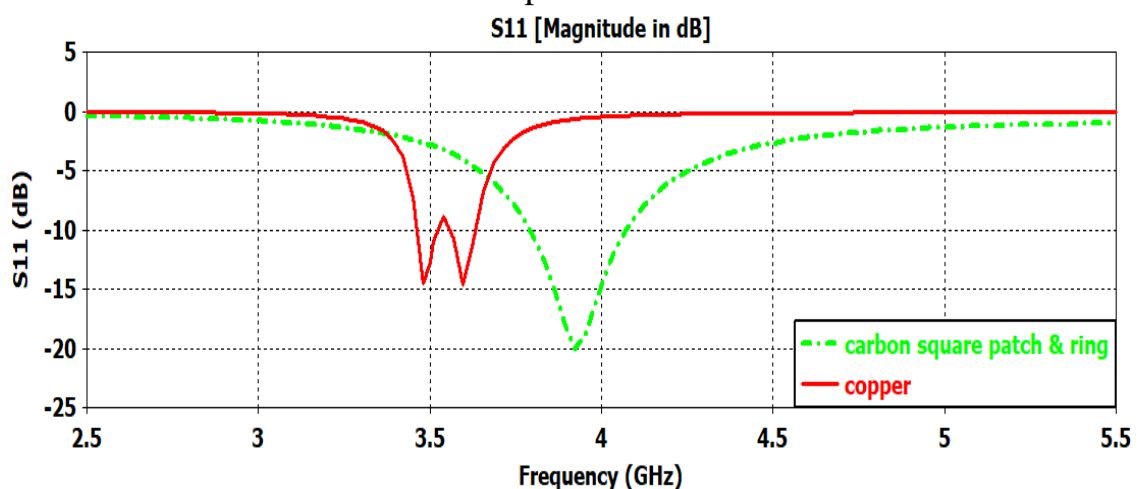


Figure 4.23 Reflection coefficient of the double ring unit cell (open inner ring) with carbon in the square patch and at the space between two rings.

4.3.6 Double Rings with Opened Inner and Carbon at the Inner Ring Opening and Carbon Ring

Figure 4.24 depicts the unit cell shape for the third case of inserting carbon paste in two regions; the opening of the inner and in between the two rings.

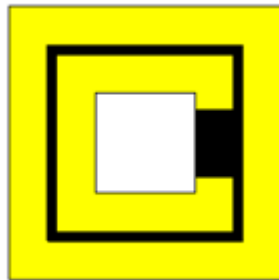


Figure 4.24 Double ring unit cell (with open inner ring) with carbon ring and carbon in the inner ring opening.

Figure 4.25 shows the obtained simulation results of the reflection coefficient (S_{11}) for the unit cell design shown in Fig. 4.24. The bandwidth and the frequency of the minimum reflection coefficient value are 225 MHz and 3.9 GHz, respectively. These values are better than those before adding the carbon paste.

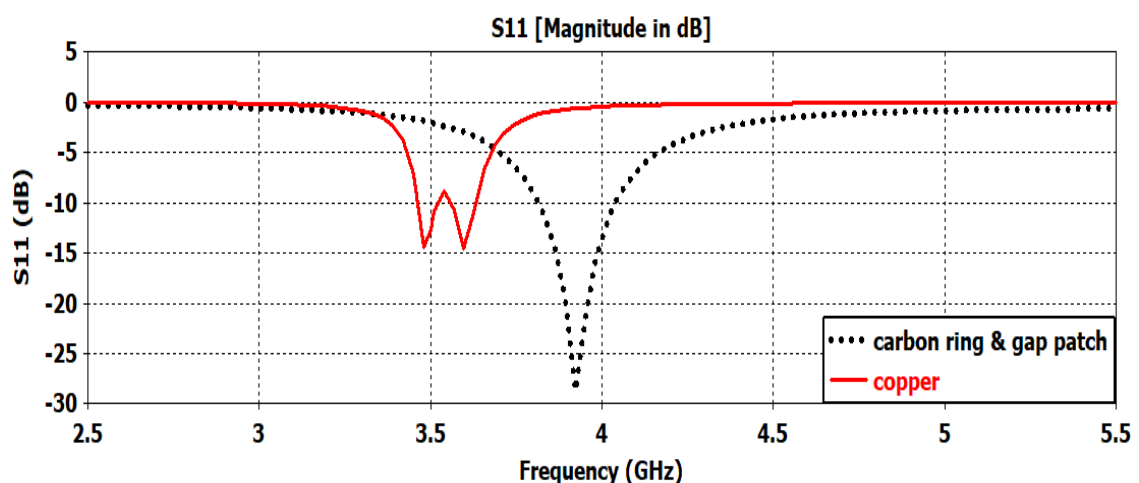


Figure 4.25 S_{11} of the double ring unit cell (open inner ring) with carbon ring and carbon in the inner ring opening together.

The geometries of the three previous cases of unit cells by adding carbon paste in two regions together are compared with the copper case as

shown in Fig. 4.26. The variations in the reflection coefficient with frequency for the three cases are shown in Fig. 4.27. The figure shows how the addition of carbon to the area between two rings and at a square patch at the center of the unit cell together increased the bandwidth to about 282 MHz, which was thought to be the best outcome of the studied cases, but at the expense of increasing the resonance frequency to 3.8 GHz (or by 8.6%). This shift in the frequency can be compensated for by increasing the size of the ring.

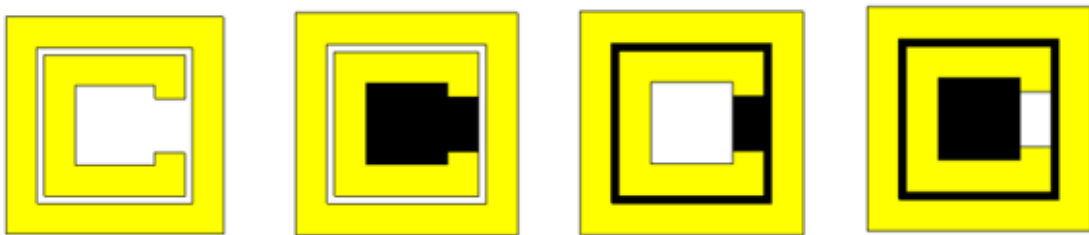


Figure 4.26 Geometries of the unit cells with carbon in two regions together compared with copper ring case.

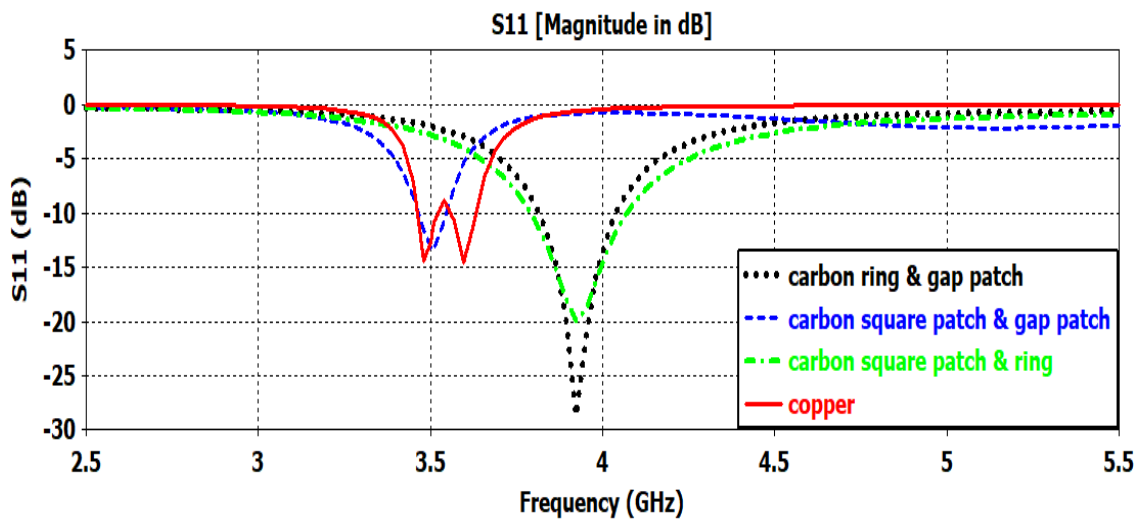


Figure 4.27 Reflection coefficient comparison of cases with carbon in two regions.

4.3.7 Double Rings with Opened Inner and Carbon Paste in between them

To demonstrate the impact of increasing the carbon region on the reflection coefficient S_{11} , the proposed unit cell is shown in Fig. 4.28-b, with the dimensions of 18 mm, $L1 = 14.15$ mm, $L2 = 0.65 * L1 = 9.1975$ mm, and $w = 2$ mm. Figure 4.29 shows the obtained reflection coefficient (S_{11}) results compared to the case without the carbon paste. The effect of adding the carbon paste is an increased bandwidth to 327 MHz, and the resonance frequency moved to 3.89 GHz.

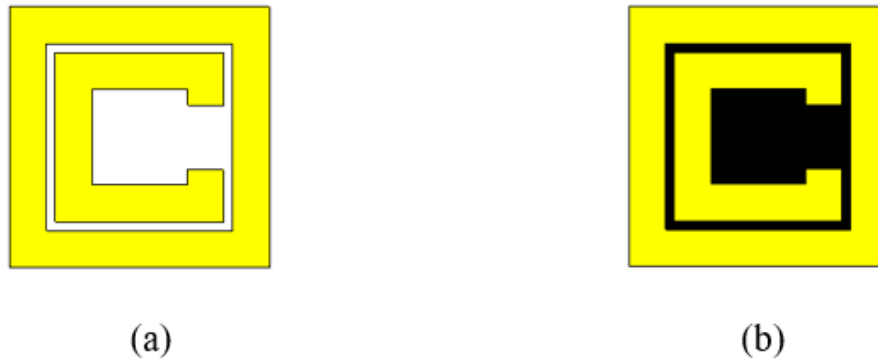


Figure 4.28 Unit cell geometry (a) copper rings (b) carbon at three regions together.

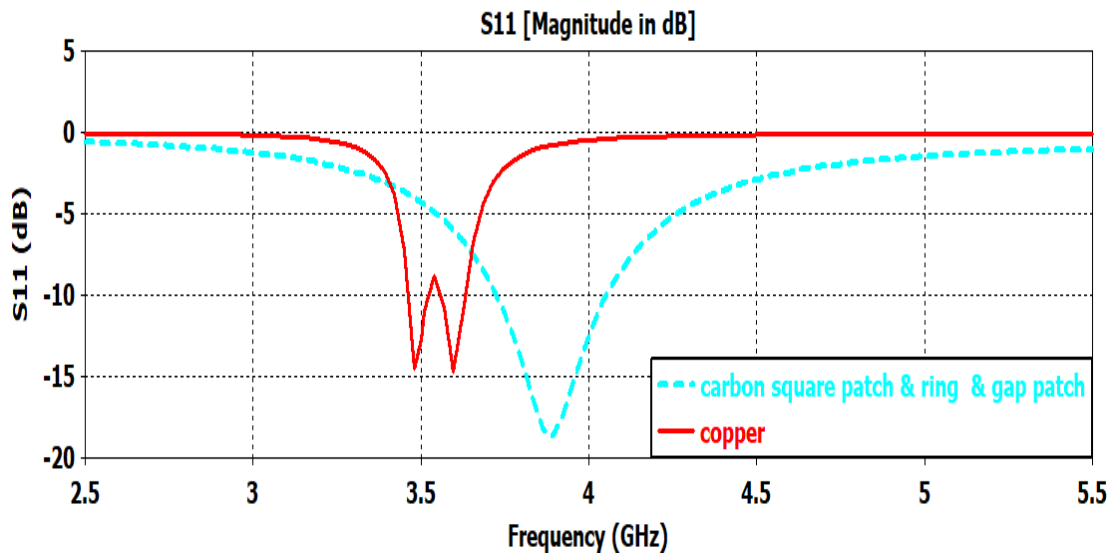


Figure 4.29 Variation of the reflection coefficient double ring unit cell (open inner ring) with carbon in three rings compared with the copper case.

The obtained results in the former sections are tabulated in Table 4.1 for comparison. It can be seen that the FSS unit cell of the double ring with an open inner ring has the best results collected according to the bandwidth of minimum reflection coefficient S_{11} by adding the carbon paste in three regions, but the value of S_{11} is less than other cases.

Table 4.1 Comparison of best results for cases of carbon region distribution.

Type of case	Resonance Frequency (GHz)	BW (MHz)	Min S_{11} (dB)
Copper rings	3.5	172	-14.2
Carbon paste at one region	3.8	175	-22.9
Carbon paste at two regions	3.92	282	-19.9
Carbon paste at three regions	3.89	327	-18.3

4.4 FSS Cells Using Rings of Carbon Paste

The proposed FSS unit cells in this section are formed of a carbon ground plane and rings printed with carbon on one side of the FR-4 substrate. The rings are divided into two cases, with the first case being a double closed carbon ring, while in the second case the inner is opened. The volume resistivity of the used carbon paste (ρ_v) = 0.833 $\Omega \cdot m$, volume conductivity of carbon paste (δ_v) = 1.2 S/m, density @25 °C = 1070 kg/m³.

4.4.1 Double Closed Rings Carbon Paste Unit Cell

In this case, the proposed unit cell includes a double ring of carbon paste with FR-4 substrate with relative permittivity $\epsilon_r=4.3$, and a thickness of $h=1.6$ mm is used. The unit cell dimensions are $L=19$ mm \times 19 mm, outer ring

side length $L_1 = 15.4$ mm, width of ring $W = 2$ mm, and the inner ring size $L_2 = 0.6 * L_1 = 9.24$ mm. Figure 4.30 shows the unit cell in two cases with carbon ground plane and copper ground plane respectively. The results of the simulations for the reflection coefficient (S_{11}) of the double ring unit cell are illustrated in Fig. 4.31, which shows that the first minimum value of the reflection coefficient has reached -21 dB at 10 GHz for the carbon ground plane case. However, the reflection coefficient (S_{11}) for the copper ground plane case doesn't reach the limit of -10 dB.



Figure 4.30 Geometry of the carbon rings unit cells (a) carbon ground plane, (b) copper ground plane.

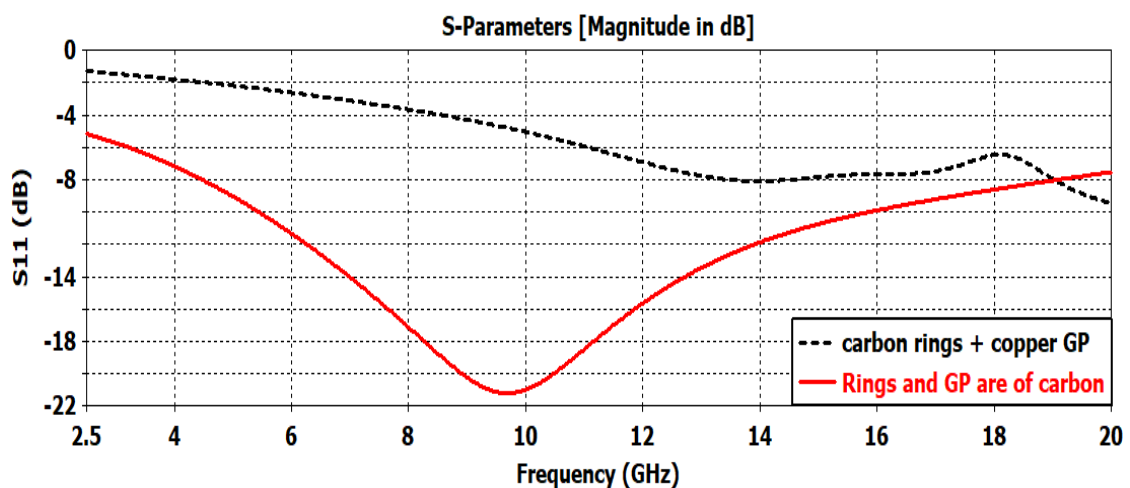


Figure 4.31 Reflection coefficient of the double ring unit cell for carbon ground plane and copper ground plane.

4.4.1.1 Carbon Ground Plane (GP) with Substrate Unit Cell

In this case, the suggested unit cell consists of FR-4 substrate with relative permittivity $\epsilon_r=4.3$ and a ground plane that's made of carbon paste (electric cond. =1.2 s/m, Rho=1070 kg/m³) with a thickness of 0.035 mm as illustrates in Fig. 4.32. Figure 4.33 shows the reflection coefficient (S_{11}) results indicating the frequency of minimum reflection coefficient at 9.7 GHz and 8.6 GHz, respectively. The corresponding bandwidths are 6.6 GHz and 10.4 GHz respectively.

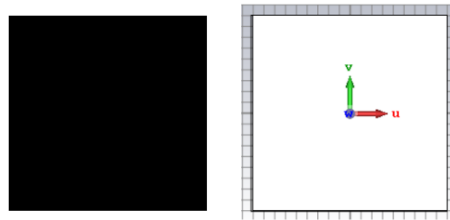


Figure 4.32 Unit cell geometry contains carbon GP and substrate.

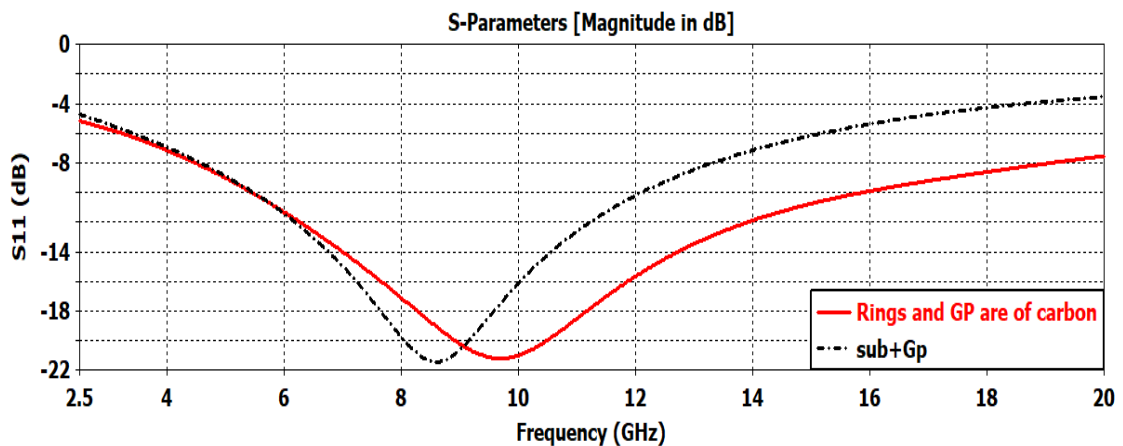


Figure 4.33 Variation of the reflection coefficient of unit cell contains carbon GP and substrate.

4.4.1.2 Ground Plane and Outer Ring of Carbon Paste

In this case, the suggested unit cell consists of FR-4 Substrate and carbon ground plane, and the outer ring is also of carbon paste. The unit cell dimensions $L=19\text{ mm}\times 19\text{ mm}$, outer ring side length $L_1=15.4\text{ mm}$, and width

of ring $W=2$ mm, as illustrated in Fig. 4.34. Figure 4.35 exhibits the reflection coefficient results (S_{11}) that indicate a bandwidth of 8.3 GHz, and the minimum value of the reflection coefficient is -41 dB at a frequency of 9.5 GHz.

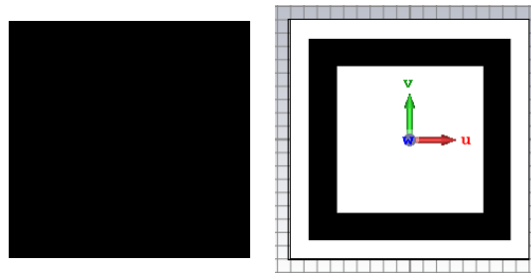


Figure 4.34 Unit cell geometry contains carbon GP and outer ring.

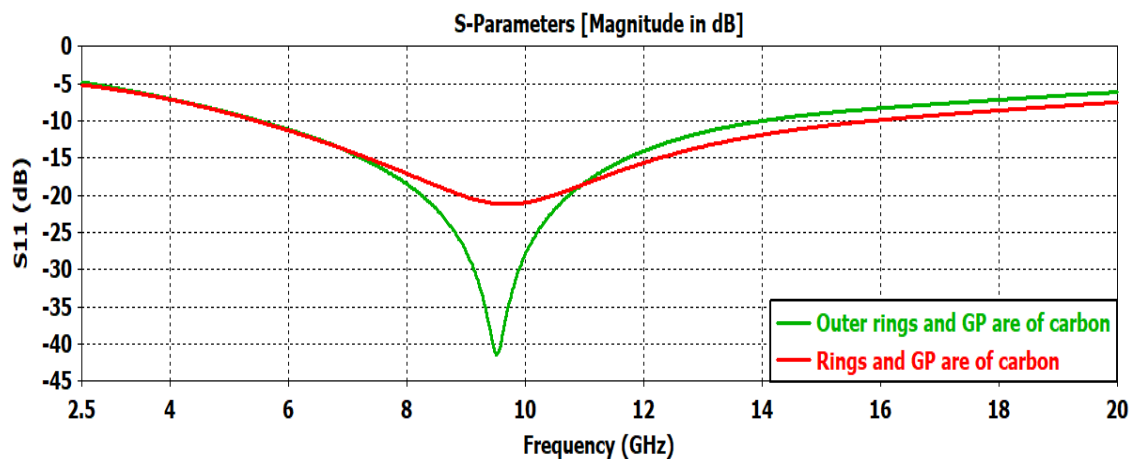


Figure 4.35 Variation of the reflection coefficient of unit cell which contains carbon GP and outer ring.

4.4.1.3 Carbon Ground Plane with Inner Ring

The proposed unit cell in this instance is composed of a FR-4 substrate, a carbon ground plane and an inner ring. The unit cell dimensions: $L=19$ mm x 19 mm, $L_2=0.6*L_1=9.24$ mm, and $W=2$ mm for the ring width, as shown in Fig. 4.36. The reflection coefficient response has achieved a bandwidth of 7.7 GHz, and the minimum reflection coefficient is -36.5 dB at a frequency of 9.6 GHz, as can be seen from Fig. 4.37.

The variation of the reflection coefficient with frequency for the previous cases are compared in Fig. 4.38, which illustrates that the carbon ground plane is responsible for the maximum effect on the bandwidth, and by using the double ring carbon paste is considered the best result among the other cases as regards to the bandwidth.

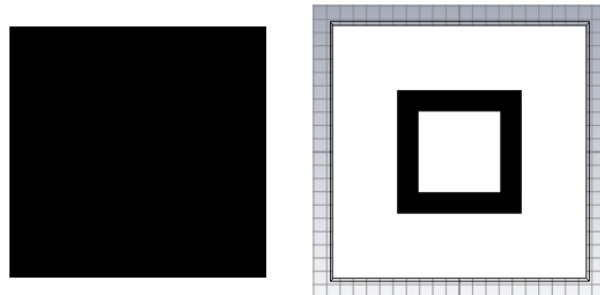


Figure 4.36 Unit cell geometry contains carbon GP and inner ring.

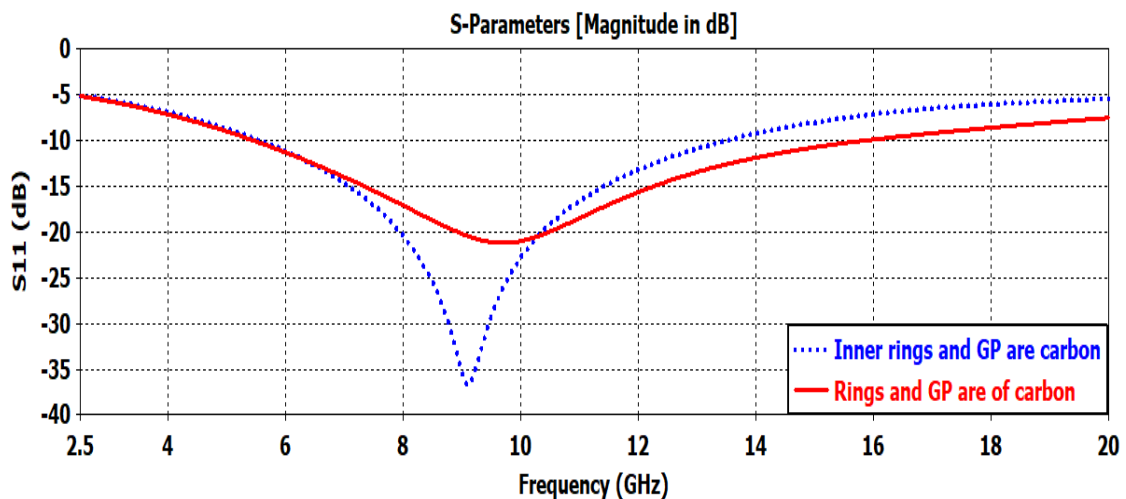


Figure 4.37 Reflection coefficient of the unit cell that contains carbon GP and inner ring.

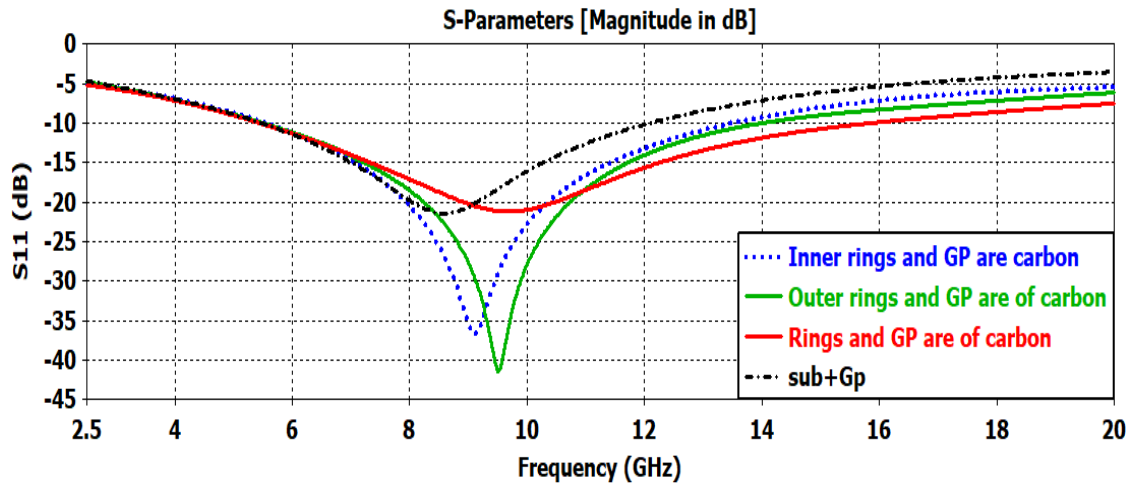


Figure 4.38 Reflection coefficient comparison for each case of closed ring carbon unit cell.

4.4.2 Double Ring (Open Inner Ring) Carbon Paste Unit Cell

In this case, a double ring of carbon paste (open inner ring) with a FR-4 substrate is employed in the suggested unit cell as shown in Fig.4.39. The unit cell in two cases with dimensions $L=18\text{ mm}\times 18\text{ mm}$, outer ring side length $L_1=15.1\text{ mm}$, width of ring $W=2\text{ mm}$, and the inner ring size $L_2=0.6*L_1=9.06\text{ mm}$. The results of the reflection coefficient (S_{11}) of the double ring unit cell is illustrated in Fig. 4.40, which shows that the minimum value of the reflection coefficient is -17.5 dB at 8.4 GHz for the carbon GP plane case, while the reflection coefficient (S_{11}) for cooper GP case doesn't reach to -10 dB even up to 20 GHz frequency.

Unit cells were employed for the ground plane (GP) with substrate only, GP with substrate and inner ring, and GP with substrate and inner ring to explore the effects of the ground plane and each ring on the resonance frequency and the reflection coefficient, as shown in the following subsections.



Figure 4.39 Geometry of double ring (open inner ring) unit cells (a) carbon GP, (b) copper GP.

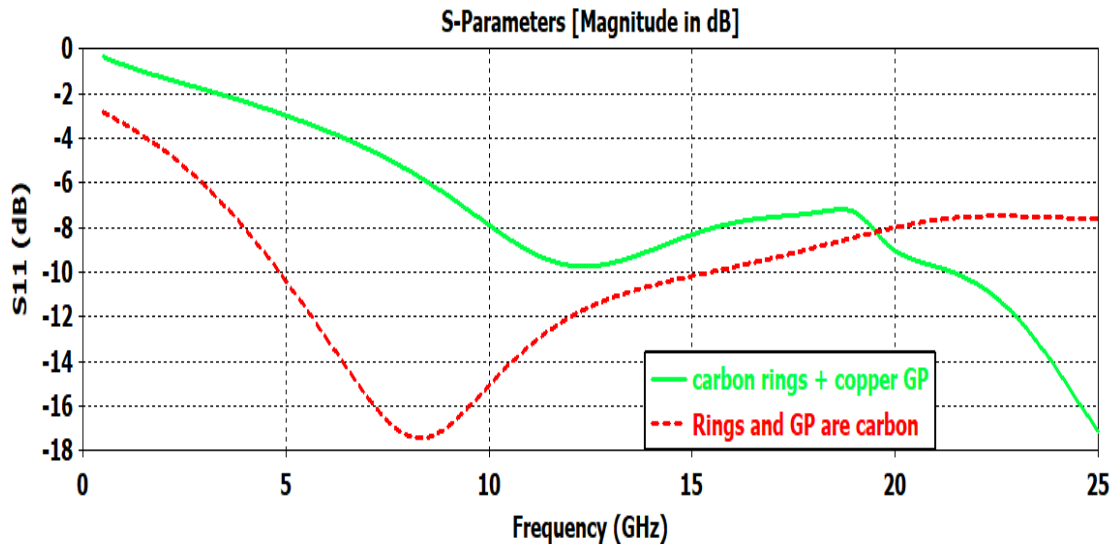


Figure 4.40 Reflection coefficient of the double ring (open inner ring) unit cell for carbon GP and copper GP.

4.4.2.1 Carbon Ground Plane with Substrate Unit Cell

As shown in Fig. 4.30, the recommended unit cell, in this case, consists of a carbon paste ground plane with a thickness of 0.035 mm and a FR-4 substrate with a relative permittivity of 4.3 and 1.2 s/m. Figure 4.41 shows the reflection coefficient (S_{11}) simulation results of the unit cell (carbon paste GP and substrate). The values are shown for the bandwidth and the frequency of minimum reflection coefficient values are 6.6 GHz and 8.5 GHz, respectively.

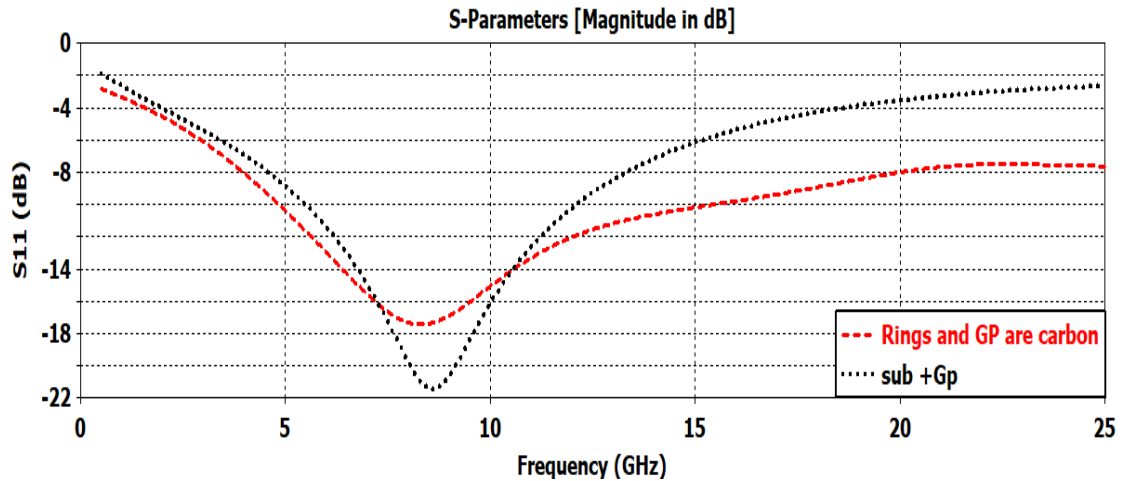


Figure 4.41 variation of the reflection coefficient of the unit cell containing carbon GP and substrate.

4.4.2.2 Carbon Ground Plane with Outer Ring

In this case, the proposed unit cell is constructed of a FR-4 substrate, a carbon GP with an electrical cond. of 1.2 s/m, and an outside ring also made of carbon paste, as shown in Fig. 4.34, and the unit cell has the following dimensions: $L=18\text{ mm}\times 18\text{ mm}$, $L_1 = 15.1\text{ mm}$ for the outer ring side, and $W=2\text{ mm}$ for the ring width. Figure 4.42 exhibits the reflection coefficient's results (S_{11}) of the unit cell where the bandwidth is 9.2 GHz, and the minimum value of the reflection coefficient is -23 dB at a frequency of 9.8 GHz. It is noticed that inserting the ring doesn't make a large effect on resonance frequency but reduces the reflection coefficient by 6 dB, and also increases the bandwidth.

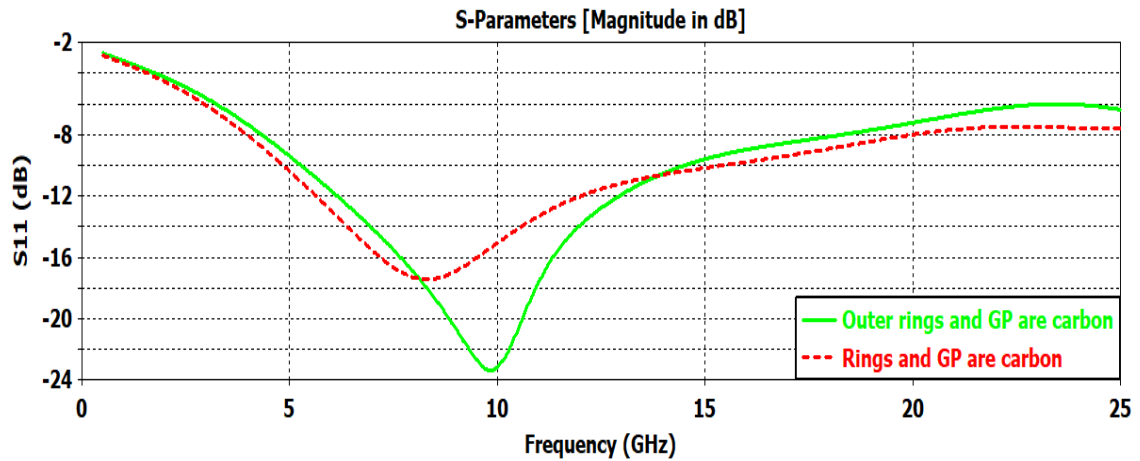


Figure 4.42 Reflection coefficient of the unit cell that contains carbon GP and outer ring.

4.4.2.3 Carbon Ground Plane with Opened Inner Ring

The proposed unit cell in this instance is composed of a FR-4 substrate, a ground plane made of carbon paste, and an outside ring also made of carbon paste. The unit cell dimensions: $L=18$ mm x 18 mm, $L_2=0.6*L_1=9.06$ mm, and the space between two ends of the inner ring is 3.5 mm, and $W=2$ mm for the ring width, as shown in Fig. 4.43. The obtained frequency response for this unit cell (Fi4.44) shows a bandwidth is 8.5 GHz, and the minimum value of the reflection coefficient is -43 dB at a frequency of 8.45 GHz.

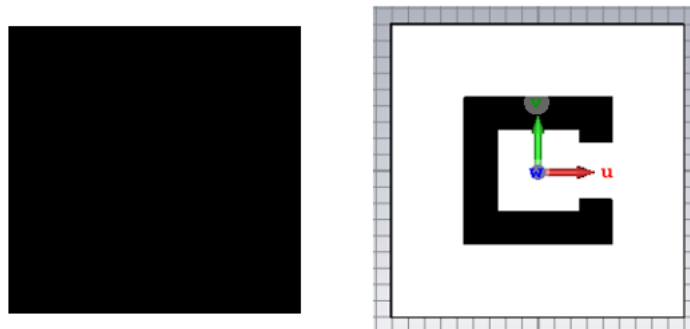


Figure 4.43 Unit cell geometry contains carbon GP and an open inner ring.

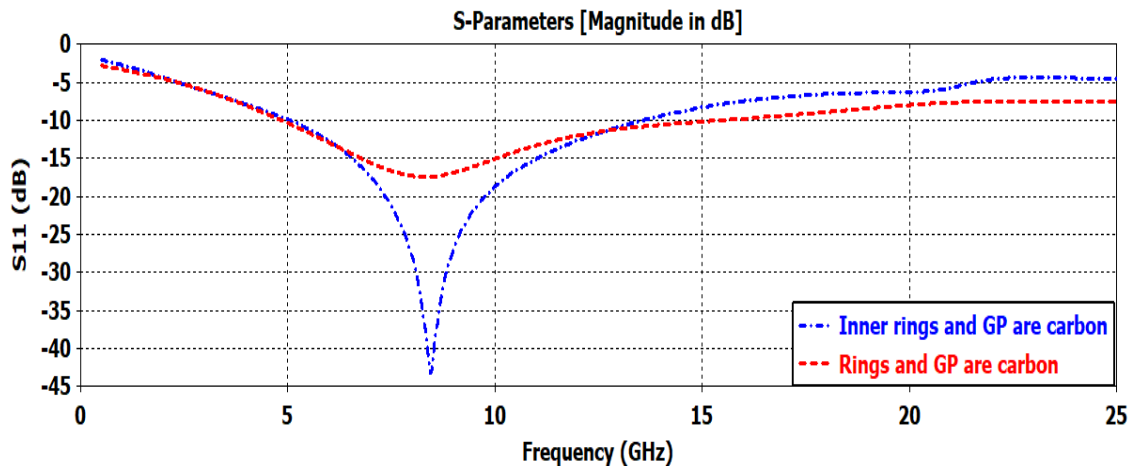


Figure 4.44 Reflection coefficient for the unit cell that contains carbon GP and inner ring.

The variation of the reflection coefficient with the frequency for the previous cases is compared as shown in Fig. 4.45. This figure illustrates that the double ring of carbon with the ground plane is considered the best result among the other cases according to the bandwidth, the value of the bandwidth is about 10.3 GHz, but the value of the reflection coefficient is somehow larger but still less than -17 dB than other cases.

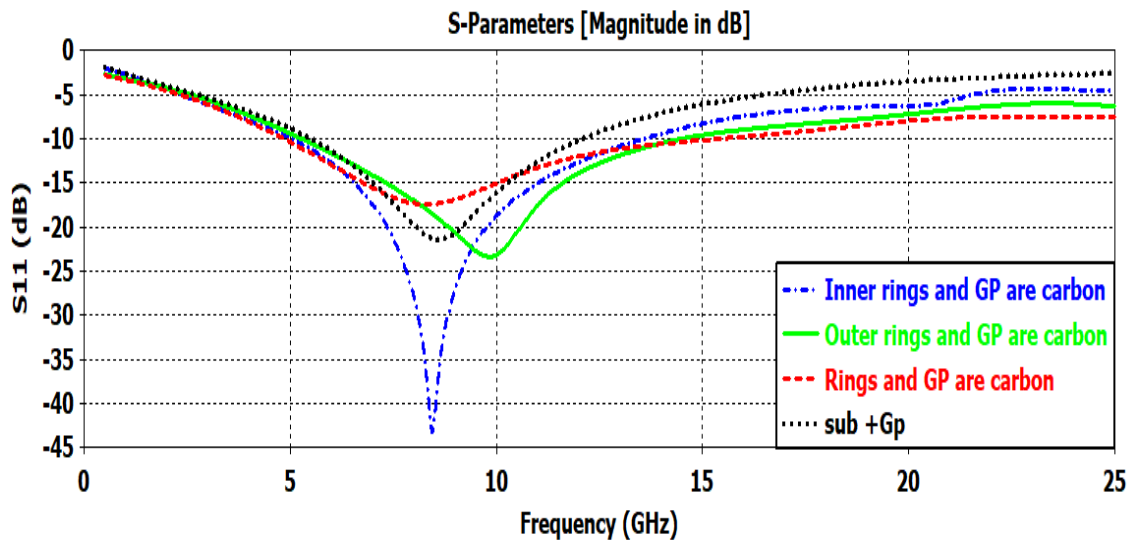


Figure 4.45 Reflection coefficient comparison for each case of carbon unit cell.

4.5 Effect of Changing Parameters on Single Ring Carbon Paste Unit Cell

This section focused on the effect of changing some parameters on the unit cell like: the side length of the ring, the width of the ring, the thickness of the carbon paste, and conductivity on the values of reflection coefficient and bandwidth. The following subsections deal with the parameter changes according to the reflection coefficient value, frequency of minimum S_{11} , and bandwidth.

4.5.1 Changing the Side Length of the Ring

In the beginning, this subsection discusses the effect of changing the side length (L_1) of the single ring unit cell. The proposed unit cell includes a single ring of carbon paste. The unit cell dimensions $L=19\text{ mm}\times 19\text{ mm}$, the width of ring $W=0.1*L_1\text{ mm}$, as seen in Fig. 4.34. The variation of reflection coefficient is shown in Fig.4.46 for various values of the side ring length (6 to 18) mm, also Table 4.2 contains more details on the results of the ring lengths.

From Fig. 4.46, it can be seen that the changing of ring length doesn't affect the resonance frequency, as it remained about 9.25 GHz, for sides sizes (L_1) between 6 mm and 18 mm. However, the minimum value of the reflection coefficient (S_{11}) varied between -24 dB to -46 dB. On the other hand, the bandwidth changed between 7 GHz to 9.5 GHz.

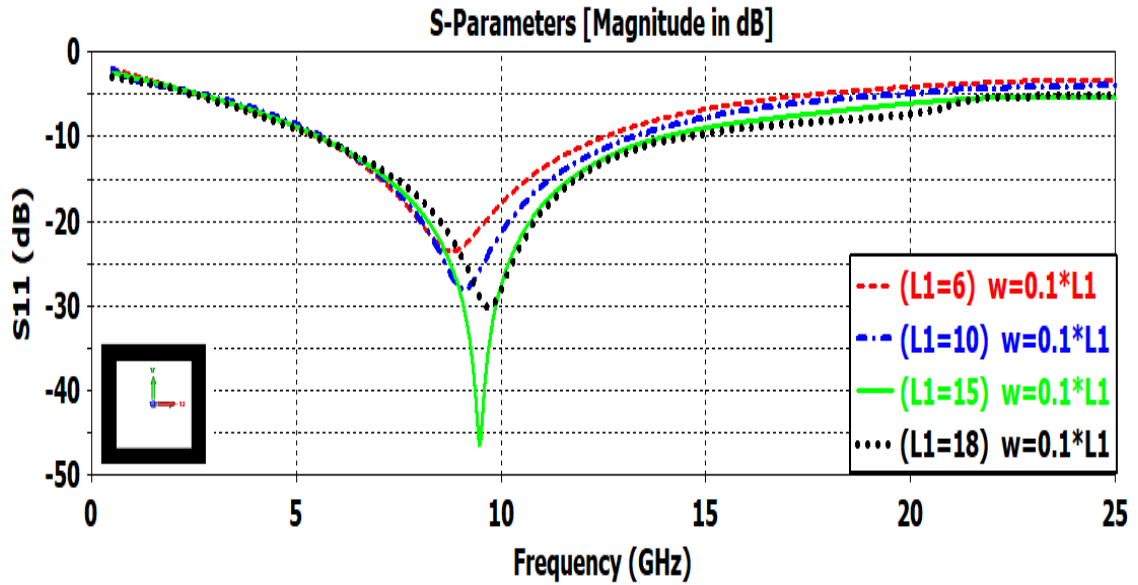


Figure 4.46 Reflection coefficient comparison for changing the side length of the ring with $w=0.1*L1$.

In this subsection, a single ring of width $W=2$ mm was used while in the previous case $0.1*L1$ was used as the width of the ring, as seen in Fig. 4.34. Figure 4.47 show the reflection coefficient response S_{11} by changing the ring widths for various ring length. Table 4.2 deals with more detailed results for various ring side lengths with using two cases of ring width to compare the results.

From Fig. 4.47 and Table 4.2, it is noticed that: The frequency of Min. S_{11} remained at about 9.35 GHz, indicating small resonance sensitivity, the value of the minimum S_{11} changed between -23.55 dB and -66.5 dB, and the bandwidth changed between 7.03 GHz and 9.566 GHz

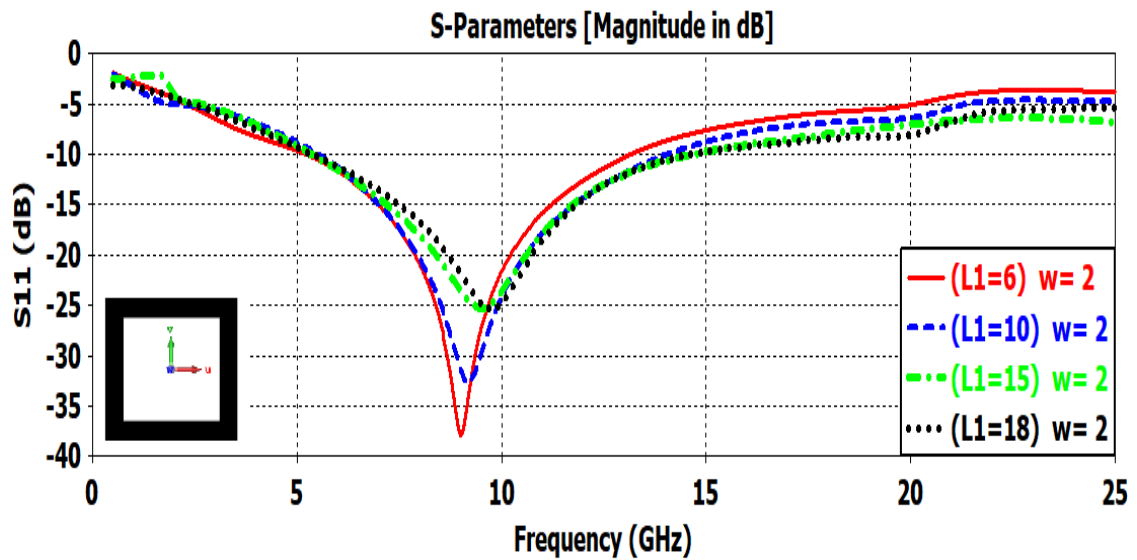


Figure 4.47 Reflection coefficient comparison for changing the side length of the ring with $W = 2$.

Table 4.2 Simulation results of changing side ring length, and ring width.

Ring side length (mm)	Ring width (mm)	Freq. of Min. S_{11} (GHz)	Min. S_{11} (dB)	BW (GHz)
6	0.6	8.8	-23.55	7.03
6	2	9.02	-37.82	7.92
8	0.8	8.94	-25.16	7.28
8	2	9.1	-66.5	7.956
10	1	9.1	-28	7.67
10	2	9.2	-32.6	8.594
13	1.3	9.34	-38.08	8.27
13	2	9.4	-26.2	9.34
14	1.4	9.42	-46.55	8.437
14	2	9.45	-25.52	9.566
15	1.5	9.48	-46.4	8.44
15	2	9.51	-25.52	9.28
16	1.6	9.54	-36.8	8.437
16	2	9.55	-25.05	8.97
17	1.7	9.62	-33.4	8.576
17	2	9.64	-25.3	8.74
18	1.8	9.7	-30.2	9.017
18	2	9.74	-25.36	9.12

4.5.2 Changing the Thickness of The Ground Plane

In the second case of the single ring unit cell, as seen in Fig. 4.34, there was a change in the carbon thickness from (0.035 to 2) mm. Figure 4.48 shows the effect of changing GP thickness on the reflection coefficient S_{11} . From Fig. 4.48 its noticed that with changing of carbon GP thickness, the value of the reflection coefficient (S_{11}) response doesn't affected and it stayed as same as for other values of GP thickness

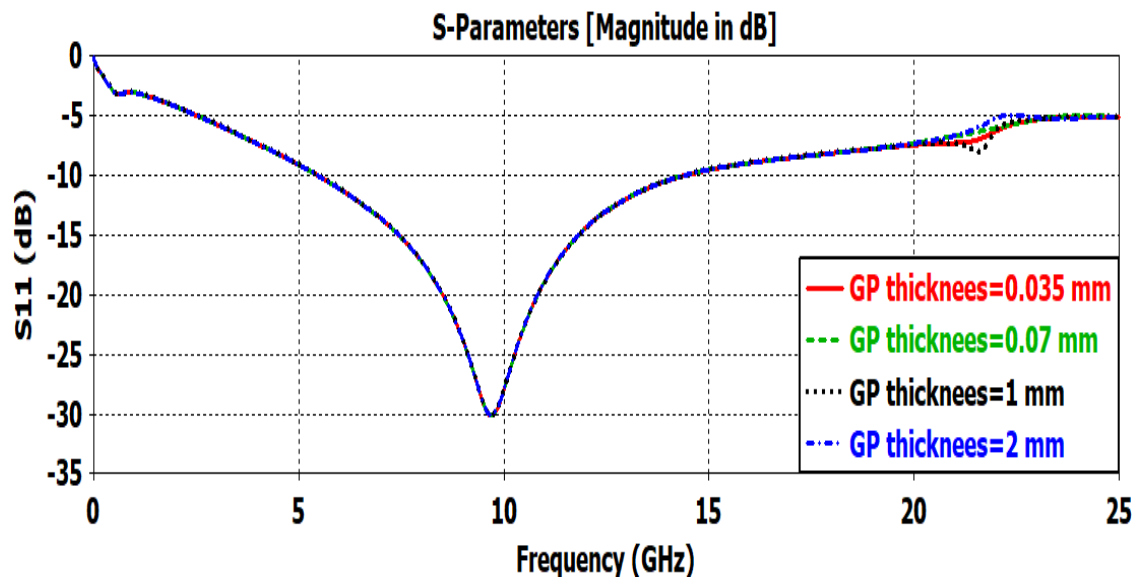


Figure 4.48 Reflection coefficient comparison for changing carbon ground plane thickness.

4.5.3 Changing the Conductivity of the Carbon Paste

The following case show the results of changing the side length of ring, width of ring and conductivity, altogether. Table 4.3 shows the S_{11} response by changing the conductivity to (1, 1.5, 5, 10, 50 and 100) s/m, and using two ring widths (0.1*L1 mm and 2 mm) for each ring length. (6, 10, 15, and 18) mm and frequency of minimum value of S_{11} .

Table 4.3 simulation results of changing length, width, and conductivity.

Ring side length (mm)	Ring width (mm)	Conductivity value (s/m)	Freq. of Min. S ₁₁ (GHz)	Min. S ₁₁ (dB)	BW (GHz)
6	0.6	1	8.24	-22.03	6.82
6	2	1	8.45	-31.75	7.38
6	0.6	1.5	9.5	-25.5	7.26
6	2	1.5	9.75	-57.2	8.02
6	0.6	5	13.85	-28.2	8.2
6	2	5	14.06	-35.55	8.67
6	0.6	10	16.3	21.5	7.9
6	2	10	16.3	-30.94	8.87
6	0.6	50	20.1	-11.04	3.15
6	2	50	19.6	-15.35	6.24
6	0.6	1000	18.76	-5.24	0
6	2	1000	19.21	-14.8	0.533
10	1	1	8.54	-25.28	7.45
10	2	1	8.634	-43.87	8.36
10	1	1.5	9.83	-32.3	7.83
10	2	1.5	9.88	-27.45	8.72
10	1	5	14.23	-45.8	8.81
10	2	5	14.65	-21	9.35
10	1	10	16.75	-29.55	8.64
10	2	10	16.5	-23.9	9.53
10	1	50	20.6	-12.55	4.6
10	2	50	20.8	-19.92	6.77
10	1	1000	15.82	-9.12	0
10	2	1000	15.98	-26	0.519
15	1.5	1	8.93	-39.36	8.41
15	2	1	9	-28.17	9.16
15	1.5	1.5	10.18	-33.23	8.55
15	2	1.5	10.15	-22.7	9.28
15	1.5	5	13.95	-23.2	9.48
15	2	5	13.6	-17	9.7
15	1.5	10	15.72	-23.7	9.06
15	2	10	15.3	-16.3	8.89
15	1.5	50	20.82	-21.76	6.74
15	2	50	20.58	-31	7.06
15	1.5	1000	18.06	-35.98	0.439

15	2	1000	17.75	-40	0.51
18	1.8	1	9.2	-36.25	9.14
18	2	1	9.28	-28.58	9.51
18	1.8	1.5	10.32	-26.34	8.67
18	2	1.5	10.33	-22.95	8.82
18	1.8	5	13.65	-19.9	7.15
18	2	5	13.6	17.7	6.69
18	1.8	10	15.35	-21.38	9
18	2	10	15.3	-18.55	5.5
18	1.8	50	17.45	-23.65	7.69
18	2	50	17.26	-27.9	2.62
18	1.8	1000	21.56	-22.4	3.82
18	2	1000	23.36	-19.6	4

From Table 4.3, it can be seen that by increasing the width of the ring with same conductivity will cause an increase in resonance frequency and the bandwidth. However, when increasing the conductivity with same width of ring the cell will suffer from increasing in the bandwidth until conductivity about 5 the bandwidth starts to decrease by increasing the conductivity.

CHAPTER FIVE
CONCLUSIONS AND
FUTURE WORK

CHAPTER FIVE

CONCLUSIONS AND FUTURE WORK

5.1 Conclusions

The radar cross-section (RCS), which is a measurement of a target's ability to reflect the incoming radar wave, is an important parameter characterizing a wide range of objects like airplanes, drones, rockets, and ships. There has been an increasing interest in the reduction of the radar cross-section of objects for a wide range of applications. Due to their lower electromagnetic wave reflection than metals, composite materials like wood and materials were first used to make airplanes in an effort to lessen their detectability. Other synthetic materials have later been used to reduce the radar cross-section.

The dissertation deals with radar cross-section of the targets and studies how it can be reduced using single-layer frequency-selective surfaces (FSS) unit cells. The goal of this study is to develop FSS unit cells with a low reflection coefficient so that they may be used to reduce the radar cross-section. The investigations comprises theoretical analysis and simulations using the CST Microwave Studio. The main contributions of this dissertation can be summarized as follows:

- 1- The targets intended for decreasing the radar cross-section are often conductive items. As a result, conductive ground planes should be present on the FSS surfaces that will be suggested as solutions for reducing the cross-section of these items.
- 2- The scattering parameters can be used for assessing the performance of the designed FSS unit cells that are suggested in order to achieve wide band capabilities. To reduce the thickness of the FSS radar absorber, the air gaps between the resonating rings and the ground plane can be removed.

- 3- The elements of the FSS unit cell, which has the form of closed ring resonates at a frequency such that the average circumference of the ring equals the effective wavelength. The value of the effective wavelength is influenced by the permittivity of the substrate, its thickness, and the ring width.
- 4- When two rings or loops are used, two minima are obtained in the frequency response of the reflection coefficient. The two resonance frequencies are related to sizes of the two rings.
- 5- The use of another smaller ring in addition to the first outer ring was agreed upon in order to combine the two bands that were acquired into one bigger band and improve the bandwidth of the absorber.
- 6- The reason of using closed rings in the unit cell is that the circular form offers similar responses to the incident vertical and horizontal polarizations.
- 7- It has been demonstrated that the dual band of the double ring design can be developed to offer a single and wide band by employing a split inner ring with the outer ring. That is based on the observation that an open ring resonates when its circumference is half the effective wavelength, circumference of the inner ring = $\frac{1}{2} \lambda_e$ at the resonance frequency. Additionally, the space between the two ends of the open ring influences the resonance frequency and may be utilized to modify it.
- 8- The intention from meandering the inner ring and expanding its circumference is to achieve nearly equal value to that of the outer ring in order to combine the bandwidth that results from the outer ring and inner ring together.
- 9- As a result of the meandering and splitting, a polarization-sensitive property is produced.

- 10- The employment of resistive sheets or rings in addition to the conducting elements showed more reduction in the reflection coefficient as the resistive sheet provides power-absorbing component.
- 11- The results demonstrate that as sheet resistance is increased above (3 /sq), reflection coefficients start to fall for all frequencies and the deep nulls due to the resonance begin to disappear at double closed resistive ring.
- 12- For the proposed FSS cells, where the carbon paste was used, the conductivity, paste thickness, ring size changes, and different combinations of components were all found to affect the performance of the FSS unit cells.
- 13- The insertion of the carbon paste into the FSS unit cell reduces the reflection coefficient and enhanced the bandwidth but caused a shifting in the resonance frequency. The shift in the resonance frequency can be compensated by a slight change in the size of the rings.

5.2 Future Works

The following aspects can be considered to extend the work done in this dissertation:

- 1- Investigation of other shapes like the circular one for the unit cell that is expected to give better performance in bandwidth and reflection coefficient as it has full circular symmetry.
- 2- Assessing the performance of the FSS for the cases of oblique incidence and the equivalent circuit under different angles of incidence.
- 3- Investigation of the convoluted unit cell and finding the equivalent circuit and the resonance frequencies.
- 4- Searching for the relation between the resonance frequency, the ring dimensions and the resistivity of the carbon paste.

REFERENCES

References

- [1] H. Ucar, "Radar Cross Section Reduction," *J. Nav. Sci. Eng.*, vol. 9, pp. 72–87, Apr. 2013.
- [2] "Radar Cross Section", *Electronic Warfare and Radar Systems Engineering Handbook*, Avionics Department of the Naval Air Warfare Center Weapons Division, 2003.
- [3] E. F. Knott, J. F. Shaeffer, and M. T. Tuley, *Radar Cross Section*. IET Digital Library, 2004. doi: 10.1049/SBRA026E.
- [4] N. Yu and F. Capasso, "Flat optics with designer metasurfaces," *Nat. Mater.*, vol. 13, no. 2, Art. no. 2, Feb. 2014, doi: 10.1038/nmat3839.
- [5] H.-J. Li, N. H. Farhat, and Y. Shen, "Radar Cross Section Reduction by Absorber Covering," *Journal of Electromagnetic Waves and Applications*, vol. 3, Feb. 1989, doi: 10.1163/156939389X00467.
- [6] E. Ongareau, A. Roussaud, E. Marouby, and J. Levrel, "Radar cross-section reduction by polarization rotation," *Microwave and Optical Technology Letters*, vol. 8, pp. 316–318, Apr. 1995, doi: 10.1002/mop.4650080616.
- [7] C. B. Wilsen and D. B. Davidson, "The radar cross section reduction of microstrip patches. 1996, p. 733 vol.2. doi: 10.1109/AFRCON.1996.562980.
- [8] S.-C. Zhao, B.-Z. Wang, and Q.-Q. He, "Broadband radar cross section reduction of a rectangular patch antenna," *Progress in Electromagnetics Research-pier - PROG ELECTROMAGN RES*, vol. 79, pp. 263–275, Jan. 2008, doi: 10.2528/PIER07101002.
- [9] S. Parit and V. G. Kasabegoudar, "Ultra Wideband Antenna with Reduced Radar Cross Section," *Int. J. Electromagn. Appl.*, vol. 6, pp. 23–30, Jun. 2016, doi: 10.5923/j.ijea.20160602.01.
- [10] W. Chen, "Radar cross section reduction using electromagnetic band-gap checkerboard surfaces," PhD Thesis, Arizona State University, 2016.

Accessed: Jun. 05, 2022. [Online]. Available: <https://keep.lib.asu.edu/items/155120>.

[11] J. Su, Y. Lu, J. Liu, Y. Yang, Z. Li, and J. Song, "A Novel Checkerboard Metasurface Based on Optimized Multielement Phase Cancellation for Super-wideband RCS Reduction," *IEEE Trans. Antennas Propag.*, vol. PP, pp. 1–1, Sep. 2018, doi: 10.1109/TAP.2018.2870372.

[12] G. Shen, M. Zhang, Y. Ji, W. Huang, H. Yu, and J. Shi, "Broadband terahertz metamaterial absorber based on simple multi-ring structures," *AIP Adv.*, vol. 8, no. 7, p. 075206, Jul. 2018, doi: 10.1063/1.5024606.

[13] J. Zhang, H. Li, Q. Zheng, J. Ding, and C. Guo, "Wideband radar cross-section reduction of a microstrip antenna using slots," *Int. J. Microw. Wirel. Technol.*, vol. 10, pp. 1–6, Aug. 2018, doi: 10.1017/S1759078718000569.

[14] L. Ali, Q. Li, T. Khan, J. Yi, and X. Chen, "Wideband RCS Reduction Using Coding Diffusion Metasurface," *Materials*, vol. 12, Aug. 2019, doi: 10.3390/ma12172708.

[15] F. Wang, K. Li, Y. Ren, and Y. Zhang, "A novel reconfigurable FSS applied to the antenna radar cross section reduction," *Int. J. RF Microw. Comput.-Aided Eng.*, vol. 29, p. e21729, Jul. 2019, doi: 10.1002/mmce.21729.

[16] M. I. Hossain, N. Nguyen Trong, K. Sayidmarie, and A. Abbosh, "Equivalent-Circuit Design Method for Wideband Nonmagnetic Absorbers at Low Microwave Frequencies," *IEEE Trans. Antennas Propag.*, vol. PP, pp. 1–1, Apr. 2020, doi: 10.1109/TAP.2020.2983756.

[17] M. Nadi, S. H. Sedighy, and M. Khalaj-Amirhosseini, "Ultra Wideband Radar Cross Section Reduction by using non-Resonant Unit Cells," *Sci. Rep.*, May 2020, doi: 10.1038/s41598-020-64362-0.

[18] R. Jaiswar, F. Mederos-Henry, V. Dupont, S. Hermans, J.-P. Raskin, and I. Huynen, "Inkjet-printed frequency-selective surfaces based on carbon nanotubes for ultra-wideband thin microwave absorbers," *J. Mater. Sci. Mater.*

Electron., vol. 31, pp. 2190–2201, Feb. 2020, doi: 10.1007/s10854-019-02751-6.

[19] S. Ünalı, H. Bodur, S. Cimen, and G. Çakir, “RCS Reduction of Reflectarray Using New Variable Size FSS Method,” *AEU - International Journal of Electronics and Communications*, vol. 117, p. 153098, Apr. 2020, doi: 10.1016/j.aeue.2020.153098.

[20] J. Y. Jeong et al., “Fabrication and characterization of resistive double square loop arrays for ultra-wide bandwidth microwave absorption,” *Sci. Rep.*, vol. 11, Jun. 2021, doi: 10.1038/s41598-021-91868-y.

[21] Y. Xi, W. Jiang, T. Hong, K. Wei, and S. Gong, “Wideband and wide-angle radar cross section reduction using a hybrid mechanism metasurface,” *Opt. Express*, vol. 29, Jun. 2021, doi: 10.1364/OE.429972.

[22] Y. Chen, X.-X. He, Y. Yang, H.-Y. Hu, F.-K. Li, and L. Yang, “Dynamic RCS Reduction Performances of Antenna Array with Coding Metasurface,” *Int. J. Antennas Propag.*, vol. 2022, p. e4644566, Mar. 2022, doi: 10.1155/2022/4644566.

[23] S. Huo et al., “Analysis of a Novel Resistive Film Absorber for Suppression of Electromagnetic Radiation in System-in-Packages,” *Int. J. Antennas Propag.*, vol. 2022, p. e7674970, Mar. 2022, doi: 10.1155/2022/7674970.

[24] P. Megh Sainadh, L. Banoth, A. Sharma, K. V. Srivastava, and S. Ghosh, “A frequency-selective absorber with wideband absorption and in-band transmission using resistive ink,” *Microw. Opt. Technol. Lett.*, May 2022, doi: 10.1002/mop.33327.

[25] M. Shukoor, S. Dey, and S. Koul, “Broadband polarization insensitive wide angular stable dual-split square ring circuit analog absorber for radar cross section and electromagnetic interference shielding applications,” *Int. J. RF Microw. Comput.-Aided Eng.*, vol. 32, May 2022, doi: 10.1002/mmce.23085.

- [26] K. R. Jha, Z. A. P. Jibrán, and S. K. Sharma, "Absorption Peak Controlled Low-Frequency Wideband Flexible FSS Absorber," *IEEE Transactions on Electromagnetic Compatibility*, pp. 1–10, 2022, doi: 10.1109/TEMPC.2022.3159746.
- [27] M. I. Skolnik, *Introduction to radar systems*, 2d ed. New York: McGraw-Hill, 1980.
- [28] L. Niu, Y. Xie, P. Wu, and C. Zhang, "ARCS: Active Radar Cross Section for Multi-Radiator Problems in Complex EM Environments," *Sensors*, vol. 20, no. 12, p. 3371, Jun. 2020, doi: 10.3390/s20123371.
- [29] R. Zaker and A. Sadeghzadeh, "Passive techniques for target radar cross section reduction: A comprehensive review," *International Journal of RF and Microwave Computer-Aided Engineering*, vol. 30, Nov. 2020, doi: 10.1002/mmce.22411.
- [30] W. Jiang, T. Hong, and S. X. Gong, "Research on the Scattering Characteristics and the RCS Reduction of Circularly Polarized Microstrip Antenna," *International Journal of Antennas and Propagation*, vol. 2013, p. e735847, Jul. 2013, doi: 10.1155/2013/735847.
- [31] H. Singh and R. M. Jha, *Active Radar Cross Section Reduction: Theory and Applications*. Cambridge: Cambridge University Press, 2015. doi: 10.1017/CBO9781316136171.
- [32] Q. Wu, J. Liu, J. Wang, F. Zhao, and S. Xiao, "Improved Active Echo Cancellation Against Synthetic Aperture Radar Based on Nonperiodic Interrupted Sampling Modulation," *IEEE Sensors Journal*, vol. PP, pp. 1–1, Apr. 2018, doi: 10.1109/JSEN.2018.2824351.
- [33] I. A. Osman, "Active Cancellation System for Radar Cross Section Reduction," 2013. [https://www.semanticscholar.org/paper/Active-Cancellation-System-for-Radar-Cross-Section-
Osman/e74ed06922bee58729fbf9435de16064330ad18d](https://www.semanticscholar.org/paper/Active-Cancellation-System-for-Radar-Cross-Section-Osman/e74ed06922bee58729fbf9435de16064330ad18d) (accessed Jun. 17, 2022).

- [34] A. Chowdhury, R. U. Nair, and H. Singh, “Active radar cross section (RCS) reduction in parallel-fed dipole phased array,” in 2017 IEEE International Conference on Antenna Innovations & Modern Technologies for Ground, Aircraft and Satellite Applications (iAIM), Nov. 2017, pp. 1–6. doi: 10.1109/IAIM.2017.8402590.
- [35] D. C. Jenn “Radar and Laser Cross Section Engineering [PDF] [5t5q7fdkiqk0].” <https://vdoc.pub/documents/radar-and-laser-cross-section-engineering-5t5q7fdkiqk0> (accessed Jun. 16, 2022).
- [36] A. Muniyasamy and K. Rajakani, “UWB radar cross section reduction in a compact antipodal Vivaldi antenna,” *AEU - International Journal of Electronics and Communications*, vol. 99, pp. 369–375, Feb. 2019, doi: 10.1016/j.aeue.2018.12.020.
- [37] R. L. Fante and M. T. McCormack, “Reflection properties of the Salisbury screen,” *IEEE Transactions on Antennas and Propagation*, vol. 36, no. 10, pp. 1443–1454, Oct. 1988, doi: 10.1109/8.8632.
- [38] H. C. Strifors and G. C. Gaunard, “Scattering of electromagnetic pulses by simple-shaped targets with radar cross section modified by a dielectric coating,” *IEEE Transactions on Antennas and Propagation*, vol. 46, no. 9, pp. 1252–1262, Sep. 1998, doi: 10.1109/8.719967.
- [39] M. Paquay, J.-C. Iriarte, Iñ. Ederra, R. Gonzalo, and P. de Maagt, “Thin AMC Structure for Radar Cross-Section Reduction,” *IEEE Transactions on Antennas and Propagation*, vol. 55, no. 12, pp. 3630–3638, Dec. 2007, doi: 10.1109/TAP.2007.910306.
- [40] F. Yang and Y. Rahmat-Samii, “Microstrip antennas integrated with electromagnetic band-gap (EBG) structures: a low mutual coupling design for array applications,” 2003, doi: 10.1109/TAP.2003.817983.
- [41] D. Singh and V. Srivastava, “An analysis of RCS for dual-band slotted patch antenna with a thin dielectric using shorted stubs metamaterial

absorber,” *AEU - International Journal of Electronics and Communications*, 2018, doi: 10.1016/J.AEUE.2018.03.039.

[42] Y. Jia, Y. Liu, Y. Guo, K. Li, and S. Gong, “A Dual-Patch Polarization Rotation Reflective Surface and Its Application to Ultra-Wideband RCS Reduction,” *IEEE Transactions on Antennas and Propagation*, 2017, doi: 10.1109/TAP.2017.2694879.

[43] K. Patel, and M. Joshi, “Broadband Radar Cross Section Reduction of Microstrip Antenna Using Polarization Conversion Metasurface,” *Progress in Electromagnetics Research B*, vol. 96, pp. 67–86, Aug. 2022,

[44] A. Murugesan, K. T. Selvan, A. Iyer, K. V. Srivastava, and A. Alphones, “A REVIEW OF METASURFACE-ASSISTED RCS REDUCTION TECHNIQUES,” *PIER B*, vol. 94, pp. 75–103, 2021, doi: 10.2528/PIERB21081401.

[45] T. Han, X. Cao, J. Gao, Y. Zhao, and Y. Zhao, “A Coding Metasurface with Properties of Absorption and Diffusion for RCS Reduction,” 2017, doi: 10.2528/PIERC17041201.

[46] D. Howe, “Introduction to the Basic Technology of Stealth Aircraft: Part 2—Illumination by the Enemy (Active Considerations),” *Journal of Engineering for Gas Turbines and Power*, vol. 113, no. 1, pp. 80–86, Jan. 1991, doi: 10.1115/1.2906534.

[47] I. A. N. O. Mohammed and A. J. A. Supervisor, “Active Cancellation Algorithm for Radar Cross Section Reduction,” Thesis, Sudan University of Science and Technology, 2014. Accessed: Jun. 18, 2022. [Online]. Available: <http://repository.sustech.edu/handle/123456789/10883>

[48] E. Nohara, M. Miacci, G. G. Peixoto, I. Martin, and M. C. Rezende, “Radar Cross Section Reduction of Dihedral and Trihedral Corner Reflectors Coated with Radar Absorbing Materials (8-12 GHz),” Oct. 2003, pp. 479–484 vol.1. doi: 10.1109/IMOC.2003.1244907.

- [49] C. K. Yuzcelik, “Radar absorbing material design,” Thesis, Monterey, California. Naval Postgraduate School, 2003. Accessed: Nov. 24, 2022. [Online]. Available: <https://calhoun.nps.edu/handle/10945/6246>
- [50] W. W. Salisbury, “Absorbent body for electromagnetic waves,” US2599944A, Jun. 10, 1952 Accessed: Jun. 19, 2022. [Online]. Available: <https://patents.google.com/patent/US2599944A/en>
- [51] M. I. Skolnik, Radar Handbook. McGraw-Hill, 1990.
- [52] T. K. Wu “Frequency Selective Surface and Grid Array : Te-Kau Wu : 9780471311898.” <https://www.bookdepository.com/Frequency-Selective-Surface-Grid-Array-Te-Kau-Wu/9780471311898> (accessed Jun. 25, 2022).
- [53] B. A. Munk “Frequency Selective Surfaces: Theory and Design | Wiley,” Wiley.com.
<https://www.wiley.com/en-us/Frequency+Selective+Surfaces%3A+Theory+and+Design-p-9780471370475> (accessed Jun. 25, 2022).
- [54] R. Mittra, C. H. Chan, and T. Cwik, “Techniques for analyzing frequency selective surfaces-a review,” Proc. IEEE, vol. 76, no. 12, pp. 1593–1615, Dec. 1988, doi: 10.1109/5.16352.
- [55] A. Rashid and Z. Shen, “Three-dimensional frequency selective surfaces,” 2010 International Conference on Communications, Circuits and Systems (ICCCAS), 2010, doi: 10.1109/ICCCAS.2010.5581918.
- [56] A. Campos, R. Maniçoba, L. Araújo, and A. D’Assunção, “Analysis of Simple FSS Cascading with Dual Band Response,” Magnetics, IEEE Transactions on, vol. 46, pp. 3345–3348, Sep. 2010, doi: 10.1109/TMAG.2010.2046023.
- [57] S. Barkeshli, T. Smith, H. S. Luh, L. Ersoy, and T. Itanami, “On the analysis and design of the frequency selective surface for the N-Star satellite Ku/S-shaped reflector,” in IEEE Antennas and Propagation Society

International Symposium. 1995 Digest, Jun. 1995, vol. 3, pp. 1656–1658 vol.3. doi: 10.1109/APS.1995.530898.

[58] A. Chatterjee, B. Mandal, and S. K. Parui, “A FSS based corner reflector for performance enhancement of a ribcage dipole antenna,” in 2015 IEEE Applied Electromagnetics Conference (AEMC), Dec. 2015, pp. 1–2. doi: 10.1109/AEMC.2015.7509246.

[59] H. U. Tahseen, L. Yang, and X. Zhou, “Design of FSS-antenna-radome system for airborne and ground applications,” IET Communications, vol. 15, no. 13, pp. 1691–1699, 2021, doi: 10.1049/cmu2.12181.

[60] R. Dewan et al., “Artificial magnetic conductor for various antenna applications: An overview,” International Journal of RF and Microwave Computer-Aided Engineering, vol. 27, Mar. 2017, doi: 10.1002/mmce.21105.

[61] Y. Zhang, B.-Z. Wang, W. Shao, W. Yu, and R. Mittra, “Artificial Ground Planes for Performance Enhancement of Microstrip Antennas,” Journal of Electromagnetic Waves and Applications -, vol. 25, pp. 597–606, Jan. 2011, doi: 10.1163/156939311794500269.

[62] E. J. Rothwell and R. O. Ouedraogo, “Antenna miniaturization: definitions, concepts, and a review with emphasis on metamaterials,” Journal of Electromagnetic Waves and Applications, vol. 28, no. 17, pp. 2089–2123, Nov. 2014, doi: 10.1080/09205071.2014.972470.

[63] A. Modi, “Metasurface-Based Techniques for Broadband Radar Cross-Section Reduction of Complex Structures,” Arizona State University, 2020. Accessed: Jun. 22, 2022. [Online]. Available: <https://keep.lib.asu.edu/items/158751>

[64] F. Yang and Y. Rahmat-Samii, “Reflection phase characterizations of the EBG ground plane for low profile wire antenna applications,” IEEE Trans. Antennas Propagat., vol. 51, no. 10, pp. 2691–2703, Oct. 2003, doi: 10.1109/TAP.2003.817559.

- [65] A. Aminian, F. Yang, and Y. R. Samii, "In-phase reflection and EM wave suppression characteristics of electromagnetic band gap ground planes," IEEE Antennas and Propagation Society International Symposium. Digest. Held in conjunction with: USNC/CNC/URSI North American Radio Sci. Meeting (Cat. No.03CH37450), 2003, doi: 10.1109/APS.2003.1220288.
- [66] C. A. Balanis, "Advanced Engineering Electromagnetics", John Wiley & Sons, 2012.
- [67] F. Yang and Y. Rahmat-Samii, "A low-profile circularly polarized curl antenna over an electromagnetic bandgap (EBG) surface," *Microw. Opt. Technol. Lett.*, vol. 31, no. 4, pp. 264–267, Nov. 2001, doi: 10.1002/mop.10006.
- [68] S. Ullah, "Design of Electromagnetic Bandgap (EBG) structures for polarization sensitive wireless communications," 2016 13th International Bhurban Conference on Applied Sciences and Technology (IBCAST), 2016, doi: 10.1109/IBCAST.2016.7429946.
- [69] M. Beruete, M. Navarro-Cía, M. Sorolla, and I. Campillo, "Polarization selection with stacked hole array metamaterial," *Journal of Applied Physics*, vol. 103, no. 5, p. 053102, Mar. 2008, doi: 10.1063/1.2841471.
- [70] Y. Jia, Y. Liu, Y. J. Guo, K. Li, and S.-X. Gong, "Broadband Polarization Rotation Reflective Surfaces and Their Applications to RCS Reduction," *IEEE Transactions on Antennas and Propagation*, vol. 64, no. 1, pp. 179–188, Jan. 2016, doi: 10.1109/TAP.2015.2502981.
- [71] R. Zaker and A. Sadeghzadeh, "A Low-Profile Design of Polarization Rotation Reflective Surface for Wideband RCS Reduction," *IEEE Antennas and Wireless Propagation Letters*, vol. PP, pp. 1–1, Jul. 2019, doi: 10.1109/LAWP.2019.2930130.
- [72] C. L. Holloway, E. F. Kuester, J. A. Gordon, J. O'Hara, J. Booth, and D. R. Smith, "An Overview of the Theory and Applications of Metasurfaces: The Two-Dimensional Equivalents of Metamaterials," *IEEE Antennas and*

Propagation Magazine, vol. 54, no. 2, pp. 10–35, Apr. 2012, doi: 10.1109/MAP.2012.6230714.

[73] J. Su, Y. Cui, Z. Li, Y. (Lamar) Yang, Y. Che, and H. Yin, “Metasurface base on uneven layered fractal elements for ultra-wideband RCS reduction,” AIP Advances, vol. 8, no. 3, p. 035027, Mar. 2018, doi: 10.1063/1.5013106.

[74] A. Y. Modi, C. Balanis, C. R. Birtcher, and H. N. Shaman, “New Class of RCS-Reduction Metasurfaces Based on Scattering Cancellation Using Array Theory,” IEEE Transactions on Antennas and Propagation, vol. 67, no. 1, pp. 298–308, Jan. 2019, doi: 10.1109/TAP.2018.2878641.

[75] J. Zhao and Y. Cheng, “A high-efficiency and broadband reflective 90° linear polarization rotator based on anisotropic metamaterial,” Applied Physics B, vol. 122, p. 255, Sep. 2016, doi: 10.1007/s00340-016-6533-6.

[76] X. Zheng, Z. Xiao, and X. Ling, “Broadband and efficient reflective polarization converter based on a three-dimensional metamaterial,” Optical and Quantum Electronics, vol. 48, p. 461, Sep. 2016, doi: 10.1007/s11082-016-0733-5.

[77] Y.-Q. Zhuang, G.-M. Wang, and H.-X. Xu, “Ultra-wideband RCS reduction using novel configured chessboard metasurface,” Chinese Phys. B, vol. 26, no. 5, p. 054101, May 2017, doi: 10.1088/1674-1056/26/5/054101.

[78] J. Su, Y. Lu, J. Liu, Y. Yang, Z. Li, and J. Song, “A Novel Checkerboard Metasurface Based on Optimized Multielement Phase Cancellation for Superwideband RCS Reduction,” IEEE Transactions on Antennas and Propagation, 2018, doi: 10.1109/TAP.2018.2870372.

[79] X. Liu, J. Gao, L. Xu, X. Cao, Y. Zhao, and S. Li, “A Coding Diffuse Metasurface for RCS Reduction,” Antennas Wirel. Propag. Lett., vol. 16, pp. 724–727, 2017, doi: 10.1109/LAWP.2016.2601108.

[80] Y. Xin, L. Lanju, Z. Yating, D. Xin, and Y. Jian-quan, “A coding metasurfaces used for wideband radar cross section reduction in terahertz frequencies,” 2015. doi: 10.7498/APS.64.158101.

- [81] Y. Zhuang et al., “Random Combinatorial Gradient Metasurface for Broadband, Wide-Angle and Polarization-Independent Diffusion Scattering,” *Scientific Reports*, vol. 7, Nov. 2017, doi: 10.1038/s41598-017-16910-4.
- [82] Y. Cheng et al., “An ultra-thin dual-band phase-gradient metasurface using hybrid resonant structures for backward RCS reduction,” *Applied Physics B*, vol. 123, Apr. 2017, doi: 10.1007/s00340-017-6728-5.
- [83] S. Leung, C.-P. Liang, X.-F. Tao, F.-F. Li, Y. Poo, and R.-X. Wu, “Broadband radar cross section reduction by an absorptive metasurface based on a magnetic absorbing material,” *Opt Express*, vol. 29, no. 21, pp. 33536–33547, Oct. 2021, doi: 10.1364/OE.440785.
- [84] Y. Zhang, J. H. Mueller, B. Mohr, L. Liao, A. Atac, and R. Wunderlich, “A Multi-Frequency Multi-Standard Wideband Fractional- PLL With Adaptive Phase-Noise Cancellation for Low-Power Short-Range Standards,” *IEEE Transactions on Microwave Theory and Techniques*, vol. 64, pp. 1133–1142, Mar. 2016, doi: 10.1109/TMTT.2016.2536022.
- [85] J. Hu, W. Zhou, Y. Fu, X. Li, and N. Jing, “Uniform Rotational Motion Compensation for ISAR Based on Phase Cancellation,” *IEEE Geoscience and Remote Sensing Letters*, vol. 8, no. 4, pp. 636–640, Jul. 2011, doi: 10.1109/LGRS.2010.2098841.
- [86] K. A. Wear, “The Effect of Phase Cancellation on Estimates of Calcaneal Broadband Ultrasound Attenuation in Vivo,” *IEEE Transactions on Ultrasonics, Ferroelectrics, and Frequency Control*, vol. 54, no. 7, pp. 1352–1359, Jul. 2007, doi: 10.1109/TUFFC.2007.395.
- [87] J. Suarez and P. R. Prucnal, “System-Level Performance and Characterization of Counter-Phase Optical Interference Cancellation,” *Journal of Lightwave Technology*, vol. 28, no. 12, pp. 1821–1831, Jun. 2010, doi: 10.1109/JLT.2010.2046879.
- [88] M. Paquay, J.-C. Iriarte, Iñ. Ederra, R. Gonzalo, and P. de Maagt, “Thin AMC Structure for Radar Cross-Section Reduction,” *IEEE Transactions on*

Antennas and Propagation, vol. 55, no. 12, pp. 3630–3638, Dec. 2007, doi: 10.1109/TAP.2007.910306.

[89] J. C. Iriarte Galarregui, A. Tellechea Pereda, J. L. M. de Falcón, I. Ederra, R. Gonzalo, and P. de Maagt, “Broadband Radar Cross-Section Reduction Using AMC Technology,” *IEEE Transactions on Antennas and Propagation*, vol. 61, no. 12, pp. 6136–6143, Dec. 2013, doi: 10.1109/TAP.2013.2282915.

[90] A. Edalati and K. Sarabandi, “Wideband, Wide Angle, Polarization Independent RCS Reduction Using Nonabsorptive Miniaturized-Element Frequency Selective Surfaces,” *Antennas and Propagation, IEEE Transactions on*, vol. 62, pp. 747–754, Feb. 2014, doi: 10.1109/TAP.2013.2291236.

[91] Y. Zheng, J. Gao, X. Cao, Z. Yuan, and H. Yang, “Wideband RCS Reduction of a Microstrip Antenna Using Artificial Magnetic Conductor Structures,” *IEEE Antennas and Wireless Propagation Letters*, vol. 14, pp. 1582–1585, 2015, doi: 10.1109/LAWP.2015.2413456.

[92] W. Chen, C. A. Balanis, and C. R. Birtcher, “Checkerboard EBG Surfaces for Wideband Radar Cross Section Reduction,” *IEEE Transactions on Antennas and Propagation*, vol. 63, no. 6, pp. 2636–2645, Jun. 2015, doi: 10.1109/TAP.2015.2414440.

[93] S. H. Esmaeli and S. H. Sedighy, “Wideband radar cross-section reduction by AMC,” *Electron. lett.*, vol. 52, no. 1, pp. 70–71, Jan. 2016, doi: 10.1049/el.2015.3515.

[94] W. Pan et al., “Combining the absorptive and radiative loss in metasurfaces for multi-spectral shaping of the electromagnetic scattering,” *Sci Rep*, vol. 6, no. 1, p. 21462, Aug. 2016, doi: 10.1038/srep21462.

[95] D. Pozar, “Microwave Engineering,” in John Wiley & Sons Inc., 2005, PP. 1–756.

[96] Y. Li, M.E. Bialkowski, K.H. Sayidmarie, N.V. Shuley,” 81-element single-layer reflectarray with double-ring phasing elements for wideband

applications”, 2010 IEEE Antennas and Propagation Society International Symposium, 1-4

الخلاصة

هناك اهتمام متزايد لخفض المقطع الراداري الخاص بالأجسام لمجموعة واسعة من التطبيقات. حيث تم استخدام المواد المركبة مثل الخشب و بعض المواد الاخرى لتصنيع الطائرات في محاولة للحد من إمكانية اكتشافها بسبب انخفاض انعكاس الموجات الكهرومغناطيسية عنها مقارنة بالمعادن.

تبحث الاطروحة في خفض المقطع الراداري للأهداف باستخدام السطوح الانتقائية للتردد (FSS) احادية الطبقة. و إنشاء خلايا (FSS) ذات معامل انعكاس منخفض هو الهدف من هذا العمل من أجل استخدامها لتقليل المقطع الراداري للأسطح المستوية. كما و يتضمن البحث تحليلاً نظرياً محاكاةً باستخدام (CST Microwave Studio.)

تمت دراسة (FSS) باستخدام حلقات مربعة مزدوجة مطبوعة على جانب واحد من الركيزة لتحسين أداء المقطع الراداري للأسطح المستوية، و تمت دراسة تأثير تغيير حجم الحلقات وعرضها على تردد الرنين، للحصول على عرض نطاق أوسع و الناتج من تقاطع نطاقي استجابة ترددية للحلقات المزدوجة ، تم استخدام حلقة داخلية متعرجة لتقريب محيطها من محيط الحلقة الخارجية ، بالإضافة إلى استخدام حلقة داخلية مفتوحة لان محيط الحلقة المفتوحة يساوي تقريبا $0.5\lambda_0$ عند الرنين. بالإضافة الى ذلك تم فحص تأثير تغيير بعض العوامل في الخلية مثل حجم الحلقة وعرض الحلقة والمسافة بين طرفي الحلقة الداخلية على تردد الرنين وقيمة معامل الانعكاس.

بالإضافة إلى الأجزاء الموصلة، تناقش هذه الرسالة أيضًا ما إذا كان من الممكن زيادة أداء الامتصاص في الخلية (FSS) لتقليل المقطع الراداري للأسطح المستوية. من أجل تقليل الطاقة المنعكسة من سطح (FSS) ، يتم إدخال خلايا وحدة (FSS) التي تمت دراستها لكل من الحلقات المزدوجة المغلقة و الحلقات المزدوجة ذات الحلقة الداخلية المفتوحة المطلية بعجينة الكربون. يتم فحص خلايا FSS المقترحة باستخدام مجموعات مختلفة من المكونات في مجال إدخال معجون الكربون، وتعديل أبعاد الحلقة، والايصالية، وسمك العجينة للأشكال المقترحة لخلايا الوحدة.

إقرار لجنة المناقشة

نشهد بأننا أعضاء لجنة التقويم والمناقشة قد اطلعنا على هذه الرسالة الموسومة (دراسة خفض المقطع الراداري للأسطح المستوية) وناقشنا الطالب (مصطفى باسم جاسم) في محتوياتها وفيما له علاقة بها بتاريخ / / ٢٠٢٢ وقد وجدناه جديراً بنيل شهادة الماجستير-علوم في اختصاص هندسة الاتصالات.

التوقيع:	التوقيع:
رئيس اللجنة: أ.م.د. يسار عزالدين محمد علي	عضو اللجنة: أ.م.د. محمد عبدالرحمن محمد
التاريخ: / / ٢٠٢٢	التاريخ: / / ٢٠٢٢

التوقيع:	التوقيع:
عضو اللجنة: أ.م.د. احمد محمد سلامة	عضو اللجنة(المشرف): أ.د. خليل حسن سيد مرعي
التاريخ: / / ٢٠٢٢	التاريخ: / / ٢٠٢٢

قرار مجلس الكلية

اجتمع مجلس كلية هندسة الالكترونيات بجلسته المنعقدة بتاريخ : / / ٢٠٢٢
وقرر المجلس منح الطالب شهادة الماجستير علوم في اختصاص هندسة الاتصالات.

مقرر المجلس: أ.م.د. صدقي بكر ذنون	رئيس مجلس الكلية: أ.د. خالد خليل محمد
التاريخ: / / ٢٠٢٢	التاريخ: / / ٢٠٢٢

إقرار المشرف

أشهد بأن هذه الرسالة الموسومة (دراسة خفض المقطع الراداري للأسطح المستوية) والمعدة من قبل الطالب (مصطفى باسم جاسم) تحت اشرافي في قسم هندسة الاتصالات / كلية هندسة الالكترونيات / جامعة نينوى، كجزء من متطلبات نيل شهادة الماجستير علوم في هندسة الاتصالات.

التوقيع:

الاسم: أ. د خليل حسن سيد مرعي

التاريخ: / / ٢٠٢٢

إقرار المقوم اللغوي

اشهد بأنه قد تمت مراجعة هذه الرسالة من الناحية اللغوية وتصحيح ماورد فيها من أخطاء لغوية وتعبيرية وبذلك أصبحت الرسالة مؤهلة للمناقشة بقدر تعلق الأمر بسلامة الأسلوب أو صحة التعبير.

التوقيع:

الاسم:

التاريخ: / / ٢٠٢٢

إقرار رئيس قسم هندسة الاتصالات

بناءً على التوصيات المقدمة من قبل المشرف والمقوم اللغوي أرشح هذه الرسالة للمناقشة.

التوقيع:

الاسم: أ.م.د محمود احمد محمود

التاريخ: / / ٢٠٢٢

إقرار رئيس لجنة الدراسات العليا

بناءً على التوصيات المقدمة من قبل المشرف والمقوم اللغوي و رئيس قسم هندسة الاتصالات أرشح

هذه الرسالة للمناقشة.

التوقيع:

الاسم:

التاريخ: / / ٢٠٢٢



جامعة نينوى
كلية هندسة لالكترونيات

دراسة خفض المقطع الراداري للأسطح المستوية

رسالة تقدم بها

مصطفى باسم جاسم

الى مجلس كلية هندسة الالكترونيات

جامعة نينوى

كجزء من متطلبات نيل شهادة الماجستير في علوم

هندسة الاتصالات

بإشراف

الأستاذ الدكتور

خليل حسن سيد مرعي



جامعة نينوى
كلية هندسة الالكترونيات

دراسة خفض المقطع الراداري للأسطح المستوية

مصطفى باسم جاسم

رسالة ماجستير علوم في
هندسة الاتصالات

بإشراف

الاستاذ الدكتور

خليل حسن سيد مرعي